Manipulation of Exciton Polariton Condensates in 1D Waveguides

By
Tingge Gao

A thesis submitted in partial fulfillment for the
Degree of Doctor of Philosophy
in the
Faculty of Science
Department of Materials Science & Technology

For my parents and my sisters

Abstract

This thesis investigates exciton polaritons in GaAs microcavity. Exciton polaritons are the eigenstates of the microcavity in strong coupling regime. In this thesis, we realize polariton lasing in a high Q microcavity and micropillars; and to manipulate polariton condensate flow along a 1D waveguide by using optical/spin method.

A high Q microcavity is investigated at low temperature and high temperature. Polariton lasing is observed only at low temperature. Micropillars are etched from the high Q microcavity. Polariton lasing threshold decreases with reducing pillar size due to strong lateral confinement, which favors polariton energy relaxation, thermalization and avoidance of exciton diffusion. A monotonic increase of the polariton lasing threshold with temperature is found which is consistent with the relation between the critical density of polariton condensate and temperature in quasi-thermalization regime.

By using polariton lasing at high wave vector states observed in the planar microcavity, we realize a polariton condensate flow along a microcavity ridge. The propagation of the condensate occurs due to polariton exciton reservoir interaction. In addition, we can manipulate the polariton condensate flow through a much weaker gate beam.

The above transistor switch could be employed to make spin devices. Firstly, we observe spin polarization oscillation of the polariton condensate flow due to the effect magnetic field generated by the TE-TM mode splitting. Secondly, a polariton condensate flow without spin polarization oscillation is found when the laser is in pulse mode. Finally, a spin dependent blueshift is introduced by making the gate beam circular polarized. The polariton condensate in different spin polarization could be reflected or transmitted through the gate spot. The gate beam acts as a spin filter to separate the polariton condensate with different spin polarization.

All these work paves the way to the application of polariton circuits or spin circuits. The spatial control of the polariton condensate flow in the waveguide allows the implementation of polariton transistors or spin filters suitable in both optoelectronic and all-optical/spin schemes.

Contents

Acknowledgement

This PhD is done under supervision of Professor Pavlos Savvidis. First of all, I would like to thank my supervisor Prof. Pavlos Savvidis. For these years, he guided me and gave me the opportunity to learn and study exciton polaritons. I am very appreciated of his energetic patience and passion to help me in every scientific and technical problem. I want to express special appreciation for Pavlos' wife Mrs Savvidis to provide us high quality figures.

I want to express special appreciation for Dr Simos Tsintzos and Dr Peter Eldridge. Simos trained me when I was new in the lab and taught me a lot about polaritons. Peter explained to me a lot of experimental physics during my PhD and some skills about IGOR. He encouraged me a lot and shared with me much stimulating discussions.

I want to thank Prof. Z. Hatzopoulos for the high-quality sample he has grown.

I also want to express my appreciation for Professor Luis Vina for his support to use his lab and Carlos for his help.

Many thanks go to Maria. She taught me much lab issues and even tolerated me some mistakes I made before.

I want to express much appreciation to Dialynas and Savvas for their help in the lab and physical examination in the hospital.

I want to thank Marina for her helping of my visa and other things.

There are many other people I am appreciated of, whose names are not listed here, for their friendly help to me.

Finally I want to thank our group members: Dr. Peter Eldridge, Dr. Simos Tsintzos
Dr. Gabriel Charistmann, Panos Tsotsis, Pramod Sharma, Kostas Daskalakis, Niccolo Somaschi
Sefanos Hatziathanasiou, Alexandros Tzimis for the fruitful coopration and discussion!

List of figures

List of tables

Chapter 1

Introduction

We work on GaAs quantum wells in this thesis. GaAs is a direct band-gap semiconductor with mature growth and fabrication techniques nowadays. The electrons and holes in GaAs can form a weak bound pair called excitons. The excitons couple with the electromagnetic field, creating a new quasi particle, exciton polariton. These polaritons are stationary states and only couple out until they reach the surface.

Low dimensional GaAs based material such as quantum well has an enhanced exciton binding energy and oscillator strength compared with the bulk material. To realize coupling between the excitons and photons, we need to insert the quantum wells into a semiconductor microcavity which confines photons along the growth direction. For example, the spontaneous emission rate of excitons in quantum well can be greatly enhanced or suppressed in weak coupling regime **[1]**. This is Purcell effect **[2]**. Exciton polaritons develop when the energy exchange rate between the excitons and cavity photons is faster than the decay rate of the excitons and out coupling rate of the cavity photons. In this regime, strong coupling holds. The first observation of 2 dimensional exciton polaritons is reported around 20 years ago in reference **[3]**.

Polaritons are composite bosons at low density regime. This is demonstrated in reference **[4]**. A threshold-less polariton laser is proposed in reference **[5]**. Exciton polaritons can condense in a single state when final state stimulation occurs. The decay of the polariton condensate emits a coherent light. This kind of laser does not need the “population inversion”, and has a much smaller threshold.

The observation of polariton laser is realized around 10 years ago. The reason is that exciton polaritons have a relaxation time which is larger than their lifetime. Polaritons decay at the so-called “bottle-neck” region before they relax to the ground state **[6]**.

When GaAs quantum wells are inserted in a high Q microcavity grown by MBE **[7]**, the lifetime of exciton polaritons is longer. They relax to the ground state before decaying out of the microcavity. In this case, polariton condensate can be formed spontaneously **[8]**. Polariton lasing is also realized in zero dimensional high Q microcavity pillars **[9]**, which confine exciton polaritons in all three dimensions.

However, detailed comparison of polariton lasing and photon lasing is still needed. Especially temperature dependent polariton lasing threshold is necessary, which indicates the direction towards room temperature polariton lasing in GaAs based semiconductor microcavity. In this thesis, exciton polaritons lasing in a high Q planar GaAs microcavity and micropillars are studied. This thesis’s focus is to compare polariton lasing at low temperature and photon lasing at high temperature, and to discuss polariton lasing threshold with temperature and detuning. We find the polariton lasing threshold increases monotonically with temperature in a micropillar, which is consistent with the critical density of polariton condensate with temperature.

We observe polariton lasing occurs at high k states in the high Q planar microcavity, this could be used to investigate the propagation of the polariton condensate along the waveguide. In one dimensional microcavity wire **[10]**, the polariton condensate can be formed spontaneously. The trapped state for the condensate exists between the wire end and the pump spot. This one dimensional microcavity wire provides a platform to study the propagation of polariton condensate. To manipulate the polariton condensate, more work is needed through optical method. In this thesis, a polariton condensate transistor switch **[11]** is realized when two laser beams are employed in a quasi one dimensional microcavity ridge. The key requirement is the polariton-exciton reservoir interaction at the gate beam spot. This kind of all-optical technique has been used to realize interesting potential landscape such as harmonic oscillator potential **[12]**, or vortex lattices formation **[13]**.

Polaritons in the semiconductor microcavity with a large Rabi splitting has also been studied recently. For example, a CeTd semiconductor microcavity is used to realize Bose Einstein condensation **[14]**. Quantum physics of the polariton condensate such as quantized vortex **[15]** is investigated.

Exciton polaritons inherent spin from the exciton part and cavity photon part. We observe spin-related phenomenon and realize a spin filter based on the work of the transistor switch in **Chapter 4**. Exciton polaritons experience an effective magnetic field generated by TE-TM mode splitting. From this, Optical Spin Hall effect is observed in reference **[16]**. In addition, exciton-exciton interaction when their spin is in singlet configuration is much weaker than the triplet configuration **[17,18]**. Based on this, an exciton polariton spin switch is demonstrated **[19]**. When a circular polarized laser is focused on a microcavity, it excites different population of polaritons and excitons with circular polarization $\boldsymbol{\sigma}$+ and $\boldsymbol{\sigma}$-. This leads to spin dependent blueshift and affects the propagating polariton condensate. The condensate with different spin polarization could be separated into two regions. In the **Chapter 5** of the thesis, a spin filter is realized **[20]** based on this idea.

Thesis outline

This thesis includes mainly four parts.

The first one is about the discussion of the basics of exciton polaritons. Starting from quantum well and microcavity, strong coupling between excitons and cavity photon modes is described. Fundamental property of exciton polaritons is reviewed, such as dispersion curve, decay rates and effective mass. Special focus is about condensation and spin of exciton polaritons.

Second part of the thesis is addressed about exciton polariton lasing in planar microcavity and micropillars. Polariton lasing is investigated in the strong coupling regime. The difference between polariton lasing and photon lasing is discussed. The polariton lasing threshold with pillar size, detuning and temperature is investigated.

The third part is about the experimental realization of a polariton condensate transistor switch. This work is carried on a microcavity ridge, which is etched from the high Q planar microcavity. Firstly, a polariton condensate flow is formed along the microcavity ridge towards the end. This results from polariton-exciton interaction at the center of the pump spot. Then a second laser is introduced, which leads to a local blueshift between the ridge end and the pump spot. This blueshift modulates the propagation of the polariton condensate flux. In addition, relaxation of the polariton condensate flow along the ridge is studied.

Finally, the spin of exciton polaritons is investigated. The TE-TM mode splitting in the microcavity ridge, results in an effective magnetic field. This magnetic field lies in the plane of the quantum well in the microcavity, and leads to spin procession of the polariton condensate. However, the polariton condensate flow without spin polarization oscillation appears when a pulse, circular polarized laser is employed. Mostly importantly, we realize a spin filter by using two laser beams. A non-resonant, linearly polarized laser forms a polariton condensate flow. The second circular polarized laser at the same wavelength introduces spin dependent blueshift. The polariton condensates with spin polarization $\sigma+$ and $\sigma-$ behave differently when they encounter the gate spot. Specifically, the polariton condensate with the same circular polarization with the second laser beam is mostly reflected back, while as the polariton condensate with the opposite circular polarization mostly transmits through the gate spot. The gate beam acts as a spin filter and separates the polariton condensate with the efficiency of around 45%.

Chapter 2

Fundamentals of exciton polaritons

As discussed in the introduction part, exciton polaritons result from strong coupling between the excitons in quantum wells and cavity photon modes. Behaving as bosons at low density, exciton polaritons can form a condensate and emits a coherent light, called polariton laser. In the **Chapter 3**, polariton lasing is realized in a planar microcavity and micropillars. A detailed description of exciton polaritons is provided in this Chapter. Here we discuss from the excitons and empty microcavity. Then weak coupling and strong coupling between the excitons and cavity photons is addressed. Finally, basic property of exciton polaritons is reviewed such as dispersion, lasing, condensation and spin.

2.1 Excitons in semiconductors

Excitons are basic excitation in semiconductors due to the Column attraction between an electron and a hole. In this thesis, we study excitons in quantum wells inserted in a semiconductor microcavity. In the following section we discuss about basic property of excitons. In section 2.5, we will review the TE-TM mode splitting of the excitons in quantum wells.

2.1.1 Excitons in bulk semiconductors and quantum wells

GaAs semiconductor is a compound of Gallium and Arsenic elements. GaAs has a Zinc-Blende lattice structure, which consists of two interpenetrated diamond lattices, as shown in **Figure 2.1**. The direct band gap of the bulk GaAs is around 1.424 eV at 0K **[21]**.

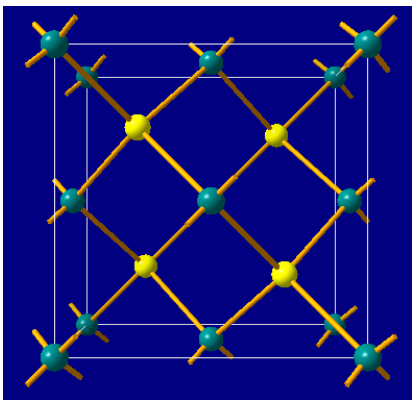

Figure 2.1: GaAs Zinc-Blende crystalline structure. The lattice points in different colors represent two different atoms Gallium and Arsenic. This is plotted by Diamond 3.1d.

Excitons in bulk semiconductors

The ground state of a perfect semiconductor is both the completely filled valence bands (for electrons) and the completely empty conduction bands (for electrons). When an electron is excited from the valence band to the conduction band by a laser, a hole is left at the valence band with the same wave vector and a positive electron charge. The Coulomb interaction

between the excited electron and the created hole pushes them to form a bound pair like a hydrogen atom or a Positronium.

The energy of excitons is determined by:

$$E_n(k) = E_g - \frac{Me^4}{2\hbar^2\varepsilon^2 n^2} + \frac{\hbar^2 k^2}{2M} \tag{2.1}$$

$$M = \frac{m_e m_h}{m_e + m_h} \tag{2.2}$$

The first part in (2.1) is the band gap of the semiconductor, the second one corresponds to the binding energy, and the third part is the kinetic energy of the excitons. The excitons' effective mass is determined by the electron effective mass and the effective mass of the hole. The 1s heavy hole exciton's effective mass is around 0.3 time electron mass in GaAs **[21]**.
There is big difference between an exciton in solid and a hydrogen atom in Vacuum. For example, the Bohr radius of excitons is much larger than a hydrogen atom with about several nanometers. There exists large dielectric screening in solids. So the electron is just loosely bound to the hole, with a binding energy of around several (4 for 1s excitons) meV in bulk GaAs **[22]**. Due to small binding energy, excitons are weak and not stable.

Wannier excitons and Frenkel excitons
Usually excitons can be classified by two kinds: the Wannier exciton and Frenkel exciton, as shown in **Figure 2.2.** The former one is the exciton which covers many unit cells in semiconductors. This kind of excitons' wave-function is delocalized in the crystal and they can move freely. In other solids such as NaCl or polymer semiconductors, excitons can also be formed in a single unit cell. This kind of excitons cannot move freely in the crystal. In this thesis, we just deal with Wannier 1s heavy hole (sometimes light hole) excitons in GaAs semiconductors.

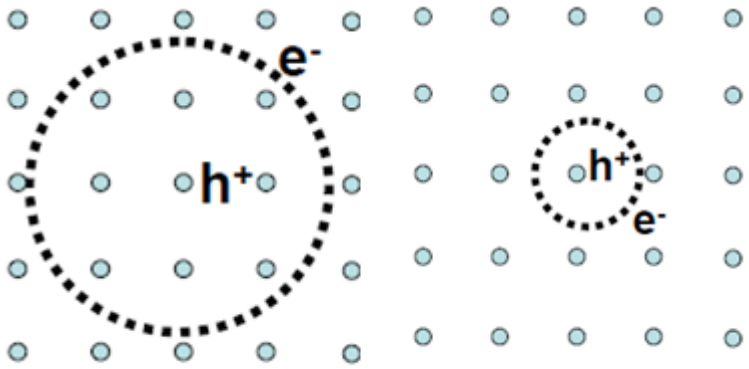

Figure 2.2 Wannier excitons and Frankel excitons in a semiconductor.

Excitons in quantum wells
In bulk GaAs semiconductors, excitons are weak. It is necessary to confine the excitons in

smaller structures. For example, we can put very narrow semiconductor slice (10nm) between two larger-band-gap semiconductor layers. We call this a quantum well. In quantum wells, the center-of-mass motion of an exciton is quantized along the direction perpendicular to the quantum well plane. The motion of the excitons along the planar quantum well is free due to translational invariance. The excitons become 2 dimensional quasi-particles, as shown in **Figure 2.3 [23].**

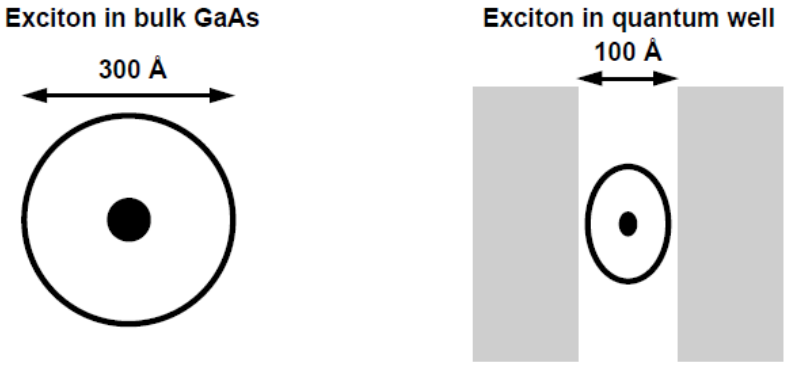

Figure 2.3 Excitons in bulk GaAs and placed in a quantum well, reprinted from **[23]**.

The quantum confinement changes the valence bands and the conduction bands of the quantum well layers. The electrons and holes are distributed at discrete energy levels in the quantum well. See **Figure 2.4.**

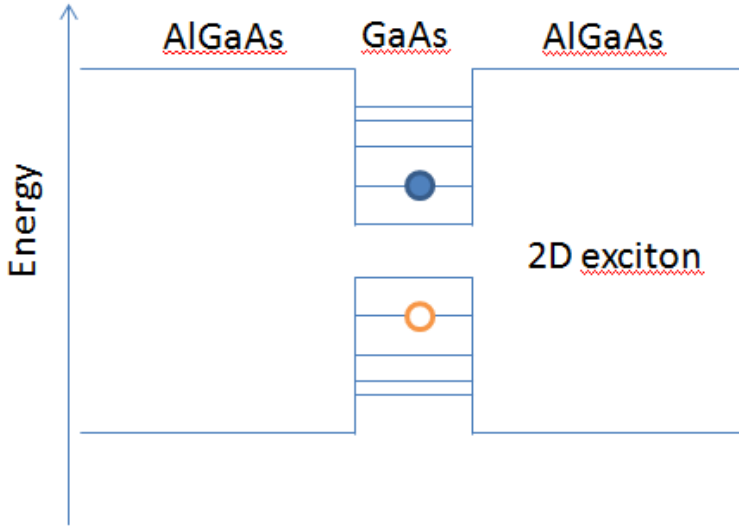

Figure 2.4 A GaAs quantum well placed between two AlGaAs barriers, the bands of the electrons and holes become into discrete levels in the quantum well.

In addition, the wave-function of the electrons and holes in the quantum well is also changed compared with the bulk materials. The overlap between the electron and the hole wave-function is larger in a quantum well. Exciton radius becomes smaller, which increases the excitons' binding energy **[23]**. When the interaction between the excitons is small compared

with the binding energy, excitons are bosons. If the density is increased larger the saturation density, the interaction between the excitons makes them to dissociate into electron-hole plasma **[24]**.

2.1.2 Exciton optical absorption

Excitons gain angular momentum from the electrons and holes. In the center of the Brillouin zone of the bulk GaAs, the conduction band has an s-symmetric structure, while the valance band owns p-symmetry. Thus the conduction band has a two-fold degeneracy, and the valence band has a six-fold degeneracy. The electron in the conduction band has an orbital angular momentum L=0 and spin angular momentum S=1/2. The electron in the valence band has an orbital angular momentum L=1 and spin angular momentum S=1/2. So in bulk GaAs, the total angular momentum of the electron in the conduction band is J=1/2. While as to the valence band, the two split-off band states with J=1/2 have an energy lower than (as to the electrons) the light hole and the heavy hole states which have total angular momentum J=3/2, as shown in **Figure 2.5 (left)**.

When placed in a quantum well, the degeneracy between the light holes and the heavy holes at k=0 is broken because the translational symmetry in the growth direction disappears. The heavy holes' total angular momentum projection onto the growth axis is $J_z^{heavyhole} = \pm 3/2$. They are closer to the band edge. The total angular momentum projection onto the growth axis of the light hole is $J_z^{lighthole} = \pm 1/2$, which is further away from the band edge, as shown in **Figure 2.5 (right)**.

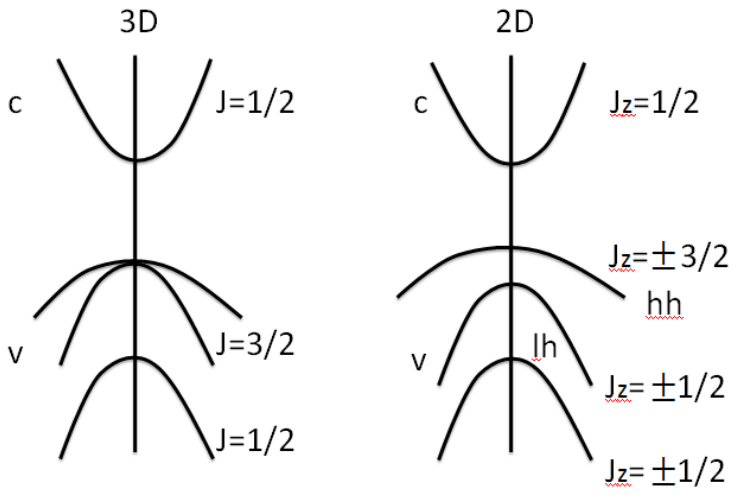

Figure 2.5 Energy band structure of Zinc-Blende crystal in bulk (left) and quantum wells (right).

Excitons are formed when an electron is bound by a hole with specific angular momentum, as shown in **Figure 2.6.** Usually the heavy-hole excitons can be described by the spin states that have projection onto the growth axis of $S_z = \pm 1, \pm 2$; while the light-hole excitons' spin projection onto the growth axis is $S_z = \pm 1, 0$ **[25].**

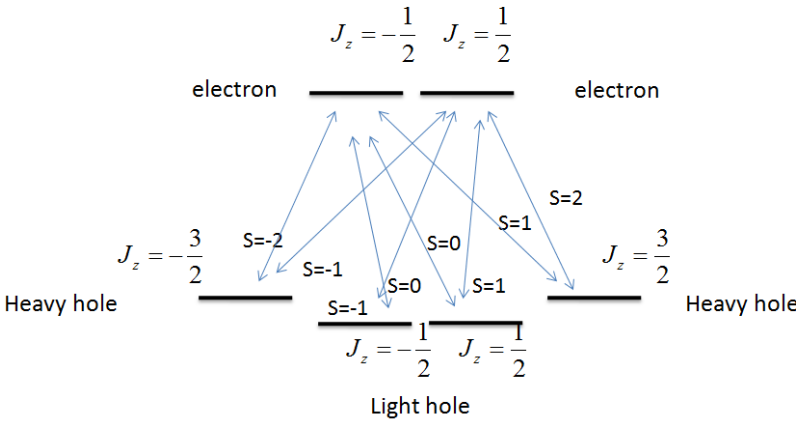

Figure 2.6 Spin states of heavy-hole exciton and light-hole exciton in a GaAs semiconductor quantum well.

The heavy-hole excitons with spin momentum projection onto the growth axis of $S_z = \pm 2$ are called dark excitons. They cannot be excited optically. In most cases, we ignore their contribution. However, the dark excitons can come into play when polariton-polariton interaction occurs**[26,27].**

2.2 Semiconductor microcavity

To realize strong coupling between excitons and photons, we need to insert the quantum well in a microcavity. The microcavity provides wavelength-scale (Integer multiple 0.5λ) confinement for the photon modes. The photons in the cavity are reflected backwards with large number of round-trips between the two high-reflectivity mirrors and can couple with the cavity material more efficiently. Here we discuss just the planar Fabry-Perot semiconductor microcavity without quantum well firstly. **Figure 2.7** shows the structure of a microcavity which does not contain quantum wells. The semiconductor microcavity is composed of a top distributed Bragg reflector, a cavity layer and a bottom distributed Bragg reflector. The distributed Bragg reflector consists of alternate semiconductor layers with the thickness of a quarter light wavelength in the cavity. The semiconductor layers in the DBR have different refractive index.

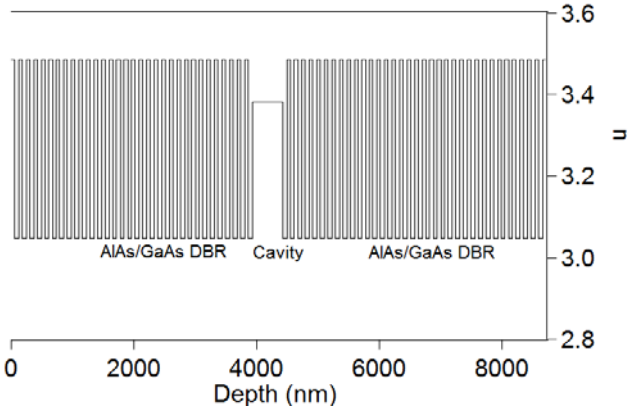

Figure 2.7 Structure of a semiconductor microcavity, right axis shows the refractive index distribution

This refractive index difference in the DBR leads to a high reflectivity region, which is called stop band, shown in **Figure 2.8**. The dip in the stop band is the cavity mode.

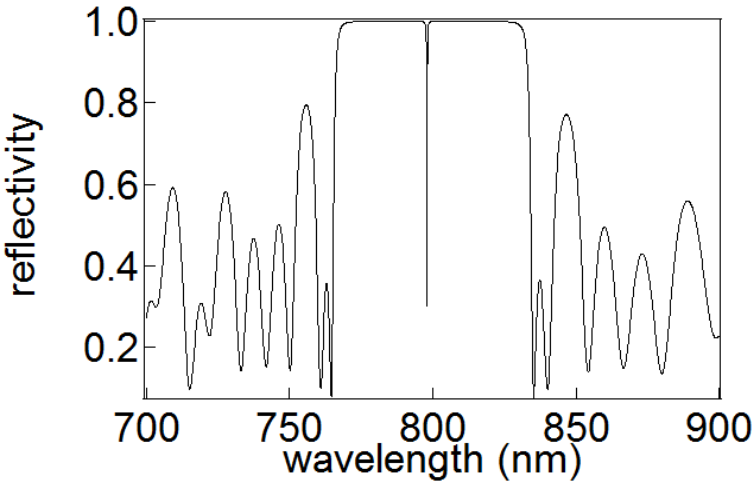

Figure 2.8 Simulated reflectivity of the microcavity, the dip is the cavity mode.

As to a semiconductor microcavity, which has equal number of the period in the top DBR and the bottom DBR, the reflectivity in the stop band is given by **[28]**

$$R = 1 - 4\frac{n_{air}}{n_{cav}}\left(\frac{n_{low}}{n_{high}}\right)^{2N} \tag{2.3}$$

where n_{air}, n_{cav}, n_{low} and n_{high} are the refractive index of the air (environment), cavity layer, low refractive index layers and high refractive index layers, N is the number of the period in the DBR.

The electric field of the light in the cavity can penetrate into the DBR with the length of:

$$L_{DBR} = \frac{\lambda_{cav}}{2n_{cav}}\frac{n_1 n_2}{n_2 - n_1} \tag{2.4}$$

So the total length for the light in the cavity should be

$$L_{effective} = L_{cavity} + L_{DBR} \tag{2.5}$$

The cavity mode frequency in **Figure 2.8**, if simply expressed, is given **[29]**:

$$\omega(\theta) = \frac{L_{cav}\omega_{cav}(\theta) + L_{DBR}(\theta)\omega_s(\theta)}{L_{effective}(\theta)} \tag{2.6}$$

where $L_{effective}$ is effective cavity length, ω_s is the center of the stop band, θ is the incident angle of the light in the cavity, the ω_{cav} is the Fabry-Perot frequency, which is determined by:

$$\omega_{cav} = \frac{m\pi c}{n_{cav} L_{cav} \cos(\theta)}, \tag{2.7}$$

m is the number of half wavelength contained in the cavity layer, when there is no phase delay in the DBR.
The reflectivity of the stop band can be very high (0.9999). The DBR acts as a very good mirror for the light in the cavity.

Dispersion curve of the cavity photon mode and effective mass
In a semiconductor microcavity, light that can be transmitted has to fulfill the requirement:

$$\frac{2\pi n_{cav} L_{cav} \cos(\theta)}{\lambda} = N\pi \tag{2.8}$$

where n_{cav} is the refractive index of the cavity; L_{cav} is the effective cavity length; θ is the incident angle of the light in the cavity and λ is the light wavelength.
The energy of the light should be

$$E_{cav} = \hbar ck = \hbar c\sqrt{k_{//}^{\ 2} + k_{\perp}^{\ 2}}, \text{ where } \begin{matrix} k_{\perp} = k\cos(\theta) \\ k_{//} = k\sin(\theta) \end{matrix} \tag{2.9}$$

If we focus the region where $k_{//} << k_{\perp}$, we have

$$E_{cav} \approx \hbar ck_{\perp}(1 + \frac{1}{2}\frac{k_{//}^{\ 2}}{k_{\perp}^{\ 2}}) = \hbar ck_{\perp} + \frac{1}{2}\hbar c\frac{k_{//}^{\ 2}}{k_{\perp}} \tag{2.10}$$

$$k_{\perp} = \frac{N\pi}{n_{cav} L_{cav}} \tag{2.11}$$

So $$E_{cav} = \hbar ck_{\perp} + \frac{1}{2}\hbar c\frac{k_{//}^{\ 2}}{k_{\perp}} = \frac{\hbar c}{n_{cav} L_{cav}} N\pi + \frac{1}{2}\hbar c\frac{n_{cav} L_{cav}}{N\pi} k_{//}^{\ 2} \tag{2.12}$$

If we define $E_{cav} = \frac{\hbar c}{n_{cav} L_{cav}} N\pi$ and $m_{cav} = \frac{\hbar N\pi}{c n_{cav} L_{cav}}$

(2.13-2.14)

Then the cavity mode energy should be

$$E_{cav} = E_{cav}(k = 0) + \frac{1}{2}\frac{\hbar^2}{m_{cav}} k_{//}^{\ 2} \tag{2.15}$$

The cavity photon thus gains effective mass because of the confinement.
The electric field can reach maximum in the cavity layer, as shown in **Figure 2.9**. Compared with the bulk semiconductor and quantum wells, the amplitude of the electric field can be increased a lot (20 times) **[24].** Thus the coupling between the excitons and the cavity photon

modes is greatly enhanced, if the quantum well is inserted at the maximal electric field position.

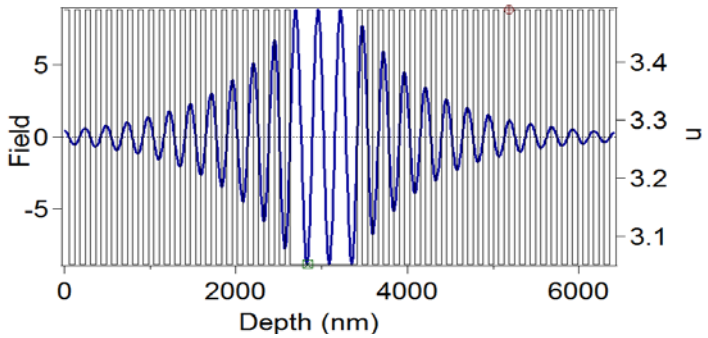

Figure 2.9 Electric field distribution of the light wavelength of the resonance cavity mode in the microcavity.

2.3 Exciton polaritons in semiconductor microcavity

The previous section of microcavity does not contain quantum well. In this thesis, we insert GaAs quantum wells in the microcavity to couple two oscillators: cavity oscillator and exciton oscillator. Depending on the coupling strength with the decay rate of the excitons and out-coupling rate of the cavity photons, we need to discuss weak and strong coupling regime.

Weak coupling and strong coupling

Usually excitons will decay irreversibly by emitting photons (**weak coupling** regime, where the coupling strength between the excitons and the electromagnetic field is small). If the quantum wells are inserted at the maximum of the electric field in the microcavity, **strong coupling** holds when the energy exchange rate is larger than the non-radiative decay rate of the excitons and out-coupling rate of the cavity photons from the cavity (or the Rabi splitting is larger than the exciton and cavity photon linewidth: $\Omega_{rabi} >> \gamma_{ex}, \gamma_{cav}$). To describe the exciton dynamics simply (just approximately), the photon emitted by the exciton will be re-absorbed by the cavity. This activates the exciton again. Such transition occurs periodically, we cannot distinguish between the exciton and the cavity photon. In this case, a new excitation is created, called exciton polaritons, as shown in **Figure 2.10**.

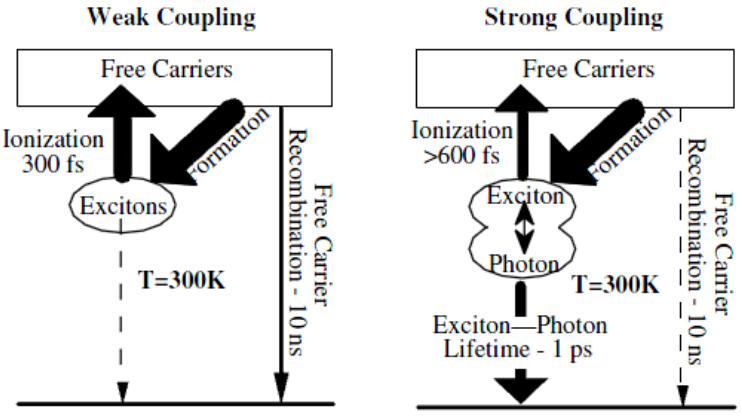

Figure 2.10 Strong coupling and weak coupling in a semiconductor microcavity, reprinted from [30].

Exciton polaritons can be viewed as the superposition of the exciton and cavity photon. They have exciton component and cavity photon component. With the exciton component, the exciton polaritons interact with each other and phonons. This helps polaritons relaxation into lower energy states. With the cavity photon component, the exciton polaritons have a very short lifetime in the 1-10ps range and a very small effective mass. This makes the exciton polaritons to condense at much higher temperature. The short lifetime of the exciton polaritons renders promising application in ultra fast optics.

Because of the translational symmetry along the planar semiconductor microcavity, the excitons interact with the cavity photon with the same in-plane wave vector. In addition, when the exciton polaritons decay, they emit photons while keeping the same in-plane wave vector and energy. We can acknowledge the information of the exciton polaritons by measuring the emitted photons at different angles.

2.3.1 Exciton polariton dispersion and effective mass

Dispersion curve

The total Hamiltonian of the microcavity is:

$$H = \sum_{k_{//}} E_{cav}(k_{//}) a_{k_{//}}^{\dagger\dagger\dagger\dagger} a_{k_{//}} + \sum_{k_{//}} E_{ex}(k_{//}) b_{k_{//}} b_{k_{//}} + \sum_{k_{//}} \hbar\Omega_{rabi}(a_{k_{//}} b_{k_{//}} + b_{k_{//}} a_{k_{//}}) \tag{2.16}$$

where $k_{//}$ is the in-plane wave vector; $E_{cav}(k_{//})$ is the energy of the cavity photon; $E_{ex}(k_{//})$ is the energy of the excitons; $a_{k_{//}}^{\dagger}$ and $a_{k_{//}}$ are the creation and annihilation operator of the cavity photon; $b_{k_{//}}^{\dagger}$ and $b_{k_{//}}$ are the creation and annihilation operator of the exciton; Ω_{rabi} is the Rabi splitting, which is determined by **[28]:**

$$\hbar\Omega_{rabi} \approx 2\hbar\left(\frac{2\Gamma_0 c N_{qw}}{n_{cav} L_{eff}}\right)^{1/2} \tag{2.17}$$

$$\hbar\Gamma_0 = \frac{\pi}{n_{cav}} \frac{e^2}{4\pi\varepsilon_0} \frac{\hbar}{m_e c} f_{ex} \tag{2.18}$$

N_{qw} is the number of the quantum well in the cavity; $\hbar\Gamma_0$ is the radiative width of a free exciton in a quantum well and is proportional to the exciton oscillator strength per unit area f_{ex} **[28].**

This Hamiltonian can be diagonalized into:

$$H = \sum_{k_{//}} E_{lp}(k_{//}) p_{k_{//}}^{\dagger\dagger} p_{k_{//}} + \sum_{k_{//}} E_{up}(k_{//}) q_{k_{//}} q_{k_{//}} \tag{2.19}$$

if we take the following transformation:

$$p_{k_{//}} = X_{k_{//}} b_{k_{//}} + C_{k_{//}} a_{k_{//}}$$
$$q_{k_{//}} = X_{k_{//}} a_{k_{//}} - C_{k_{//}} b_{k_{//}} \quad (2.20)$$

They can be viewed as the new creation and annihilation operator of the eigenmodes of the microcavity, where $X_{k_{//}}$ and $C_{k_{//}}$ are called Hopfield coefficients **[31]**. These new eigenmodes are lower-branch and upper-branch exciton polaritons in a microcavity.

If we do not consider the decay or out-coupling of excitons and cavity photon modes, the energy of the exciton polaritons is:

$$E_{lp}(k_{//}) = \frac{E_{ex}(k_{//}) + E_c(k_{//})}{2} - \frac{1}{2}\sqrt{(E_{ex}(k_{//}) - E_c(k_{//}))^2 + 4\hbar^2\Omega_{rabi}^2}$$
$$E_{up}(k_{//}) = \frac{E_{ex}(k_{//}) + E_c(k_{//})}{2} + \frac{1}{2}\sqrt{(E_{ex}(k_{//}) - E_c(k_{//}))^2 + 4\hbar^2\Omega_{rabi}^2} \quad (2.21)$$

When the wave vector is small, the energy of the lower-branch polaritons and upper-branch polaritons is:

$$E_{lp}(k_{//}) = E_{lp}(k_{//} = 0) + \hbar^2 k_{//}^2 / 2m_{lp}^*$$
$$E_{up}(k_{//}) = E_{up}(k_{//} = 0) + \hbar^2 k_{//}^2 / 2m_{up}^* \quad (2.22)$$

So here the dispersion of exciton polaritons is approximately parabolic; while it behaves dramatically different when the wave vector is increased.

If we define

$$\delta(k_{//}) = E_{ex}(k_{//}) - E_c(k_{//}) \quad (2.23)$$

Then the Hopfield coefficients are:

$$\left|X_{k_{//}}\right|^2 = \frac{1}{2}\left(1 + \frac{\delta(k_{//})}{\sqrt{\delta(k_{//})^2 + 4\hbar^2\Omega_{rabi}^2}}\right), \left|C_{k_{//}}\right|^2 = \frac{1}{2}\left(1 - \frac{\delta(k_{//})}{\sqrt{\delta(k_{//})^2 + 4\hbar^2\Omega_{rabi}^2}}\right) \quad (2.24)$$

$\delta(k_{//} = 0)$ is called detuning between the cavity photon modes and the excitons.

Figure 2.11 plots the dispersion curve of the lower-branch and upper-branch polaritons at different detuning and corresponding Hopfield coefficients.

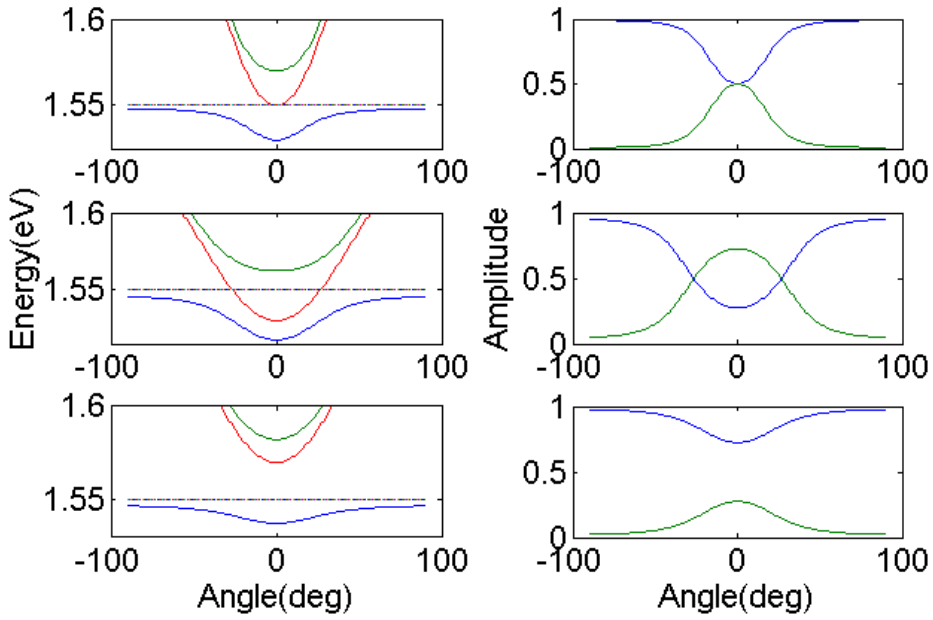

Figure 2.11 Exciton polariton dispersion curve and Hopfield coefficients as a function of angle when the detuning changes (top: zero detuning; middle/bottom: negative and positive detuning).

Figure 2.12 is the energy of lower-branch and upper-branch polaritons as a function of the detuning where the cavity photons is linearly changed while the exciton energy is kept constant. These two branches of polaritons show a clear **anti-crossing** at zero detuning.

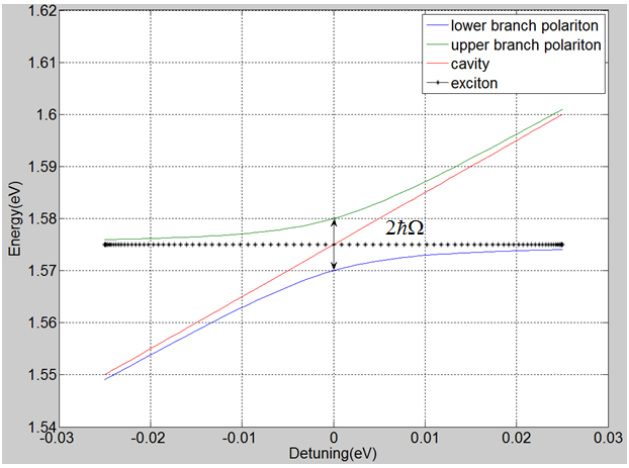

Figure 2.12 Lower branch and upper branch exciton polaritons as a function of detuning. The cavity mode and exciton is also plotted.

Effective mass

The exciton polaritons' effective mass depends strongly on the wave vector because of this specific dispersion curve.

$$m_{lp} = \frac{m_{ex} m_{cav}}{\left|X_{k_{//}}\right|^2 m_{cav} + \left|C_{k_{//}}\right|^2 m_{ex}}$$
$$m_{up} = \frac{m_{ex} m_{cav}}{\left|X_{k_{//}}\right|^2 m_{ex} + \left|C_{k_{//}}\right|^2 m_{cav}} \quad (2.25)$$

It is well known that the effective mass of the cavity photon is much smaller than the excitons, $m_{cav} << m_{ex}$, in the region where $k_{//} \approx 0$,

The effective mass of lower and upper-branch polaritons is

$$m_{lp}(k_{//} \approx 0) \approx \frac{m_{cav}}{\left|C_{k_{//}}\right|^2} \approx 10^{-4} m_{ex} \quad (2.26)$$

$$m_{up}(k_{//} \approx 0) \approx \frac{m_{cav}}{\left|X_{k_{//}}\right|^2} \quad (2.27)$$

At small wave vector region, the effective mass of the lower-branch polaritons is around 4 orders of magnitude smaller than the excitons, or 5 orders of magnitude smaller than the electron mass. At large wave vector region, the effective mass of the lower-branch polaritons increases dramatically to be around the same order of magnitude as the excitons.

2.3.2 Exciton polariton decay

Considering the finite lifetime of the cavity photons and excitons, the energy of the exciton polaritons is as follows:

$$E_{lp}(k_{//}) = \frac{E_{ex}(k_{//}) + E_c(k_{//}) + i(\gamma_{cav} + \gamma_{ex})}{2} - \frac{1}{2}\sqrt{(E_{ex}(k_{//}) - E_c(k_{//}) + i(\gamma_{cav} - \gamma_{ex}))^2 + 4\hbar^2\Omega_{rabi}^2}$$
$$E_{up}(k_{//}) = \frac{E_{ex}(k_{//}) + E_c(k_{//}) + i(\gamma_{cav} + \gamma_{ex})}{2} + \frac{1}{2}\sqrt{(E_{ex}(k_{//}) - E_c(k_{//}) + i(\gamma_{cav} - \gamma_{ex}))^2 + 4\hbar^2\Omega_{rabi}^2} \quad (2.28)$$

where γ_{cav} is the coupling rate of a cavity photon out of the microcavity due to the imperfection of the DBR mirror, γ_{ex} is the non-radiative decay rate of the excitons.

The decay rate of exciton polaritons is directly determined by the excitons and cavity photons.

$$\gamma_{lp} = \left|X_{k_{//}}\right|^2 \gamma_{ex} + \left|C_{k_{//}}\right|^2 \gamma_{cav}$$
$$\gamma_{up} = \left|X_{k_{//}}\right|^2 \gamma_{cav} + \left|C_{k_{//}}\right|^2 \gamma_{ex} \quad (2.29)$$

The lifetime of exciton polaritons mainly depends on the cavity photons because the excitons' lifetime is much longer:

$$\gamma_{lp} \approx \left|C_{k_{//}}\right| \gamma_{cav} \quad (2.30)$$

Usually the relaxation time of exciton polaritons is longer compared with their lifetime. They decay by emitting photons out of the microcavity before relaxing to the ground state. In a high

Q semiconductor microcavity, the lifetime of the cavity photons and exciton polaritons can be greatly increased. Reference **[32]** claims that they realize a semiconductor microcavity with exciton polaritons' lifetime of around 100ps.

2.4 Polariton lasing and condensation

In the introduction part, we have discussed about polariton lasing, which is the spontaneous decay of the polariton condensate from the microcavity. However, at high temperature or high pump power, Rabi splitting is decreased and strong coupling is lost easily. Sometime the transition from strong coupling to weak coupling is not easy to be identified. It is necessary to compare the lasing mechanism in strong coupling regime (polariton lasing) and in weak coupling regime (cavity photon lasing) in view of high similarity between them. In the **Chapter 3**, cavity photon lasing is observed at 70K. In addition, there is no strict Bose Einstein condensation in an infinite two dimensional system. Exciton polaritons experience a KT transition towards superfluity and local condensation. The description of polariton condensation starting from Bose Einstein statistics needs to be discussed here.

2.4.1 Cavity photon lasing and exciton polariton lasing

When a VCSEL is pumped by a laser, the electrons in the valence band are activated into the conduction band. The activated high energy electrons relax to the bottom of the conduction band through incoherent process. Correspondingly, the high energy holes relax to the top of the valence band. This leads to a population inversion: there are more electrons in higher energy states (the bottom of the conduction band) than lower energy states (the top of the valence band). The population inversion and net gain result in amplified coherent light and occurrence of photon lasing, as shown in **Figure 2.13(top).**

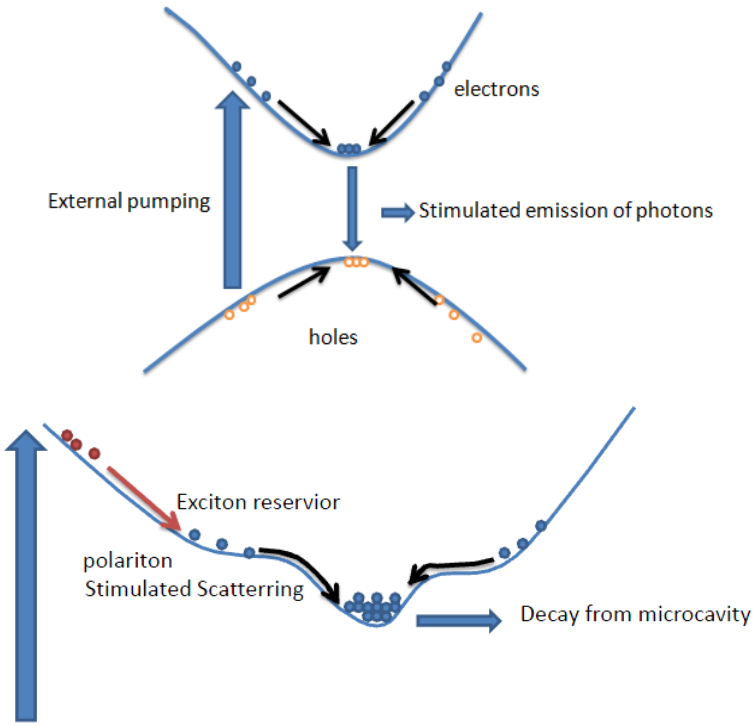

Figure 2.13 Photon lasing (top) and polariton lasing (bottom) in a semiconductor microcavity.

When strong coupling between the excitons and cavity photons holds, it is necessary to treat the microcavity as an ensemble of exciton polaritons. As shown in **Figure 2.13(bottom),** the activated electrons and holes form an exciton reservoir. These high energy excitons relax through scattering with acoustic phonons towards the ground states along their dispersion curve. When the population number at the ground state is larger than unity, stimulated scattering of polaritons occurs (usually exciton-exciton scattering is needed to realize this). The exciton polaritons macroscopically occupy the ground state. The decay of these polaritons by emitting photons out of the microcavity, because of their finite lifetime, is a polariton laser **[5]**. This kind of coherent light does not need population inversion. To make sure polariton lasing occurs, either two thresholds should be observed or polariton dispersion curve should be kept.

2.4.2 Exciton polariton condensation

As discussed before, exciton polaritons do not experience strict Bose Einstein condensation in a microcavity, as alkaline atoms condensate. However, the exciton polariton condensate has many similarities with them [14]. In the following we discuss the Bose statistics of the exciton polaritons in a two dimensional microcavity.

Bose condensate of an ideal Bose gas

As to an ideal Bose gas, the bosons obey the Bose-Einstein distribution function:

$$f_{BE}(E) = \frac{1}{\exp(\frac{E-\mu}{k_B T}) - 1} \tag{2.31}$$

Where E is the energy of a single particle, μ is the chemical potential of the Bose gas, T is the temperature and k_B is Boltzmann constant.

The total particle number of the Bose gas is

$$N = \sum_{allenergylevels} f_{BE}(E) = \sum_{allenergylevels} \frac{1}{\exp(\frac{E-\mu}{k_B T}) - 1}, \tag{2.32}$$

which can be rewritten as:

$$N = f_{BE}(E_0) + \sum_{allexcitedstates} f_{BE}(E_{i\neq 0}) \tag{2.33}$$

The first term is the mean occupation number in the single-particle ground state; the second term is the sum of the mean occupation number in the excited single-particle states of the Bose gas. When the temperature is high, the chemical potential is much lower than E_0, so the mean occupation number in the single-particle state is much less than unity. If the temperature is decreased, the chemical potential is larger. The mean occupation number of the single-particle state is increased. The Bose-Einstein condensation occurs when a large number (macroscopic)

of particles are occupying the ground state, if a critical temperature is reached.
To be strict, the Bose condensate occurs when

$$\lim_{R\to\infty}\frac{N_0}{R^2}=n_0>0 \tag{2.34}$$

Where R is the system size and N_0 is the population number in the ground state.

For a uniform Bose gas in a three dimensional box with volume V, the critical temperature for Bose Einstein condensation is

$$k_B T_c=\frac{2\pi}{[\zeta(3/2)]^{2/3}}\frac{\hbar^2 n^{2/3}}{m} \tag{2.35}$$

where n is the particle density, m is the single particle mass.

Exciton polariton condensate

As to a uniform non-interacting Bose gas in two dimensions, Bose Einstein condensation can only occur at zero temperature **[33]**. Kosterlitz and Thouless predict that there is a phase transition from normal state to a coherent (superfluity) state in a two dimensional system. This phase transition exists at a finite temperature, which is called KT transition temperature T_{KT}.

Above the KT transition temperature, there is only normal state and no superfluity state. Below the KT transition temperature, there are normal state and superfluity state together. The superfluity state number is related to the KT transition temperature as following **[34]**:

$$n_s(T_{KT})=\frac{2m^* k_B T_{TK}}{\pi\hbar^2} \tag{2.36}$$

And the total particle number is the sum of the normal state and superfluity state:

$$n(T)=n_s(T)+n_n(T) \tag{2.37}$$

The KT transition of exciton polaritons allows the appearance of superfluity and local quasi-condensation. From (2.35), the critical temperature is inversely proportional to the mass of the single particle. As to the exciton polaritons, the critical temperature can be greatly increased because the effective mass is much smaller than the alkaline atoms. Bose-Einstein condensation has been claimed to be realized at room temperature in a GaN semiconductor microcavity **[35]**.

2.5 Spin of exciton polariton

Exciton polaritons inherent spin from the exciton component and cavity photon component. We can control the polariton spin by using laser with specific polarization and analyze the spin state of the polaritons by measuring the Stokes parameters of the emitted light from the microcavity. The spin polarization dynamics is governed by the effective magnetic field generated by the TE-TM mode splitting in microcavity. In the **Chapter 5**, spin dynamics is investigated in a microcavity ridge. We will discuss the pseudospin vector formula and TE-TM mode splitting in the following section. (Here we say polarization of polaritons which means

the polarization of the emitted light by the polaritons)

2.5.1 Pseudospin vector formula for exciton polariton

For excitons in quantum well, Bir-Aronov-Pikus mechanism dominates the spin relaxation **[18]**. The exciton's dark states are usually neglected. The exciton polaritons in a planar microcavity can be seen as a two level system. Pseudospin is introduced to describe the polaritons in microcavity **[18]:**

$$\rho_k = N_k[I/2 + \vec{S}_k \bullet \vec{\sigma}_k] \tag{2.38}$$

Where $\vec{S}_k$ is the pseudospin of the exciton polaritons; $\vec{\sigma}_k$ is the three Pauli matrix; N_k is the number of the exciton polaritons; k is the in-plane wave vector. The in-plane component of the pseudospin vector S_k is used to analyze the in-plane dipole moment orientation of the exciton polaritons; while the out-of-plane component S_k describes the polariton spin projection onto the growth direction.

The pseudospin vector of the exciton polaritons can be described by a Poincare sphere in **Figure 2.14**. The North and South poles of the Poincare sphere represent the right-hand circularly polarized and left-hand circularly polarized state. The linearly polarized state is located at the equator of the sphere. For example, the linearly horizontal polarization lies at (1, 0, 0) on the sphere, the linearly vertical polarization appears at (-1, 0, 0) on the sphere (here the circular polarized or linear polarized state means the light polarization emitted by the polaritons, and we note points (1,0,0) or (-1,0,0) means the coherent state which's pseudospin S_x =1/2 or -1/2).

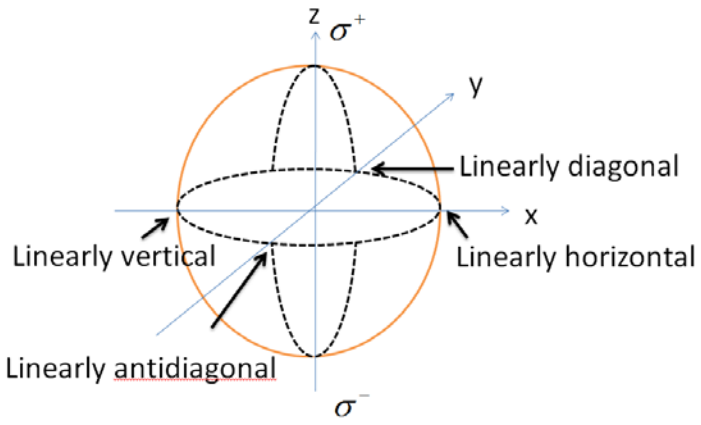

Figure 2.14 Poincare sphere representing the pseudospin vector of the exciton polaritons and polarization of emitted light by the polaritons.

Ideally, when right hand circularly polarized light is focused onto the semiconductor microcavity, the exciton polaritons with the spin projection onto the growth axis of +1 will be

excited. Linearly polarized light excites the exciton polaritons with spin projection +1 and -1, the total spin projection is zero. The polarization of the light emitted by the microcavity can be analyzed by Stokes parameters, which is calculated by the following formula:

$$S_x = \frac{I_{horizontal} - I_{vertical}}{I_{horizontal} + I_{vertical}}, S_y = \frac{I_{diagonal} - I_{antidiagonal}}{I_{diagonal} + I_{antidiagonal}}, S_z = \frac{I_{right-hand} - I_{left-hand}}{I_{right-hand} + I_{left-hand}} \quad (2.39)$$

$S_x = \pm 1$ corresponds to horizontal or vertical linearly polarization; $S_y = \pm 1$ represents diagonal or anti-diagonal linearly polarization and $S_z = \pm 1$ describes right-hand circularly or left-hand circularly polarized states.

2.5.2 TE-TM mode splitting in semiconductor microcavity

Depending on the orientation of the exciton's wave vector with its polarization field, there is an energy splitting called Longitudinal-Transverse Splitting or TE-TM mode splitting **[36].** To simply express, the TE-TM mode splitting of a 1s heavy hole exciton in a quantum well is **[36]**:

$$E_{TE-TM} \approx (3/16)\Delta^{3D}_{TE-TM} |< \chi_{e1} | \chi_{h1} >|^2 (E_B^{2D} / E_B^{3D})^2 a_B^{3D} k \quad (2.40)$$

Where Δ^{3D}_{TE-TM} is the TE-TM mode splitting in a bulk semiconductor material; χ_{e1}, χ_{h1} are the electron and hole envelope function; $E_B^{2D}, E_B^{3D}, a_B^{3D}$ are the exciton binding energy in 2 dimensional, 3 dimensional semiconductor and the Bohr radius. This splitting increases linearly with the exciton's wave vector. There is no splitting when the wave vector is zero.
TE-TM mode splitting also exists in an empty microcavity with an incident angle θ **[29]**:

$$\omega^{TE}(\theta) - \omega^{TM}(\theta) \approx \frac{L_{cav} L_{DBR}}{(L_{cav} + L_{DBR})^2} \frac{2\cos(\theta_{eff})\sin(\theta_{eff})}{1 - 2\sin^2(\theta_{eff})} \delta \quad (2.41)$$

$$\theta_{eff} \approx \arcsin \frac{n_0}{n_{cav}} \sin(\theta) \quad (2.42)$$

Where δ is the energy difference between the cavity mode and the center of the stop band. The TE-TM modes splitting for the cavity mode vanishes at normal incidence.
The TE-TM mode splitting of polaritons in a microcavity can be expressed simply as **[18]**:

$$E_{TE-TM}(k) = | X_k |^2 E_{ex}(k) + | C_k |^2 E_{cav}(k) \quad (2.43)$$

Where $| X_k |, | C_k |$ are Hopfield coefficients and $E_{ex}(k), E_{cav}(k)$ are TE-TM mode splitting for the excitons and cavity photon mode, respectively. In general it is larger when the wave vector increases. However, the TE-TM mode splitting is not monotonic with the wave vector at specific detuning **[18].** As the same as the excitons in quantum well **[36]**, the TE-TM mode splitting generates an effective magnetic field which leads to spin flip. The pointing direction of the effective magnetic field caused by the TE-TM mode splitting lies in the planar microcavity plane, as following **[36]**,

$$\vec{\Omega}_{eff}(\vec{k}) \propto \cos(2\theta)\,\vec{i} + \sin(2\theta)\,\vec{j} \tag{2.44}$$

The effective magnetic field points at an angle of 2θ, where θ is the pointing direction of the in-plane wave vector, as shown in **Figure 2.15.**

Due to the effective magnetic field, the pseudospin vector dynamic of the exciton polaritons is (the exchange field due to population number difference in different spin polarization and the anisotropic polariton-polariton interaction is ignored here):

$$\frac{d\vec{S}_k}{dt} = [\vec{S}_k \times \vec{\Omega}_{eff}(k)] \tag{2.45}$$

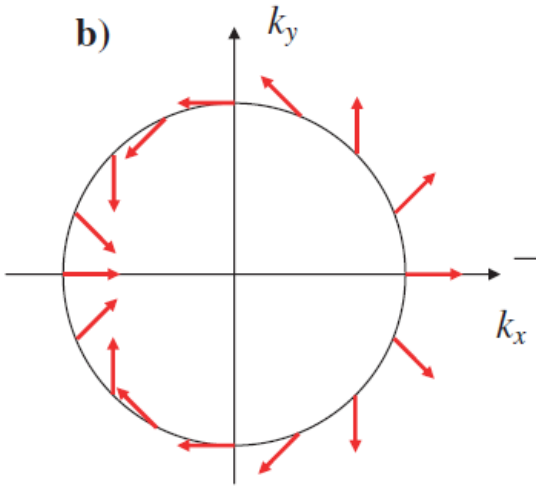

Figure 2.15 The pointing direction of the effective magnetic field changes with the wave vector of the polaritons, the arrows indicate the pointing direction of the effective magnetic field. Reprinted from [16]

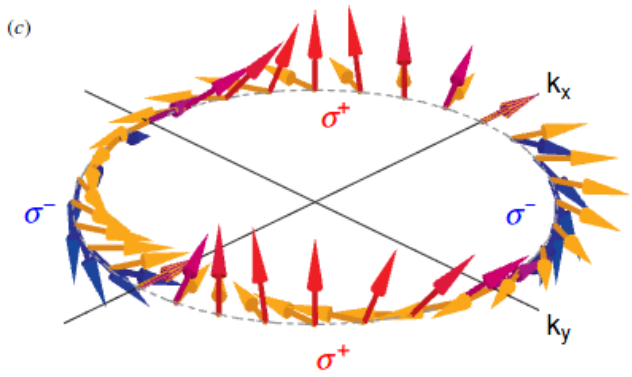

Figure 2.16 The rotation of the polarization of an exciton polariton will depend on the wave vector of the polaritons, so the polarization of the polariton will change from linear polarization to circular polarization if the initial polarization is linear and pointing along the kx. Reprinted from [18]

This effective magnetic field rotates the polarization of exciton polaritons very complexly. For example, in **Figure 2.16,** an initially linear polarized polariton will become right-hand circular polarized or left-hand circular polarized when it is scattered elastically in a ring in momentum

space.

There are other contributions to the effective magnetic field from the structure of the microcavity **[18]**. The absence of cylindrical symmetry along the growth direction leads to an additional in-plane magnetic field. This kind of magnetic field points in a direction which is fixed along a specific angle. It still exists when the wave vector is zero.

Although the effective magnetic field causes big influence on the dynamics of the polaritons, however, it is only valid when the density is low. If the population density is large such that exciton-exciton interaction cannot be ignored, the scattering intensity between the excitons (and polaritons) with the same spin polarization is much larger than the excitons with the opposite spin polarization. Based on this interaction difference, a spin switch has been realized by reference **[19]**.

2.6 Summary

The basics of exciton polaritons in semiconductor microcavity are discussed in this Chapter. Exciton polaritons, result from strong coupling between excitons and cavity photons, provide an excellent platform to study condensation and lasing. When stimulated scattering occurs, exciton polaritons show a phase (KT) transition. In this Chapter, polariton lasing and photon lasing is compared, in view of high similarity between them. Finally, the effective magnetic field generated by the TE-TM mode splitting is discussed. The spin polarization of the exciton polaritons is described by using pseudospin vector formula.

Chapter 3

Polariton lasing in planar microcavity and micropillars

3.1 Introduction

In the **Chapter 2** we have discussed about polariton lasing. Compared with common photon lasing, polariton lasing does not need population inversion and has a smaller threshold. GaAs based microcavity is very promising to realize an electrically pumped polariton lasing due to very well developed growth and fabrication techniques. Although it is claimed that an electrical injected polariton laser has been realized, however, they need to use magnetic field to enhance the coupling strength in the microcavity.

Among the work about GaAs based microcavity which includes the observation of polariton condensation in reference **[37]** injected resonantly at large angle, polariton lasing in reference **[8]** by non-resonant pumping and Bose condensation by using stress-tuning method **[38],** there is still necessity to compare polariton lasing and photon lasing when temperature and detuning is changed. Especially temperature dependent polariton lasing threshold is needed, in view of the fact that the critical density of polariton condensate increases monotonically with temperature in equilibrium or quasi-equilibrium regime. In this case, polariton lasing threshold increases with temperature. In this chapter our research fulfills this gap. We realize exciton polariton lasing in a similar GaAs microcavity as reference **[8]**. Both polariton lasing in a planar microcavity and micropillars are discussed. Polariton lasing in planar microcavity at low temperature and photon lasing at high temperature are compared. We find a linear increase of polariton lasing threshold in a micropillar. This shows the same trend of the critical density of the polariton condensate in the temperature range investigated.

3.2 Sample

Figure 3.1(left) shows the structure of the microcavity. 4 sets of 3 GaAs quantum wells are inserted at the antinodes of the electric field inside the 2.5λ cavity. The DBR consists of alternative AlAs and Al0.15Ga0.85As layers with the thickness of a quarter light wavelength in the cavity. The bottom DBR is gown on a GaAs substrate. The top DBR and the bottom DBR are not doped.**Figure 3.1(right)** is the SEM imaging of the cross section of the semiconductor microcavity. The interface is very smooth and the microcavity is grown with a very high quality.

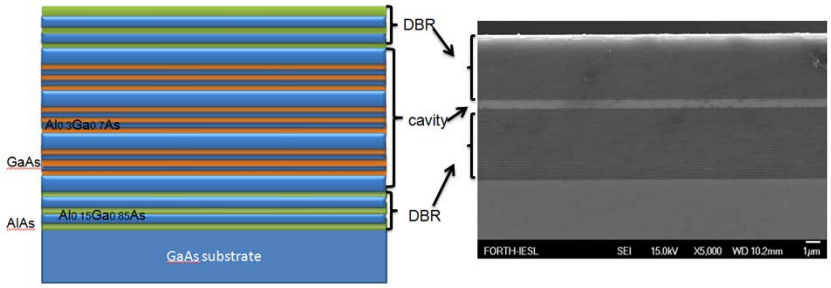

Figure 3.1 Left: structure of the semiconductor microcavity used in experiment, the thickness of the DBR and cavity is not in real scale, just to see the details of the cavity. Right: SEM imaging of the cross section of the microcavity.

Figure 3.2 is the simulated electric field distribution in the microcavity for light wavelength of around 802 nm. The maximal electric filed is located at the position where the quantum wells are inserted. This promises maximal coupling between the excitons in quantum wells and the cavity photon modes. At each maximal electric field position, three quantum wells are used. With this, the total exciton density can be distributed within 12 quantum wells. The effective exciton density for each quantum well is greatly reduced **[39]**. The large number of the quantum well also increases the Rabi splitting of the microcavity.

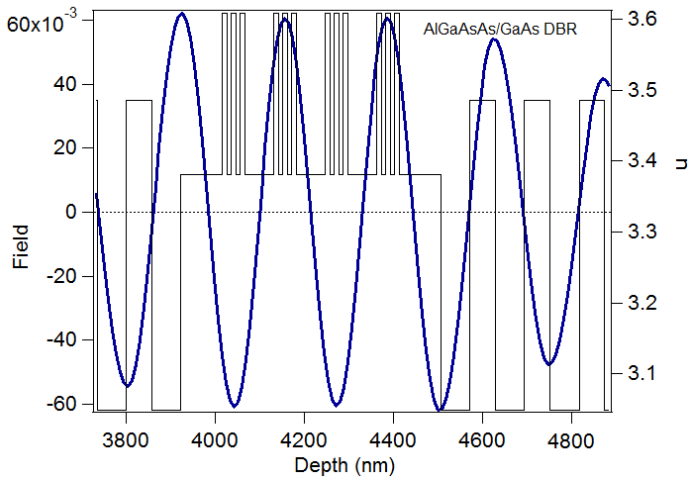

Figure 3.2 The Refractive index and electric field distribution in the high Q microcavity.

The simulated polariton modes are shown in **Figure 3.3(left)**. The enlarged graph of the polariton modes can be found in **Figure 3.3(right).** The experimental reflectivity and simulated one agree very well.

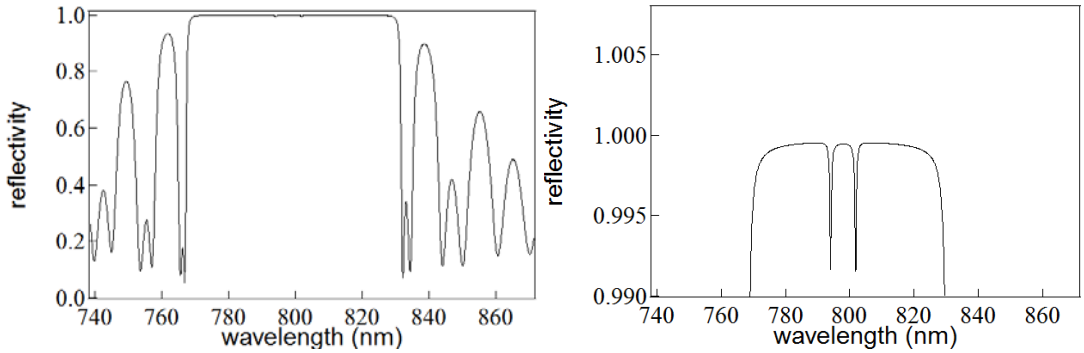

Figure 3.3 Left: Reflectivity of the semiconductor microcavity; right: Enlarged graph of the stop band of the microcavity.

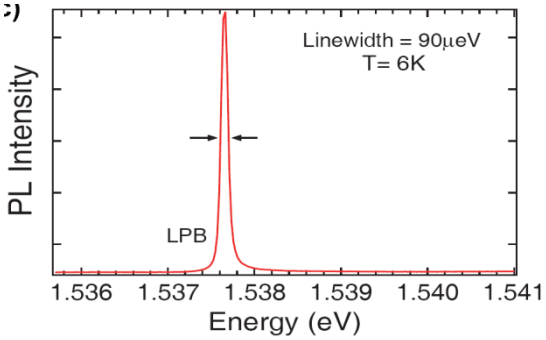

Figure 3.4 Low-branch polariton emission at 6K (taken at Univ. Southampton)

Figure 3.4 shows the low-branch polariton emission at 6K with a large negative detuning, which can be used to estimate the Q factor of the microcavity. From Figure 3.4, we find the Q factor is around 16,000 and the lifetime of the cavity photon is around 18-20 ps.

Figure 3.5 demonstrates angle resolved PL and corresponding lower-branch polaritons and upper-branch polaritons energy with angle taken at around 20K. The microcavity' Rabi splitting is around 9 meV.

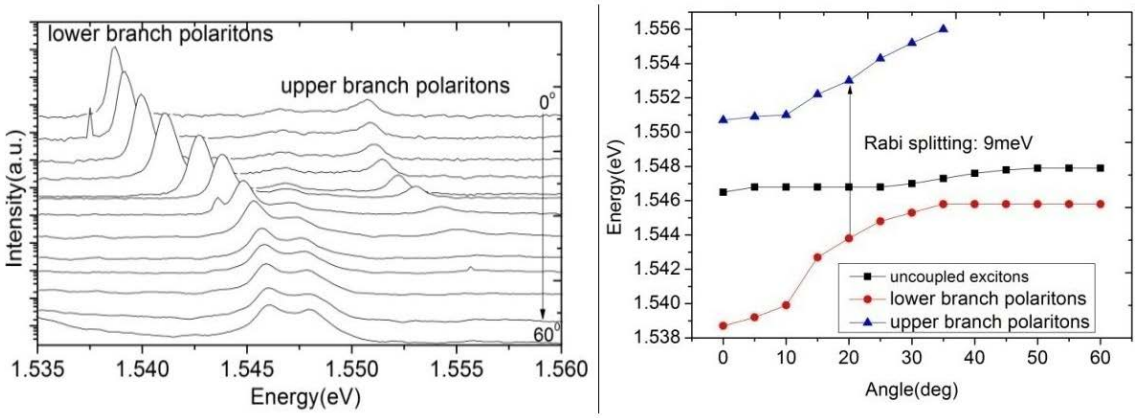

Figure 3.5 Left: angle-resolved PL taken at ultralow power, the spectra is shifted for clarity; right: measured lower-branch and upper-branch polariton energy as a function of angle.

3.3 Setup

The setup used in the experiment can be found in **Figure 3.6**. The sample is placed in a cold cryostat which can cool the sample to around 20K. The pump laser is a continuous wave Ti:Sapphire laser, which is focused onto the sample by using an objective. The objective's magnification is 50 times. It has a working distance of 13 mm. The magnification of the objective makes sure to see the surface of the sample clearly. The wavelength of the laser is tuned at around the first minimum of the reflectivity above the microcavity's stop band, to guarantee high absorption. The laser is chopped by using a mechanical chopper to reduce the heating. The spot onto the sample is around 2-5 microns. The emitted light from the sample is collimated by the same objective and sent to the spectrometer with additional lens. A combination of two lens in **Figure 3.6** are used to put the Fourier plane onto the slit of the spectrometer.

When investigating the micropillars, a white light is shined onto the sample. The reflected

white light is send to a thorlabs CCD camera, which can be found in the **box a** in **Figure 3.6.** A lens in **box b** with a focus length of 5 cm is used to focus the real space imaging onto the CCD camera. In the experiment, we can move the cryostat in 2 directions and monitor the position of the laser spot onto the sample.

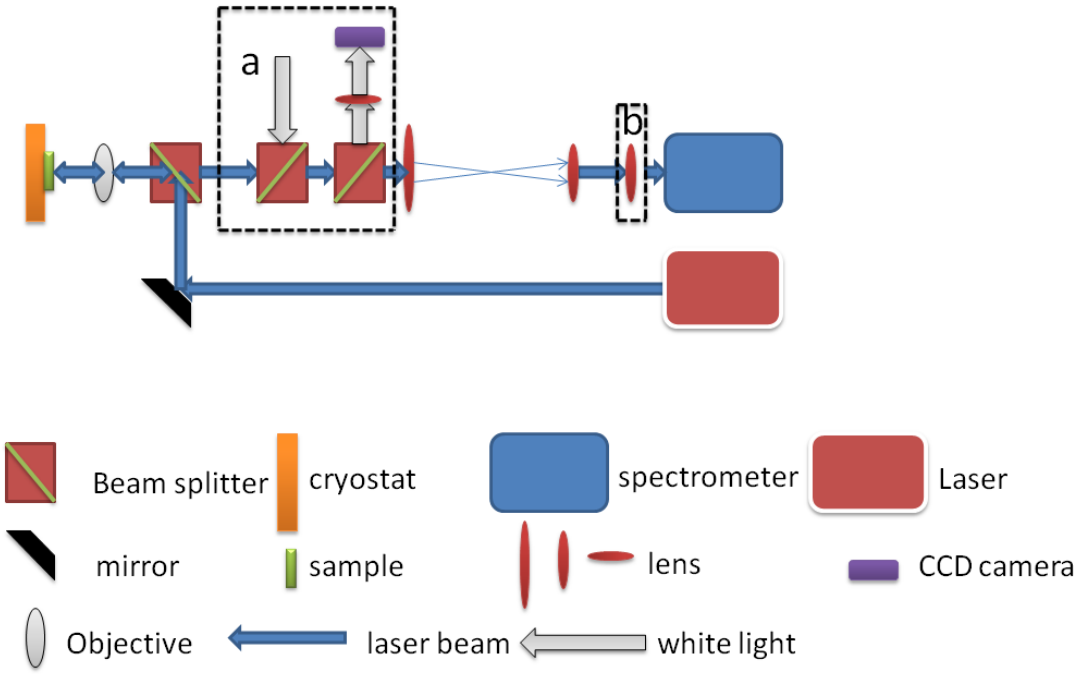

Figure 3.6 Experimental setup for the momentum space imaging, the box a indicates the optics for micro PL experiment, where white light is used to shine the surface of the sample, the lens in box b is used to take real space imaging.

3.4 Polariton lasing in planar microcavity

3.4.1 Bottle-neck effect and high Q microcavity

As bosons, exciton polaritons can condense into the ground states when the mean occupation number reaches unity. This is only observed recently, like in reference **[37]**. The reason is due to the bottle-neck effect. It occurs because the relaxation time of exciton polaritons is larger than their lifetime. Most of exciton polaritons decay at the bottle-neck region (where the polariton density of states decreases greatly) before relaxing further to the ground states, as shown in **Figure 3.7**. If the laser power is increased further, the exciton is approaching the Mott density, strong coupling is lost **[6]**.

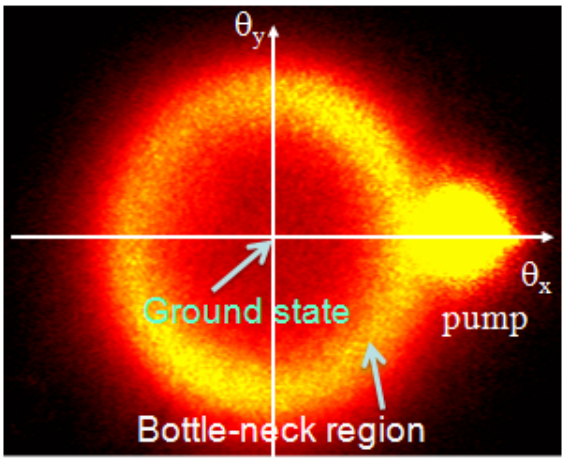

Figure 3.7 Momentum Space imaging with both the pump and polariton emission ring, reprinted from **[4]**

The bottle-neck effect can be avoided in the semiconductor microcavity which has larger saturation density **[14]**. The pump power could be high enough to fasten the relaxation process by exciton-exciton scattering in the strong coupling regime. Another way is to optimize the cavity quality that makes the cavity photons and polaritons lifetime longer. The polaritons relax to the ground state before they decay out of the microcavity **[8]**. The following is about the polariton lasing through the second method.

3.4.2 Polariton lasing in planar microcavity

Figure 3.8 shows the polariton lasing in a high Q planar GaAs microcavity at 20K.

At low power, the excitons formed by a non-resonant pump laser firstly scatter with LO phonons very quickly (100fs). A population of excitons with large wave vector and high energy is formed called an exciton reservoir. Then they experience a slower relaxation along the exciton polariton dispersion curve with acoustic phonons. Now we just observe the emission from the lower-branch polaritons which occupy the states that have a mean population number much smaller than unity, in **Figure 3.8(left)**.

When the pump power is increased, the relaxation becomes faster due to the physical processes such as exciton-exciton scattering. When the population number of low energy states is increased to unity, polariton lasing occurs, as shown in **Figure 3.8(right)**. The lasing energy is far away from the cavity photon mode. This shows that we see unambiguously a polariton laser.

The polariton lasing occurs accompanied by the superlinear increase of the integrated intensity of the emitted light from the microcavity with the pump power, as in **Figure 3.9**. The nonlinearity starts at around 10mW, which is the threshold power. The integrated intensity of the emitted light increases linearly, with the pump power below and above the threshold. In **Figure 3.9**, the linewidth of the emitted light decreases greatly from 1.6 meV to 0.5 meV near the threshold. When the power is increased further, the linewidth becomes larger because of polariton-polariton interaction in the condensate or polariton-exciton reservoir interaction.

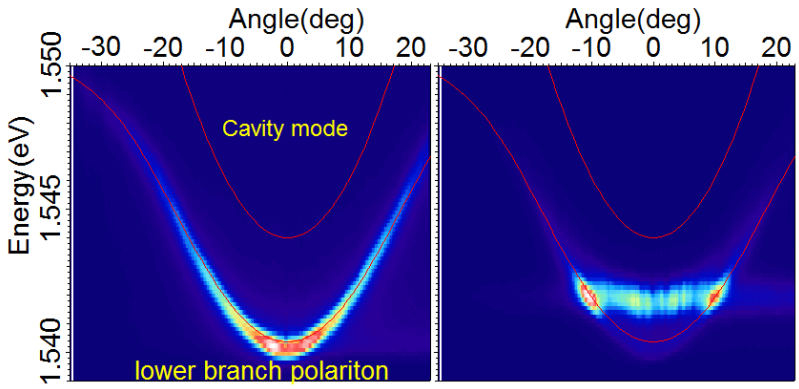

Figure 3.8 Energy vs angle imaging when the power is below threshold (left) and above threshold (right)

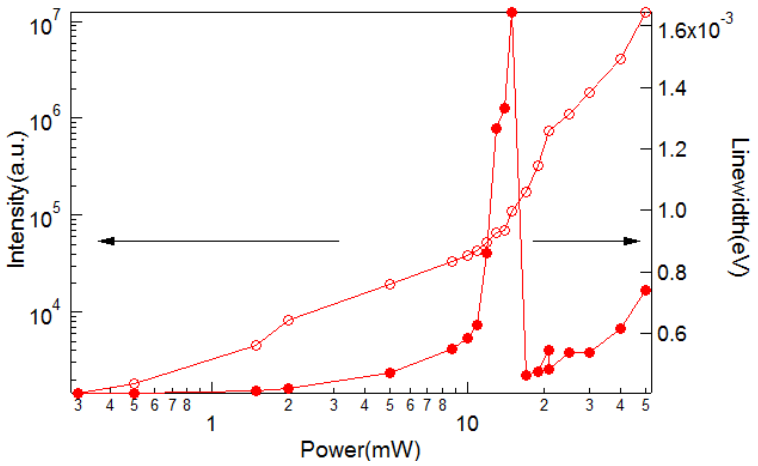

Figure 3.9 Left: integrated intensity of the light as a function of pump power; Right: linewidth of the emitted light as a function of pump power

Above the threshold, we find polariton lasing occurs at high-k states, shown in **Figure 3.8(right)**. This is caused by strong interaction between polaritons in the condensate or polariton-exciton reservoir interaction. This strong interaction is larger especially when a small pump spot is used **[14]**, where the relaxation into the ground state is hindered. The macroscopic occupation of the polaritons into the ground state can be realized when a large spot (25 micrometers) is employed.

To conclude, polariton lasing is observed in a planar microcavity at 20K. The nonlinear increase of the integrated intensity of the emitted light, the decrease of the linewidth confirm the occurrence of polariton lasing.

3.4.3 Photon lasing at high temperature

The necessity to increase temperature

The final goal of polariton laser should be to occur at room temperature and find real application in industry. When the temperature is increased, the oscillator strength and the Rabi splitting are reduced. Strong coupling in microcavity could be lost at lower pump power (higher pump power also reduces Rabi splitting). It is necessary to check whether polariton lasing is still observed or not at higher temperature such as 70K.

Results and discussion

From **Figure 3.10,** the integrated intensity of the light from the microcavity shows a clear nonlinearity with the pump power. A kind of lasing occurs at around 30mW.

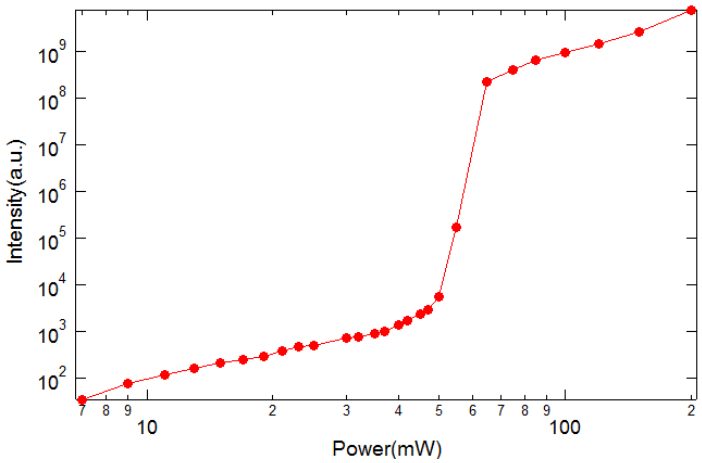

Figure 3.10 Integrated intensity of PL as a function of pump power at 70K.

To make clear it is polariton lasing or photon lasing, momentum space imaging is needed to take. In the following I measure the angle-resolved spectra and plot them together in **Figure 3.11.** When the pump power is small, the microcavity is still in the strong coupling regime. Now light hole exciton is also included to the coupling with the cavity photons. We observe lower-branch, middle-branch and upper-branch polaritons. However, strong coupling is lost when the pump power is just above the threshold. We find that the lasing energy follows the cavity mode, as shown in **Figure 3.11(middle).** When the power is increased further, the lasing occurring at the cavity mode is clearer. At this power we do not observe the emission from lower-branch polaritons. Surprisingly, the photon lasing threshold is not much larger than the polariton lasing threshold at low temperature (30mW vs 10mW, in reference **[38]**, the threshold changes by around 1 order of magnitude).

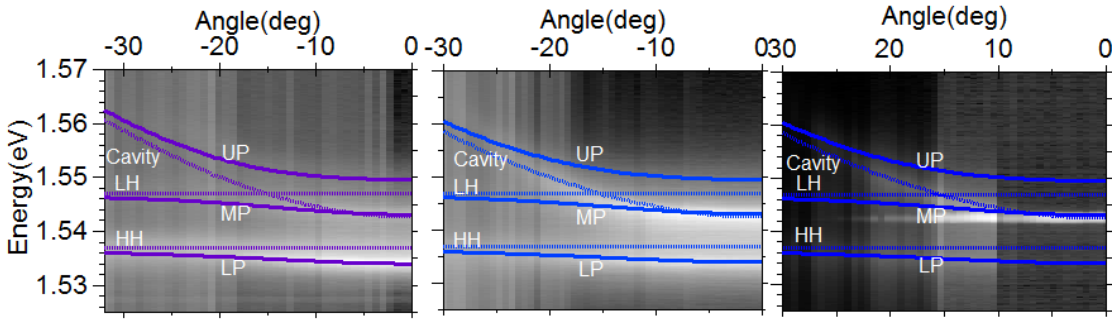

Figure 3.11 Energy vs angle imaging below threshold (left), just at threshold (middle) and above threshold (right)

Discussion about whether middle-branch polariton lasing

In **Figure 3.11(middle),** the lower-branch polariton is still visible. It seems that the middle-branch polariton is lasing. This should not be true. The appearance of the emission from the lower-branch polaritons when lasing occurs cannot be seen as the evidence that strong coupling regime is kept. In fact, the emission of the lower-branch polaritons comes from the outer region of the pump spot where strong coupling still exists. But strong coupling is lost in the center of the pump spot, where weak coupling lasing occurs. This is more obvious when the pump spot is not homogeneously distributed. Usually we can put a pin-hole with diameter of 50 micrometers in the real space imaging plane of the pump spot, to choose a specific small area (several micrometers depending on the lens and objective used) that truly reveals the coupling between the excitons and the cavity photons.

Compare photon lasing and polariton lasing

The photon lasing looks very like the polariton lasing. Especially in a similar structure like a VCSEL, we could also observe a threshold behavior of the integrated intensity of the emitted light from the cavity with the pump power, the decrease of the linewidth at threshold, even the increase of the spatial order when cavity photon lasing occurs **[41]**. In a paper from reference **[40],** they claim that even in a microcavity that has a large Rabi splitting, a small blue-shift above lasing threshold does not guarantee that it is in the strong coupling regime.

To make a systematic investigation of polariton lasing at low temperature and photon lasing at high temperature, we compare the polariton lasing or photon lasing when the detuning is changed. The lower-branch polaritons, HH excitons, LH excitons, cavity modes and polariton or photon lasing energy are plotted with the detuning (now the detuning is defined by the energy difference between the cavity mode and HH excitons). When strong coupling lasing occurs, there should be a rigid blue-shift of the dispersion curve of the polaritons; while as the photon lasing energy should just follow the cavity photon mode. The result is summarized in **Figure 3.12** and **Figure 3.13.**

From **Figure 3.12** it shows that the lasing energy at 70K is very close to the cavity mode at low power. Considering the changes in the refractive index of the microcavity when the pump power is very high, the renormalized cavity mode is red-shifted **[40].** The difference between the lasing energy and the cavity mode at high power is even smaller and can be ignored. We could say that lasing just occurs at the renormalized cavity mode. In addition, the lasing energy at some positive detuning (larger than 2meV) is higher than the un-coupled excitons. This is direct evidence that we observe clearly the cavity photon lasing.

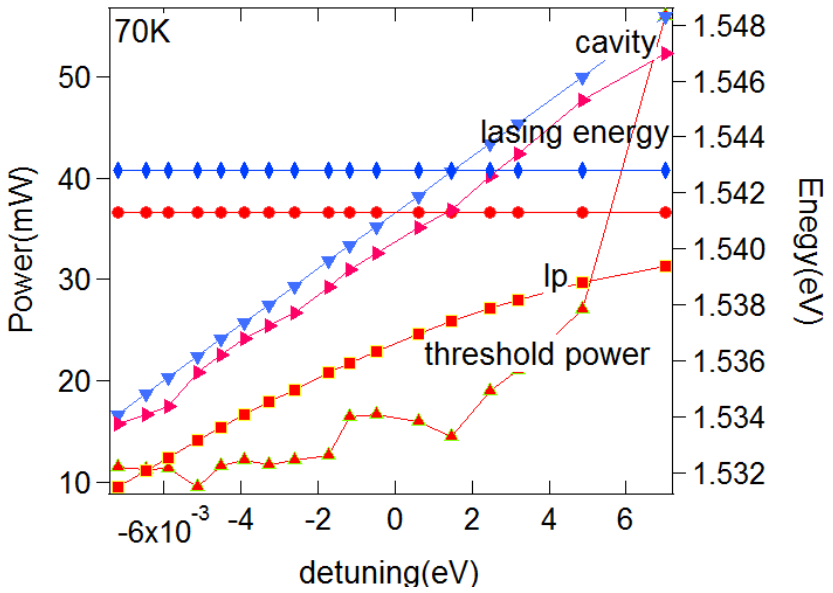

Figure 3.12 Cavity mode, low power lower-branch polariton, lasing peaks and threshold power as a function of detuning at 70K.

It is different when the temperature is at 24K, in **Figure 3.13.** The lasing energy is far from the cavity mode when the detuning is changed. There is a rigid blueshift of the lasing energy from the small power lower-branch polaritons. We find that the lasing energy never goes beyond the un-coupled excitons, not like the case at 70K.

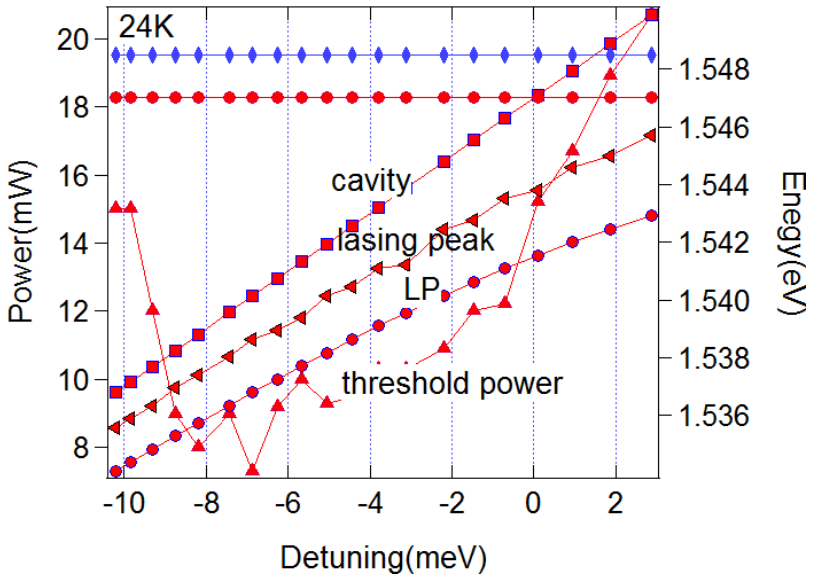

Figure 3.13 Cavity, low-power lower branch polaritons, lasing peaks and threshold power as a function of detuning at 24K.

In the strong coupling regime, the polariton lasing threshold is minimal at around -7meV. The reason why this occurs can be seen in the work of micropillars later.

To conclude, clear photon lasing is observed at 70K. The comparison between the photon lasing and polariton lasing undoubtedly demonstrates different coupling in the microcavity.

However, more work should be continued. The most convincing evidence should be that strong coupling is lost when the pump power is much larger than the polariton lasing threshold. Then a second lasing occurs when the power is increased further than the weak coupling lasing threshold, like the work performed by reference **[42].** A second threshold is also observed in our group. This is the convincing evidence that strong coupling is lost and photon lasing occurs.

3.5 Polariton lasing in micropillars

3.5.1 Observation of polariton lasing in micropillars

The importance of micropillars

The micropillar structure can be used in electrically injected exciton polariton devices such as polariton LED and LD. To explore the possibility of electrical pumped polariton devices, it is necessary to investigate polariton dynamics in micropillars by using optical method. The lateral confinement in micropillars enhances polariton relaxation and thermalization, which could reduce the polariton lasing threshold.

The micropillars

The micropillars are etched in FORTH/IESL, which can be seen in **Figure 3.14.** From **Figure 3.14(right)**, the micropillar has smooth surface and clear steep slope. The etching material is just the top DBR, the quantum wells are exposed to the air. To decrease the emission from these quantum wells, a layer of gold is deposited onto the etched surface.

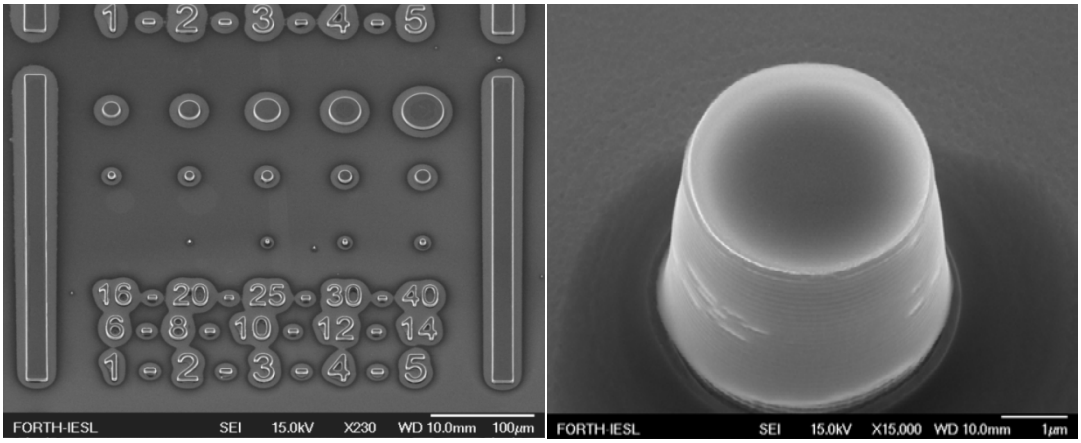

Figure 3.14 Left: SEM of the etched micropillars and ridges. Right: SEM imaging of a single micropillar with diameter of 2 micrometers.

Results and discussion

In the experiment, several pillars are investigated with the diameter of 6, 8, 12, 16, 25 and 40 micrometers. In **Figure 3.15(top),** we find that the dispersion curve of exciton polaritons changes when the micropillar diameter varies. As to smaller pillars with the diameter of 6 micrometers, the dispersion curve transits to discrete levels, as shown in **Figure 3.15(top 1).** This is consistent with the expectation that the lateral confinement makes the 2D exciton polaritons to become 0D particles. When the pillar size increases, the confinement is weaker, the discrete levels transform into continuous curves. In addition, the energy of the lower-branch

polaritons at normal incidence decreases when the pillar size is smaller. This is opposite to other research which shows the cavity mode should be blueshifted. The reason should be that the detuning variance is large in this set of micropillars (in perfect condition, the detuning difference should be very small to be ignored, but some detuning changing inhomogeneous region exists here).

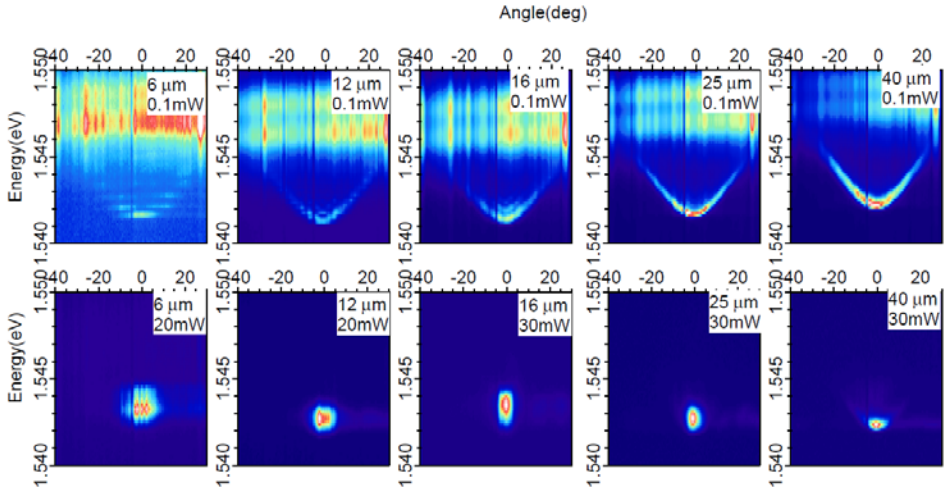

Figure 3.15 (top) Energy vs angle imaging of exciton polaritons at low power of different micropillars; (bottom) Energy vs angle imaging of exciton polaritons at high power of different micropillars

Polariton lasing is observed in a large variety of micropillars, as shown in **Figure 3.15(bottom).** **Figure 3.16** shows the integrated intensity of the emitted light from the microcavity as a function of pump power. We find that the threshold of the polariton laser is smaller when the pillar size decreases.

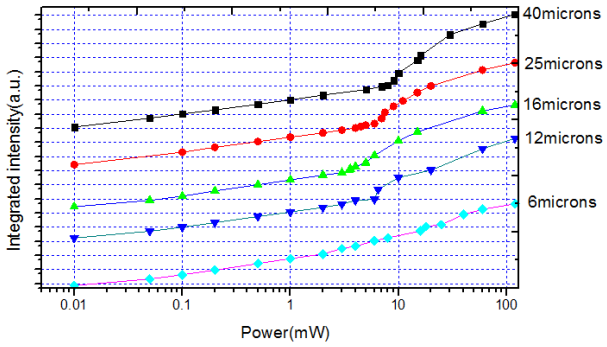

Figure 3.16 Integrated intensity of the emitted light from the microcavity with the pump power of different micropillars, the detuning is -2meV.

Relaxation dynamics in micropillars

In the planar microcavity, we find the polariton lasing occurs at high k states rather than the ground state (in this thesis, we always use a small pump spot). When the exciton polaritons are confined in a micropillar, the lasing behavior is different as following:

(1) Lasing at high k state and relaxing to the ground state

In the pillars with the diameter of 40 micrometers, the polariton lasing first occurs at high k states. Then the lasing polaritons relax to the ground state with further increasing the power, as shown in **Figure 3.17.** This has been observed by reference **[43]**. They find polariton lasing

firstly at high-energy states, then the lasing polaritons transit to the ground states at higher power. They use a theoretical model to simulate the dynamic transition between these two lasing states by including exciton-exciton interaction or polariton-polariton interaction. Our experiment uses a much larger pillar (40 micrometers vs 4-5micrometers), and we observe more clearly the transition process.

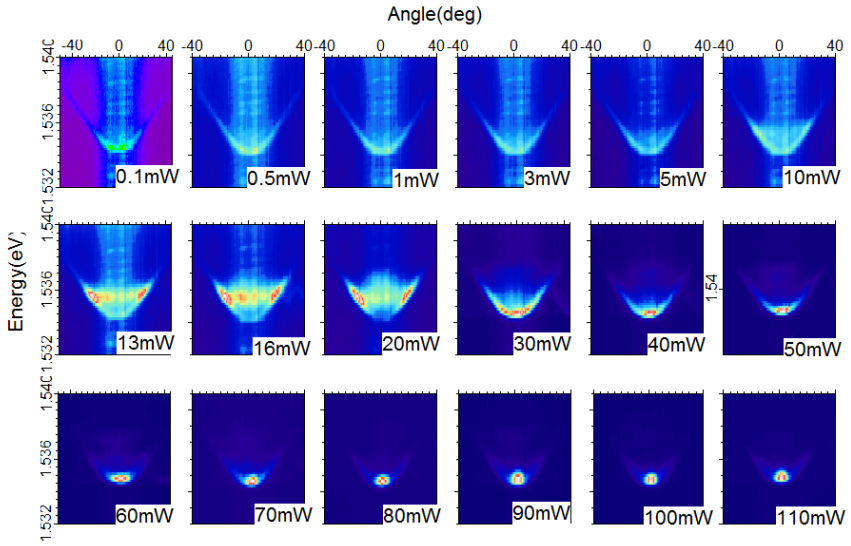

Figure 3.17 Energy vs angle imaging as a function of pump power, the lasing occurs firstly at high k states while moves to the ground states with increasing power.

(2) Polariton lasing directly at the ground state

In the smaller micropillars with more positive detuning, polariton lasing occurs directly at ground state, as shown in **Figure 3.18.** (The two horizontal lines correspond to un-coupled excitons in the microcavity, whose intensity is very low when stimulated scattering of polaritons occurs.) As mentioned before, the confinement in the micropillars fastens the polariton-polariton interaction or polariton -exciton reservoir interaction, which enhances relaxation into the ground state and overcomes the bottle-neck effect.

Through (1) and (2), it is clear that the micropillars have stronger confinement and allow faster relaxation process.

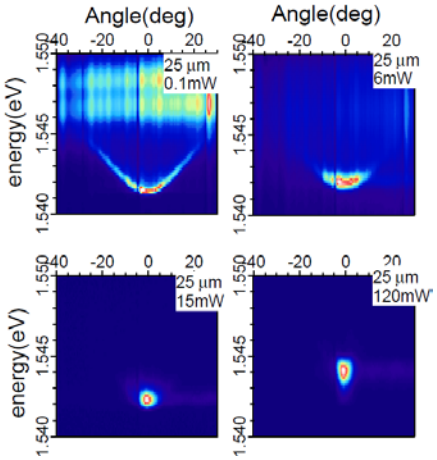

Figure 3.18 Energy vs angle imaging below threshold (0.1mW) and above threshold (6, 15 and 120mW), the pillar size is 25microns.

In addition, we observe in **Figure 3.18** that the lasing energy has blueshift when the pump power is increased further due to polariton-polariton interaction. This is consistent with the result of the planar microcavity.
To summarize, the above result clearly confirms that the confinement in micropillars enhances the relaxation of the exciton polaritons and attenuates the polariton lasing threshold.

3.5.2 Polariton lasing threshold changes with the pillar size and detuning

In **Figure 3.16**, we have found that the polariton lasing threshold is smaller when the pillar size decreases at detuning of -2 meV. **Similar work should be continued at other detuning.** The lateral confinement in micropillars modulates the cavity photon dispersion. With changing detuning, we can investigate how the confinement affects the cavity mode and polariton lasing threshold.

Results and discussion

In **Figure 3.19,** we compare the thresholds of polariton lasing of different pillars when the detuning is changed. (The detuning is varied when different sets of micropillars are chosen, where the detuning difference between the micropillars in one set can be ignored here.)

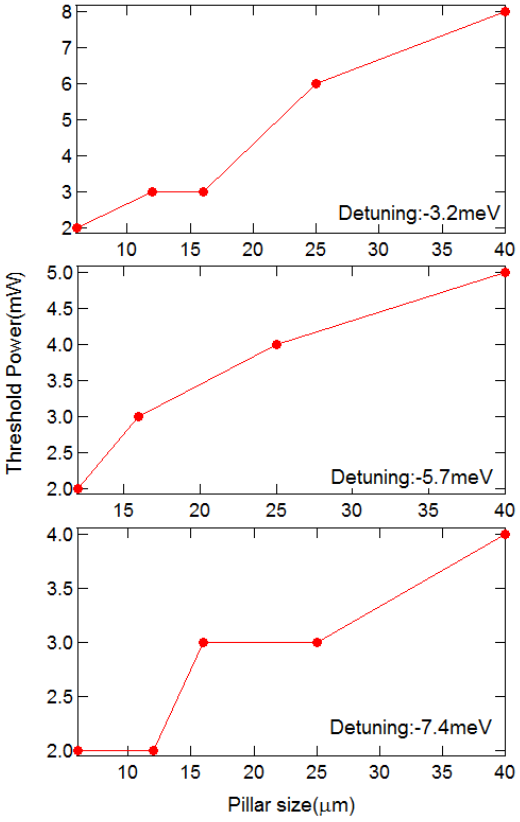

Figure 3.19 Polariton lasing threshold of different micropillars when the detuning is changed at 25K

In **Figure 3.19,** the polariton lasing threshold tends to be smaller when the diameter of the micropillars decreases at detuning -3.2meV, -5.7meV and -7.4meV. The decrease of the threshold is due to more efficient relaxation mechanism and avoidance of exciton diffusion in smaller micropillars. The polariton relaxation rate with acoustic phonons is inversely

proportional to the square root of the microcavity volume. In smaller micropillars, the relaxation rate is smaller so polariton lasing threshold is reduced. The exciton diffusion length can reach several micrometers at low temperature. In small micropillars, excitons will be reflected back from the pillar wall and contribute to the stimulated scattering. The polariton lasing threshold thus becomes smaller. In addition, the polariton lasing threshold decreases when the detuning becomes more negative. Our result is different from reference **[8]**, which shows polariton lasing threshold is minimal around zero detuning. Here we propose the explanation for this below:

When the detuning is more positive, the exciton component becomes larger. This increases the critical density of the polariton lasing **[8],** because the density of states is larger. It is also reported that the polariton lasing threshold is minimal at negative detuning by reference **[44].** The reason, they claim, is that there is a de-trapping effect from the ground states of polaritons, especially when the energy-trap depth (the energy difference between the polariton ground state and the excitons) can be comparable to the thermal excitation. It is more difficult to confine the exciton polaritons in the energy-trap when the detuning is more positive (where the energy-trap is shallow). Thus more pump power is needed to realize polariton lasing. In the present cryostat, the sample is pasted onto a silicon substrate, which does not conduct heat efficiently. So the real temperature of the sample is higher than the cryostat. I estimate the real temperature is around 40-50K when the cryostat reaches around 20K. The thermal energy is around 4-5meV, which can be comparable to the energy-trap for the positive detuning. When the detuning is negative, the trap can be as large as 9meV. Here the de-trapping effect of the exciton polaritons can be ignored. Now the polariton relaxation into the ground state can be easily realized and threshold power is smaller.

3.5.3 Polariton lasing threshold changes with the temperature

As discussed before, polariton lasing is the spontaneous emission of the condensate in the microcavity. However, building a polariton laser does not mean that a thermalized or quasi thermalized polariton condensate has to be realized. When the polariton condensates reach equilibrium or quasi-equilibrium with the host crystal, the critical density can be derived from the Bose statistics and the dispersion, as shown in **Figure 3.20.** We can see that the critical density increases monotonically with temperature.

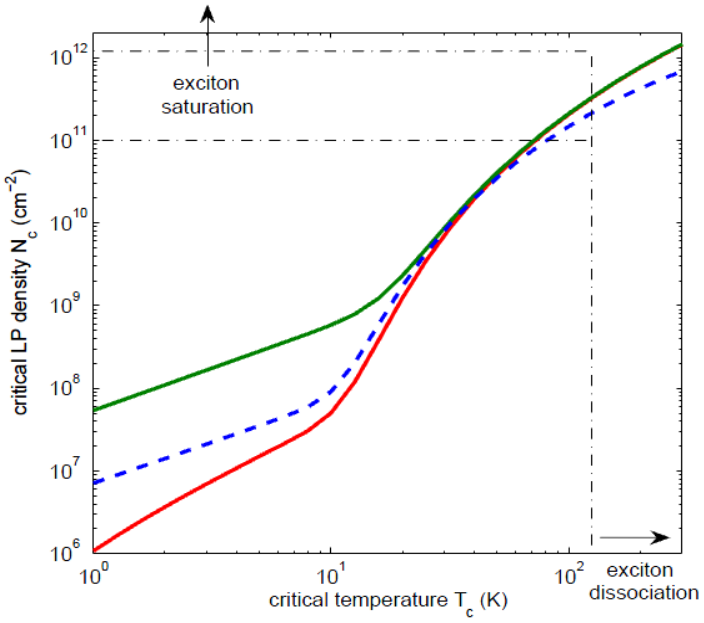

Figure 3.20 Critical density of KT transition (dashed line) and quasi-BEC in a system with square size of 20 microns (the lower red solid line) and 1 m (the upper green solid line); vertical dash-dotted line is the upper-limit of exciton-dissociation temperature. The horizontal dash-dotted lines show the exciton saturation density with 1 QW (the lower one) and with 12 QWs (the upper one). Reprinted from [44]

Results and discussion

We increase the temperature, and keep the detuning between the excitons and cavity photon constant. With increasing the temperature, polariton lasing threshold is larger. This is clearly shown in **Figure 3.21.**

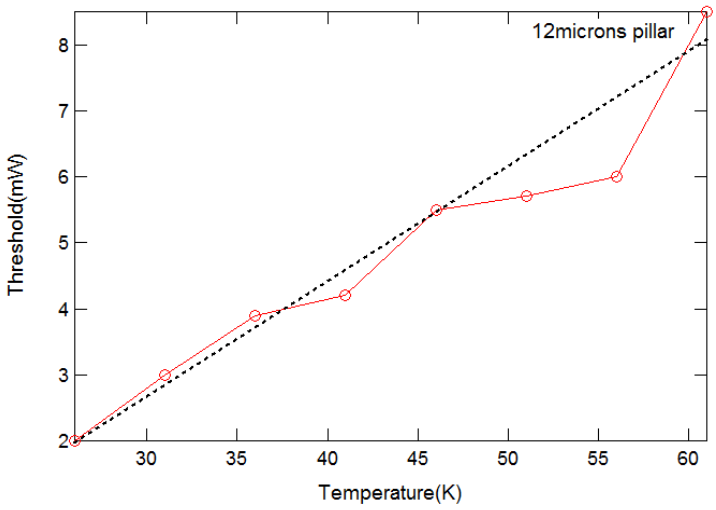

Figure 3.21 Polariton lasing threshold of the micropillar with the diameter of 12 microns when the temperature is changed from 26K to 61K

We can see that the above linear increase of the polariton lasing threshold is consistent with **Figure 3.20** in the temperature range investigated. A linear increase in the polariton lasing threshold with temperature is also observed in reference **[44].** To check whether the polariton condensate is thermalized or not, we plot the integrated intensity (integrate from the energy vs angle imaging data) just at the threshold corresponding to **Figure 3.21**. The relative population number of polaritons is proportional to the integrated intensity divided by the cavity photon component. At each temperature, we get the cavity photon fraction by simulated Hopfield coefficients. **Figure 3.22** shows the integrated intensity after the cavity photon component correction. We find that a linear behavior is clearly seen, which shows that the polariton condensate reaches quasi-equilibrium (from fitting by using a Boltzmann distribution, we find the fitted temperature is higher than the micropillar; for example, we find a fitted temperature of 50K when the cryostat is 26K).

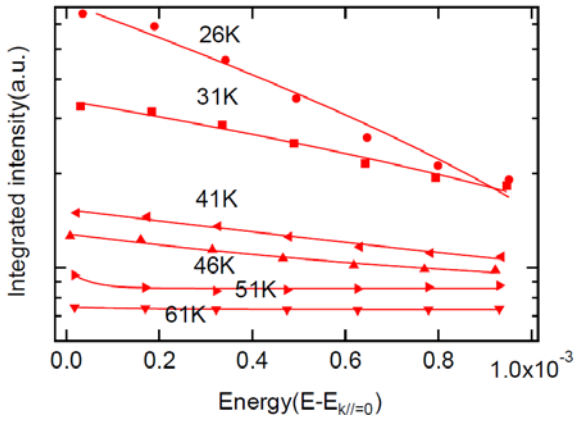

Figure 3.22 Integrated intensity of the emitted light taken from the energy vs angle imaging data corrected by the cavity photon faction with the energy difference from the state which has a zero wave vector, the lines are fitted by a Boltzmann distribution. Left axis: log; bottom axis: linear. (the temperature indicated is the cryostat temperature)

The increase of the polariton lasing threshold with temperature can also be explained by considering that the polaritons can be thermally excited away from the ground states, which prevents macroscopic occupation and lasing. Thus more power is needed to realized polariton lasing.

To conclude, polariton lasing is observed in a large variety of micropillars, in which the confinement enhances the polariton relaxation. The threshold decreases with pillar size and detuning. A linear increase of polariton lasing threshold with temperature is observed. To be further, the micropillars can be applied in some polariton devices. Future work could be also continued in view of the giant polariton-polariton interaction in small micropillars such as polariton blockade regime.

3.6 Conclusion

In this Chapter, polariton lasing in a high Q planar microcavity and micropillar is observed. The polariton lasing occurs at high wave vector states in a planar microcavity due to polariton-exciton reservoir or polariton-polariton interaction within the condensate. Polariton

lasing is found to be at the ground state in micropillars due to strong lateral confinement. In addition, we observe both polariton lasing at low temperature and photon lasing at high temperature. The lasing mechanisms at these two temperatures are compared and discussed. When increasing the temperature, we find polariton lasing threshold increases linearly in a micropillar between 26K and 61K, where a quasi-thermalized polariton condensate is realized.

Chapter 4

Transistor switch based on the polariton condensate

4.1 Introduction

Achieving higher and higher speed of operation in electronics is experiencing increasing obstacles. Moore's law, which lasts for several decades, is approaching the inherent limits of semiconductor materials **[45-48]**. Although a number of novel approaches are used to improve the electronics' operating frequency and power consumption **[49-51]**, it is widely accepted that charged carriers will be replaced by information carriers that do not suffer from scattering and resistance effects in the future. However, up to now, a viable optical analogue to an electronic transistor has not to be identified as switching and operating powers of these devices are too high **[52]**.

Polariton, as hybrid states of light and electronic excitations in semiconductor microcavity, offers a promising solution in view of the fact that they behave as a natural bridge between these two systems. The cavity polaritons' exciton component allows them to interact with each other strongly, resulting in nonlinear functionality. On the other hand, their photonic component restricts their de-phasing, which allows them to carry information with minimal data loss. Notably from the view of solid state physics, polaritons are bosonic particles with a particularly light effective mass. So polaritons can macroscopically condense into single low-energy state, which shows many similarities to atomic Bose Einstein condensates **[14,53-55]**.

The macroscopic quantum properties of polariton condensates combined with their photonic nature make them ideal candidates in the application of quantum information devices and all optical circuits **[19,56-58]**.

Several recent works address the possibility of optical manipulation of polariton condensate flow, however, these stop short of demonstrating actual switch gating of polariton condensate flow, which is a prerequisite for implementation of integrated optical circuits **[11,59,60]**.

Polariton propagate

Exciton polariton condensate has much larger particle-particle interaction because of the exciton component. The polaritons in the condensate repel each other due to polariton-polariton interaction or polariton-exciton reservoir interaction. In this case, the polariton condensate can propagate backwards away from the pump spot center when they gain non-zero wave vector, with the group velocity which is determined by its dispersion curve:

$$v_{group} = \frac{1}{\hbar}\frac{dE}{dk} \tag{4.1}$$

The polaritons will propagate with the momentum

$$\vec{p} = \hbar \vec{k} \tag{4.2}$$

and energy

$E(\vec{k})$

Sample

The sample is a microcavity ridge, etched from a high Q planar microcavity. The microcavity ridge is around 20x300 micrometers. The ridge is in the orientation such that the long side is along the detuning-changing direction. With the detuning difference along the ridge, the created exciton polariton condensate goes towards the more-negative end, as shown in **Figure 4.0(a).**

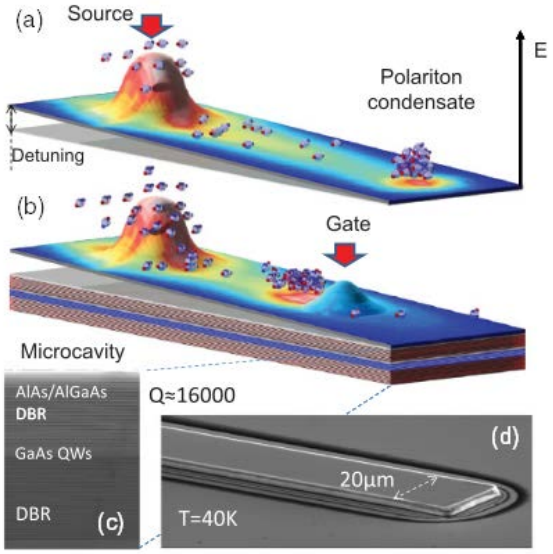

Figure 4.0 Schematic of the polariton condensate transistor based on a microcavity ridge (a) without and (b) with the gate; SEM images: (c) the cross section of bulk sample and (d) a 20μm ridge.

Position-varying blueshift

Around the pump spot center, the exciton reservoir density changes at different position, which causes different blueshift, as shown in **Figure 4.1.** The blueshift is maximal at the center of the pump spot, and becomes smaller at larger distance.

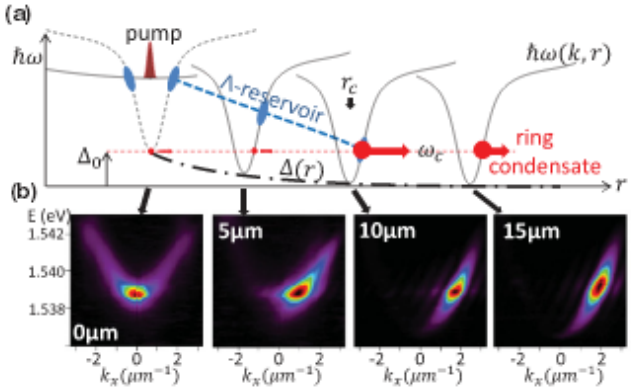

Figure 4.1(a) Schematic diagram of the polariton condensate expelled from the pump position with increasing the wave vector. (b) The energy vs angle imaging taken at different position from the pump position, reprinted from [61].

Proposal of transistor switch

If we introduce a second non-resonant laser in the pathway of the polariton condensate flow, the blueshift resulted from this laser forms a local blueshift. The polariton condensate ejected by the pump laser can be either reflected or transmit through, depending on the height of the blueshift. This looks like an electronic transistor switch, where the pump laser acts as source, the second gate beam behaves as gate electrode, and the ridge end can be seen as the drain electrode or collector. Now the carrier is not electrons, but polaritons. The advantage of polaritons is that the group velocity of the polaritons can reach around 2.5 um/ps, which is one order of magnitude higher than the drift velocity of the electrons at high electric field (the saturated drift velocity of the electrons in AlGaAs/GaAs/AlGaAs 2D electron gas channel is around 0.4 um/ps in reference **[45]**).

4.2 Experiment setup

The experiment setup, as shown in **Figure 4.2(a)** is similar as the one used in **Chapter 3**. However, to investigate the transportation of exciton polariton condensate, the sample is aligned in such a way that the microcavity ridge is parallel with the slit of the spectrometer. So we can measure the energy distribution of the exciton polariton condensate along the ridge. The two lasers come from the same continuous wave Ti:Sapphire laser. They are focused onto the microcavity ridge in a way that is shown in **Figure 4.2(b)**. An objective is used to focus the laser spot of about 2-5microns onto the ridge and to collect the PL from the sample. The first laser is the source beam, which acts to inject the exciton polariton condensate. This condensate propagates along the ridge towards to the more negative-detuning direction. The second is the gate beam, which induces a blueshift between the pump spot and the ridge end. It controls the polariton condensate flow. The laser wavelength is at around the first reflectivity minimum of the Bragg mode above the stop band of the microcavity, as done in **Chapter 3**.

There is a blocking element which can block the gate beam, with which we can see how polariton condensate flow forms when there is only source beam.

When investigating the real space imaging of the ridge, a lens is used in front of the slit of the spectrometer, with the distance of its focus length, while the slit is totally open. To resolve energy information of the polariton condensate flow along the ridge, the slit of the spectrometer is closed as in the case of taking spectra. Here we usually put the center of the ridge onto the slit of the spectrometer.

White light is shined onto the surface of the sample and we can monitor the positions of the source spot and gate spot. In the experiment, the source beam spot is put around 60 micrometers from the ridge end.

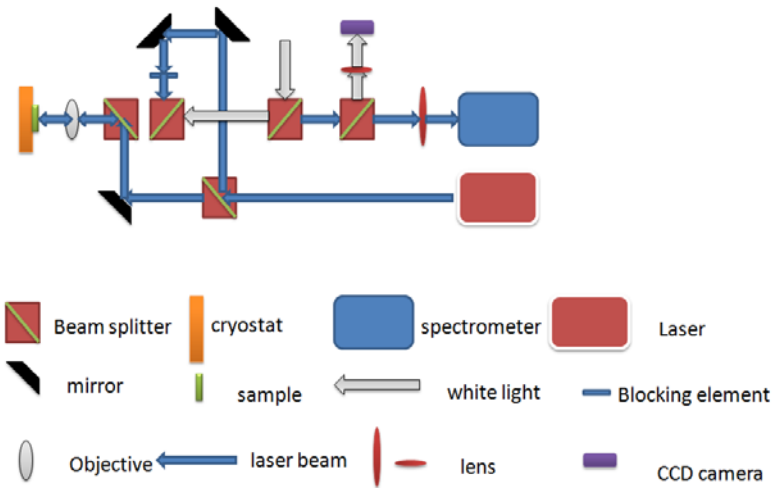

(a)

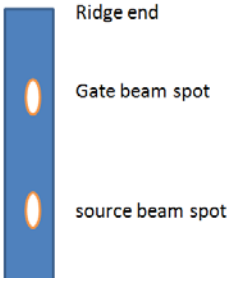

(b)

Figure 4.2 (a) Experimental setup for two beams when blocking element is off; (b) Two spots alignment on the ridge

4.3 Results and discussion

4.3.1 One beam case

With only source beam, we find that there is huge difference between below threshold and above threshold, as shown in **Figure 4.3** (a) i, (b) i and (c) i.

Below threshold real space image in **Figure 4.3(a)i** reveals the emission is concentrated at the source whilst angularly resolved emission **Figure 4.3(c)i** confirms that the emission originates from the lower polariton (LP) branch. The spectrally-resolved image **Figure 4.3(b)i** shows the relaxation bottleneck at higher energies and evidences long polariton lifetimes through the extension of the polariton emission to the end of the ridge.

In **Figure 4.3** (a) ii, (b) ii and (c) ii, however, the physics process is much different when the power is above threshold, while the source spot causes the formation of exciton polariton condensate. From **Figure 4.3** (c) ii, we can see that the condensate gains non-zero wave vector due to polariton-exciton reservoir interaction. We estimate the group velocity of the polariton condensate is around 2.5 um/ps. This condensate flux flows towards the more-negative-detuning direction because of the potential gradient, which is clearly seen in **Figure 4.3** (b) ii.

From the time-resolved experiment performed in Madrid on the same sample, the polariton condensate is reflected backwards when it propagates to the end of the ridge. The backwards-transporting condensate is reflected again when it propagates to the pump spot.

Thus there is multiple reflection of the polariton condensate between the ridge end and the pump spot.

From **Figure 4.3**(b) iii-iv, the polariton condensate has a smaller energy than the pump spot. This means a non-ballistic propagation of polariton condensate occurs. We find the energy of the trapped condensate is around the same as the lower-branch polaritons at the ridge end when the power is very low.

In addition, from **Figure 4.3** (c) iii, iv, (b) iii, iv, it is clear that the condensate at the ridge end forms with a zero wave vector. The change in the wave vector is caused by the multiple reflectance of the condensate flow from the pump spot and the ridge end. During this process, the kinetic energy of the polaritons is lost.

Here there is no interference between the forward-moving condensate and backward-moving condensate, as shown in reference **[10].** This has more advantage because this parasitic interference will bring in some problem in optical circuits, which favors clean and definite optical control along the waveguide.

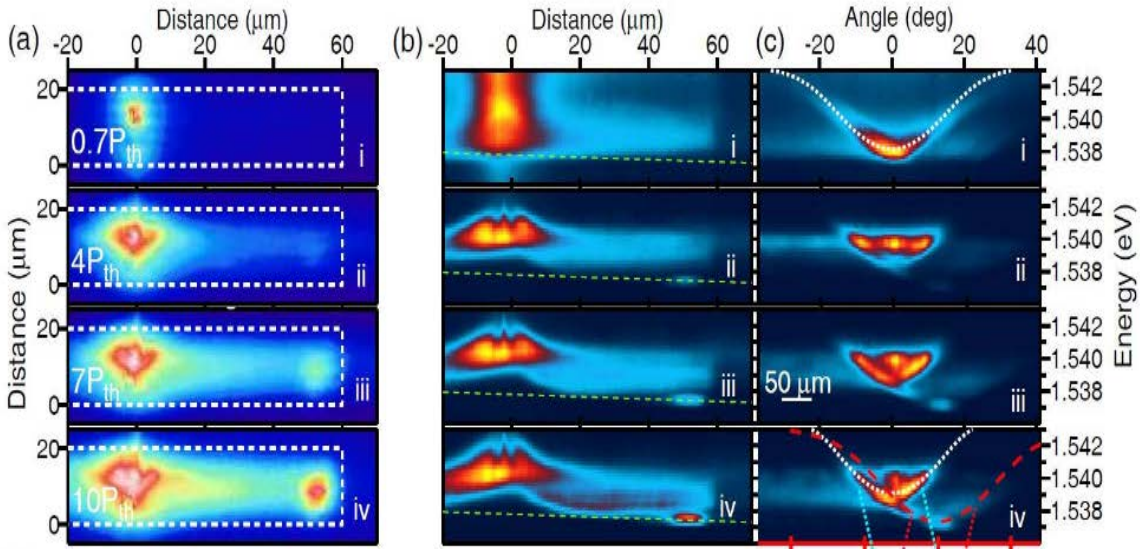

Figure 4.3 Real space imaging, energy resolved imaging and energy vs angle imaging taken at different power

Line profile along the ridge

From the line profile we can compare the intensity along the ridge more clearly. **Figure 4.4** plots the line profile along the center of the ridge at different power. The intensity at the ridge end increases nonlinearly and becomes larger than the pump position. This means more and more polaritons do not decay at the pump spot while they transport along the ridge. **Figure 4.4** clearly shows the propagation of the exciton polariton condensate flow.

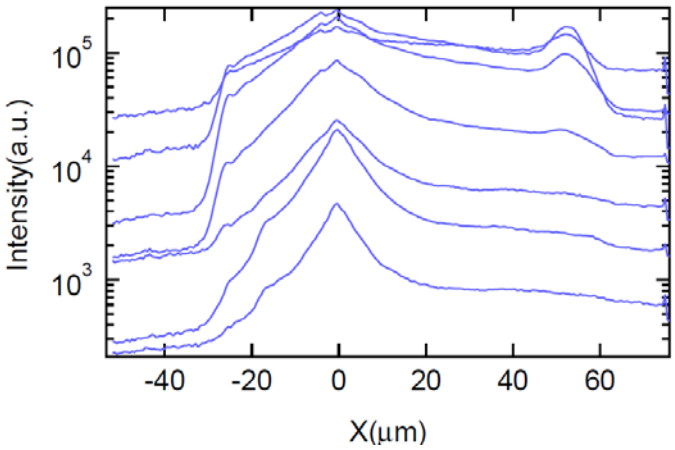

Figure 4.4 Line profile of the real space imaging along the ridge taken at different power

Power dependent spectra at ridge end

The condensate at the end of the ridge forms nonlinearly, the power dependent spectra is needed to investigate the nonlinear process. In the following part we plot the line profile from the energy versus distance imaging of the exciton polaritons condensate at the ridge end with pump power, in **Figure 4.5(a)**. From these power dependent spectra we can see that the condensate appears suddenly above the polariton lasing threshold with a very small linewidth.

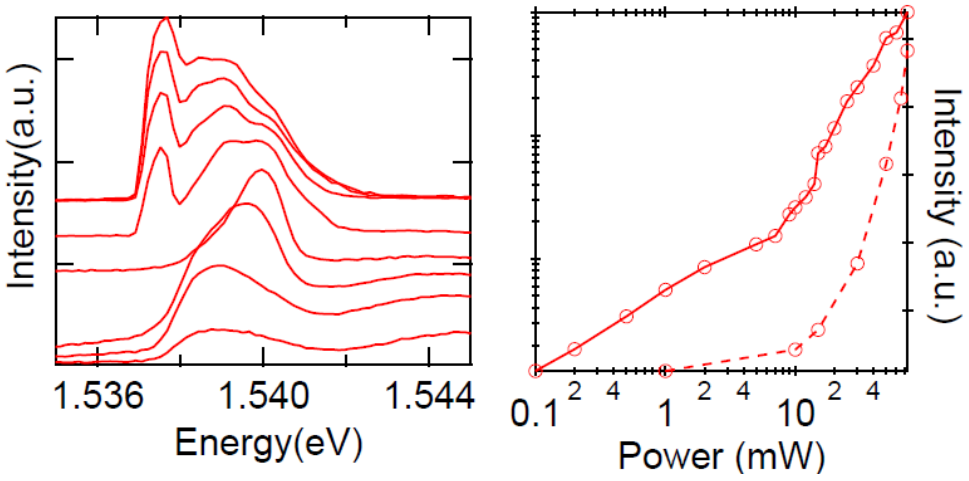

Figure 4.5 Power dependent spectra at the ridge end (left, log scale versus linear scale) and integrated intensity of this position and the pump position (right, log scale versus log scale).

Figure 4.5(b) is the integrated intensity of the emitted light from the pump position and the ridge end as a function of the pump power. It is clear that there is also nonlinear increase with the pump power at the ridge end, with a larger threshold than the pump position. It is reasonable because the condensate flow is from the pump spot and the polaritons experience relaxation during the propagation process.

4.3.2 Relaxation along the ridge

From **Figure 4.3**, we find that the polariton condensate experiences relaxation along the ridge and a trapped condensate forms at the ridge end. It is necessary to measure the energy versus angle dispersion at different position along the propagation path to investigate the relaxation process. We find these are sub-branch polaritons due to lateral confinement and these sub-branches play an important role in the polariton relaxation dynamics.

Subbranch polaritons due to lateral confinement

In our sample, there exist discrete energy levels due to lateral confinement of the ridge. The momentum space imaging can be simulated by adopting the following formula **[62]**:

$$E_n(k_{//}) = \sqrt{E^2_{cav} + \frac{\hbar^2 c^2}{\varepsilon}\left(\frac{\pi^2}{L^2}(n+1)^2 + k^2_{//}\right)}$$

(4.3)

Where n is the number of the nodes of the electric field vertical the ridge, L is the width of the ridge, E_{cav} is the cavity mode energy at normal incidence without considering the lateral confinement.

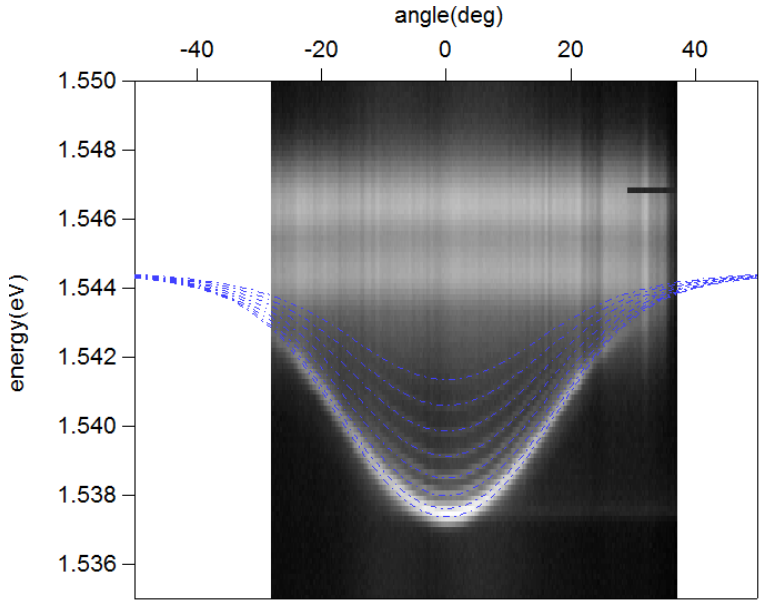

Figure 4.6 Low power energy versus angle imaging (along the ridge)

In **Figure 4.6,** the dotted points are the simulated result from the formula above. The number n indicates the parity of the field distribution of the photon modes in the direction vertical to the ridge. When n is an even number, the field distribution of the cavity mode vertical to the ridge is symmetric. While as the field distribution of the cavity mode vertical to the ridge is anti-symmetric when n is an odd number. Some research shows that these subbranch polaritons are linearly polarized due to strain **[10]**.

Results and discussion

To explore the relaxation of the polariton condensate, we measure the momentum space dispersion along the ridge with different pump power. To do this, we need to put the Fourier imaging of the objective onto the slit of the spectrometer. Then a second slit is used with the orientation such that the two slits are perpendicular to each other. The second slit is controlled by a translation stage. With moving the translation stage, we can measure the momentum space imaging at different position along the ridge. The result is shown in **Figure 4.7.**

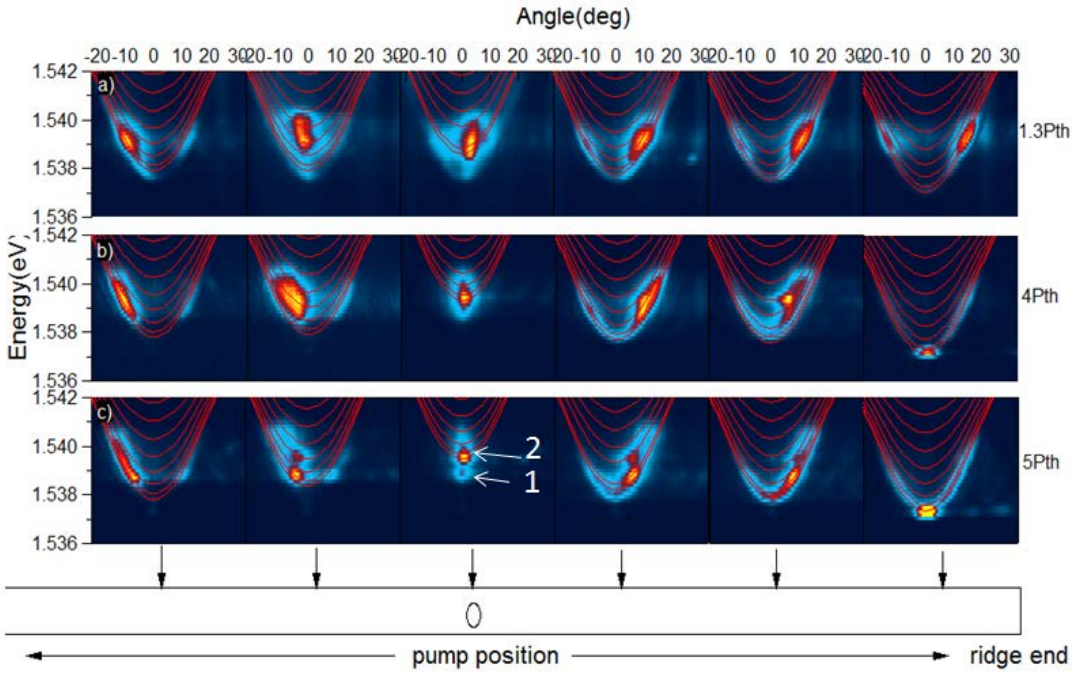

Figure 4.7 Energy versus angle imaging at various positions along the ridge at different power above threshold, 1 and 2 dictates different sub-branch polaritons

From **Figure 4.7**, we can see that the exciton polaritons that propagate to the ridge end have a larger population with a positive wave vector. While as the exciton polaritons transporting backward the pump position have a larger population with a negative wave vector. This confirms that the polariton condensate gains opposite wave vector at the pump spot center (at two sides).

When the pump power is 4 or 5 times the polariton lasing threshold, we find there is something interesting:

1) Dynamic transition occurs between different sub branches polaritons.

At the pump position, we find that several sub-branch polaritons are occupied. For example, at the power 5 times polariton lasing threshold, two sub branches are clearly seen at the pump spot. However, variant sub-branches are occupied at different positions along the ridge. From the pump spot center, where sub branch 2 dominates the emission, to the position closer to the ridge end, we can see sub branch 1 overwhelms sub branch 2. Here we firstly find the transition dynamics between different sub branch polaritons in a propagation process.

2) Lowest energy level forms at the ridge end.

At the ridge end, it is clear that a new condensate appears at the energy determined by the detuning at the ridge end. Here it seems that some parametric scattering occurs. However, more

work is needed to check the physical process here.

4.3.3 Weak coupling regime

High pump power can push the excitons at the pump spot beyond saturation density. This leads to the dissociation of the excitons and thus the strong coupling is lost. So it is possible that weak coupling lasing occurs in the center of the pump spot but strong coupling exists in the outer region. In this case, the exciton polariton condensate at outer part of the pump spot can also appear. In the following we plot the near field imaging at around 28K where strong coupling regime is kept and 70K when weak coupling lasing occurs. The result can be seen in **Figure 4.8.** We can see that propagation only exists in the strong coupling regime. When weak coupling lasing occurs, the emitted light is mainly located at the center of the pump position. And there is no any propagation of the cavity photons along the ridge.

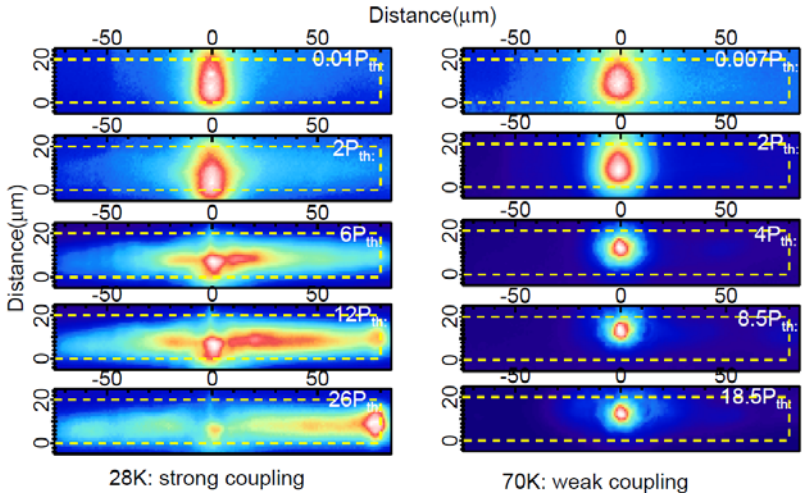

Figure 4.8 Real space imaging of the ridge above threshold at 28K (left) and 70K (right)

4.3.4 Two beam case

When a second laser beam is introduced, the propagating exciton polariton condensate will "feel" the interaction with the exciton reservoir created at gate spot, which will block the transportation of the condensate depending on the interaction strength. As in **Figure 4.9** (a) i, ii, iii, (b) i, ii, iii, (c) i, ii, iii, the counts at ridge end are reduced with increasing the gate beam power. This is like an electronic transistor switch. The second beam acts like a gate electrode, while the ridge end is a collector. In an electron transistor, the free transport of the 2 dimensional electron gas is controlled by the gate electrode. Here the control gate beam modulates the propagation of the polariton condensate.

From energy resolved imaging in **Figure 4.9** (a) ii, iii, (b) ii, iii, (c) ii, iii, the condensate between the source spot and gate spot is formed. With increasing the gate beam power, the middle condensate is repelled more towards the source spot. This is because the blueshift caused by the gate beam is larger, which pushes the polariton condensate towards the source spot more closely. When the gate beam power is 0.47 times the polariton lasing threshold, the total intensity at the ridge end is reduced by 90%. The gate beam power is only 1/20 of the source beam.

In **Figure 4.10 (left),** the intensity profile along the ridge is plotted when the gate beam power is changed. From this figure, the gating behavior of the second beam is very clear.

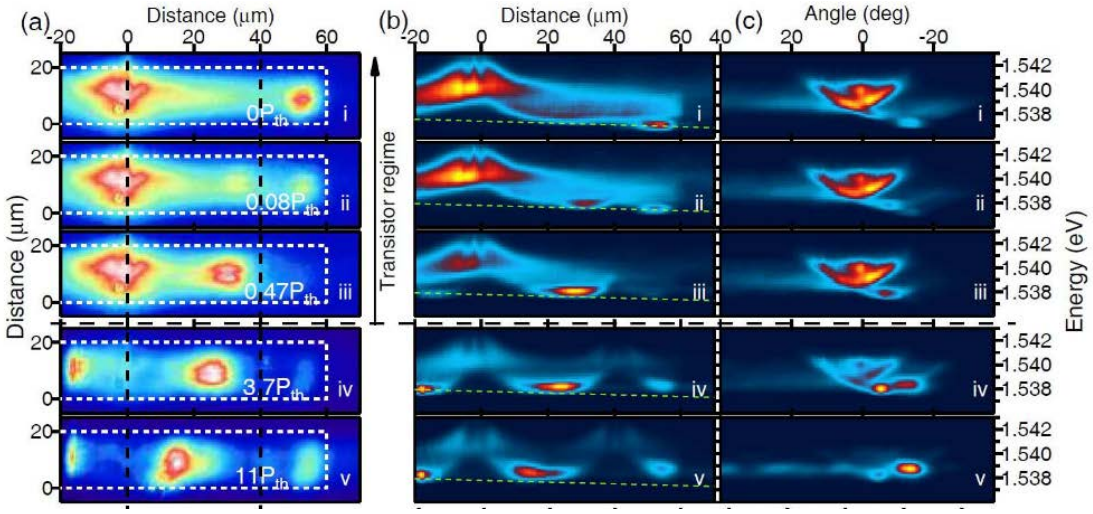

Figure 4.9 Real space imaging, energy resolved imaging and k space imaging at different powers when two beams are introduced

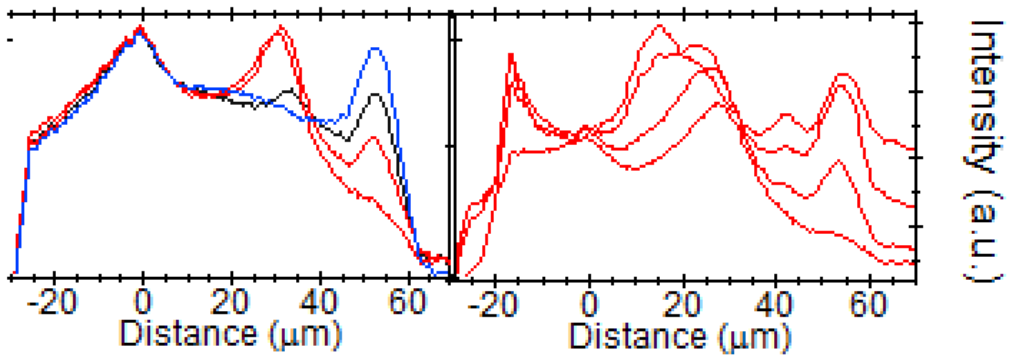

Figure 4.10 the line profile of the real space imaging along the ridge at transistor switch regime and beyond transistor switch regime

However, when the power of the gate beam is high enough, the second laser also creates exciton polariton condensate, which flows towards the ridge end. So the counts at ridge end become larger when the gate beam power is increased further, as shown in **Figure 4.9** (a) iv, v, (b) iv, v, (c) iv, v. The condensate between the source position and gate position is repelled more towards the source spot when the gate beam power is higher. This is consistent with the **Figure 4.10 (right).**

This gating behavior can be seen more clearly when the source power and gate power is scanned independently, as seen in **Figure 4.11.**

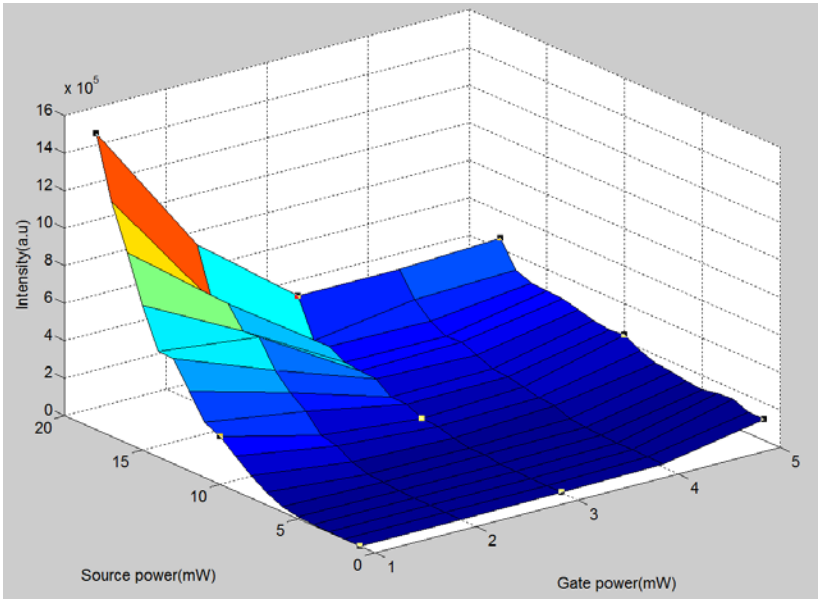

Figure 4.11 The intensity at the ridge end when the source power and gate power are scanned independently

From **Figure 4.11,** the gating by the second beam works very well, only at a region where the gate beam does not go beyond the polariton lasing threshold, either does not inject polariton condensate towards the ridge end.

Compare to the electron and exciton based transistor

If we discuss the performance of this prototype polariton condensate transistor, we can see that the polariton dispersion yields a group velocity of 2.5μm/ps. This is nearly 30 times faster than the speed of electrons in modern silicon transistors, which ensures a short transit time from gate to collector (10 ps). So, in the current scheme the switching time of the device is limited by the polariton lifetime (18 ps), which allows operation frequencies of tens of Gigahertz, one order of magnitude faster than those of exciton-based transistors **[63]**.

Further work is needed to reduce the operation power of the polariton transistor through either resonant condensate injection or implementation of electrically controlled gating.

4.3.5 Theoretical simulation

The theoretical simulation is done by Tim Liew by using a Gross-Pitaevskii equation for the polariton mean field $\psi(x)$;

$$i\hbar\frac{d\psi(x)}{dt}=(\hat{E}+V(x)+\alpha|\psi(x)|^2)\psi(x) \tag{4.4}$$

where $\hat{E}$ is the kinetic energy operator of polaritons, which reproduces the lower- -branch polariton non-parabolic dispersion by using a coupled model;

The second part comes from

$$V(x)=V_0(x)-\beta x+P(x) \tag{4.5}$$

In which the first one is the confinement potential for the walls of the ridge; the second is the potential gradient; the final part is pump induced blueshift. The blueshift is composed of Gaussian spot with intensity and position corresponding to the lasers used in the experiment.
External pump induced blueshift has been shown to permit the engineering of the polariton potential by using resonant **[64]** and non-resonant **[65]** excitation before. In this experiment, the pump laser excites high energy excitons that induce a blueshift of polaritons through polariton-exciton reservoir interactions.
The polariton-polariton interaction strength, can be estimated by: **[66]**

$$\alpha \approx 6E_B a_B^2 \tag{4.6}$$

If we use standard values for the exciton binding energy E_B and Bohr radius a_B in GaAs quantum wells, the polariton density at the collector spot (ridge end) can be estimated from the observed blueshift as $7.5\times10^{9}\,cm^{-2}$ when the interaction strength is around $0.004 meV\,\mu m^{2}$.

The Gross-Pitaevskii equation can be solved numerically using imaginary time propagation to yield the ground state of the system (The maximum pump-induced (reservoir-induced) blueshift was taken as 2meV, estimated from the observed blueshift at the pump position. β =9meV/mm).
The simulated result can be seen in **Figure 4.12**

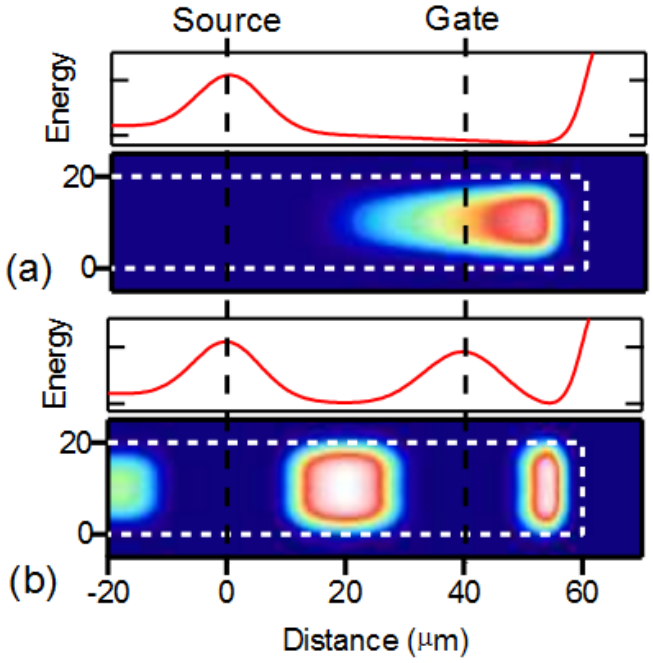

Figure 4.12 Simulated Real Space imaging when one pump beam is used and two beams are introduced

In **Figure 4.12**, the simulated result when there is only source beam (**Figure 4.12(a))** and when both the source beam and gate beam (above threshold and beyond transistor switch regime) appear (**Figure 4.12(b))** agrees well with the experiment.

4.3.6 Some questions

One question is that this transistor acts just as a switch, not as an amplifier. Now the amplification is not well defined in view of the fact that the source, gate and collector are independent, not like an electronic transistor. Recently, reference **[67]** shows an amplification scheme by performing time resolved experiments. More work can be done if more experimental methods are available.

4.4 Conclusion

In summary, a prototype polariton condensate transistor switch is realized by utilizing a high-finesse microcavity sample fabricated into ridges. In this Chapter we show that the polariton condensate flux on the ridge can be controlled using a gate beam that is 20 times weaker than the source. This spatial control with attenuation approaching larger than 90% (from later experiment) allows the implementation of all-optical polariton transistors suitable in both optoelectronic and all-optical schemes **[55,68]**.

In the short term they could be used in optical inter-core communication for transferring data within and between chips. In the long term they could enable the elimination of electronics all together.

Chapter 5

Spin related phenomenon of polaritons in a microcavity ridge

5.1 Introduction

It is widely known that long range electron-hole exchange interaction is a leading spin relaxation mechanism for Heavy-Hole Excitons in quantum wells **[18]**. This interaction generates an effective magnetic field (called Maialle field) which lies in the quantum well plane. The amplitude of the effective magnetic field depends on the TE-TM mode splitting. In a strongly coupled semiconductor microcavity, the polaritons' TE-TM mode splitting is amplified due to the cavity mode component. The effective magnetic field generated by the TE-TM mode splitting introduces a polariton pseudospin vector evolution, like the effective Rashba and Dresselhaus field on the electrons in semiconductors. The advantage of polaritons is the long coherence length which can reach 1 mm in planar microcavities **[18]**. This is several orders of magnitude longer than the electrons in semiconductors. In addition, the effective magnetic field's pointing direction depends on the wave vector of the polaritons. It varies when the wave vector changes. The polaritons' spin shows much more interesting physics and application potential. The research of exciton polaritons' spin leads to a newly emerging area: spin-optronics **[16]**, the counterpart to spintronics with electrons.

Recently, spin oscillation is observed in a high Q microcavity **[65]**. Different from previous study which depends on resonantly pumping or quasi-resonantly pumping, this work uses non resonant laser to study the spin procession in a planar microcavity. They observe the polarization of the polaritons oscillates during ballistic propagation due to the effective magnetic field. This kind of polarization oscillation above polariton lasing threshold needs to be studied in 1D microcavity wire or ridge which provides a good platform to investigate the pseudospin vector propagation and oscillation along the waveguide.

In this chapter, the following topics are discussed:

(1) We study polariton condensate flow propagation along the ridge under a CW circularly polarized non-resonant laser. We observe some patterns due to the reflection of polariton condensate flow at the edge of the ridge. This kind of patterns (called spin texture in the following) is interesting because no such texture is found in planar microcavity or much narrow (4-5 micrometers) microwires. In addition, we find that the spin polarization of the polaritons show periodical oscillation due to the effective magnetic field.

(2) We find that the periodical oscillation of the polaritons' spin polarization disappears when a pulse circularly polarized non-resonant laser is used. A polariton condensate flow with around constant spin polarization (called spin bullet later) is observed.

(3) The polariton condensate transistor switch realized in **Chapter 4** could be used to realize spin based devices. When the gate beam becomes circularly polarized, it introduces spin-dependent blueshift. The polariton condensate flow with different spin polarization can be either reflected and distributed between the source spot and gate spot, or can transmit through the gate spot and be located between the gate spot and the ridge end. From this, we realized to separate the polaritons with different spin polarization by the circular

polarized gate beam.

5.2 Spin polarization in a microcavity ridge

In the following we firstly discuss the spin polarization when a circularly polarized laser is focused onto the ridge at low power (below threshold) and at high power (above threshold). The polariton relaxation time changes abruptly at the stimulated scattering threshold, which leads to the increased spin polarization degree with the pump power.

5.2.1 Experiment setup

The experiment is performed at Madrid. The sample is placed in a stable cryostat which can cool the sample to around 10K. The experiment setup can be seen in **Figure 5.1**.

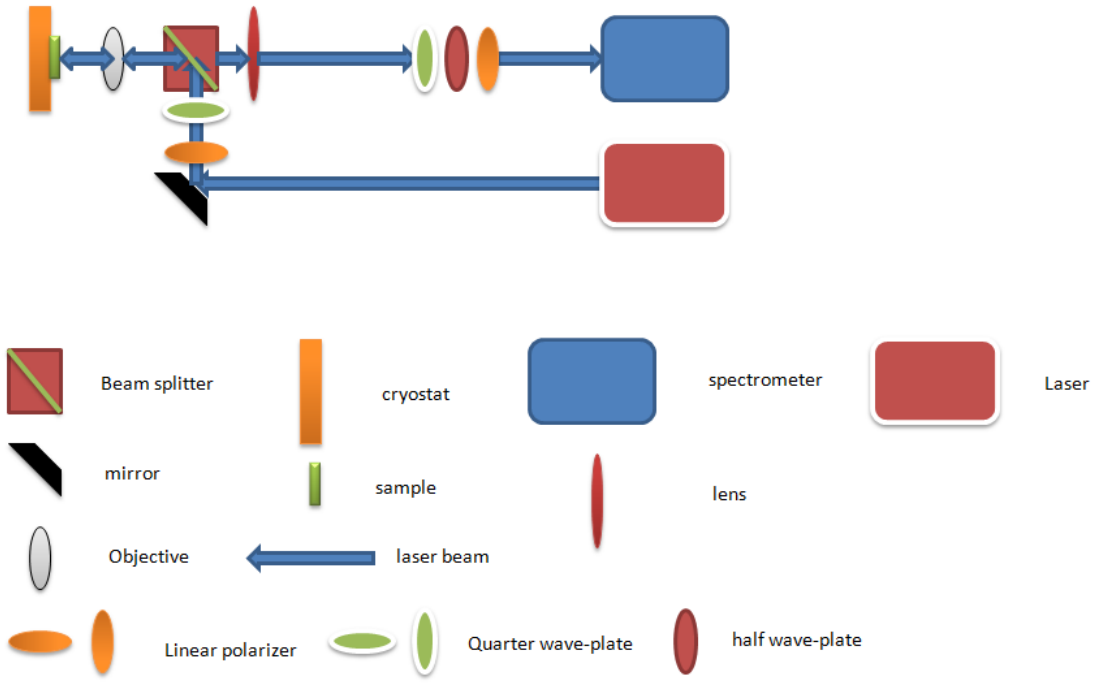

Figure 5.1 Experimental setup used for spin measurements

A large lens with a focus length of 1 meter is used to put the real space imaging of the sample onto the slit of the spectrometer. A linear polarizer is put in the optical path to remove other polarization light so only linear polarized laser is employed; a quarter waveplate is added to change the laser from linear polarization to circular polarization. To detect the signal with different polarization, a quarter waveplate, a half waveplate and a linear polarizer are combined in front of the slit of the spectrometer. Considering the sensitivity of the spectrometer to the light with different linear polarization, in the experiment, we fix the quarter waveplate and the linear polarizer. We can rotate the half waveplate by 45 degree to detect the signal with right-hand circular polarization and left-hand circular polarization. When the detection of other polarization state is necessary, for example, the Stokes parameters, we can change the quarter waveplate and the half waveplate at specific angles. The specific angle needed to be rotated can

be seen in the following table if the initial angle for the quarter waveplate and the half quarter waveplate is 0:

$\lambda / 4$	$\lambda / 2$	Linear polarizer	Polarization
45^0	0	0	Horizontal
45^0	45^0	0	Vertical
0	22.5^0	0	Diagonal
0	67.5^0	0	Anti-diagonal
0	0	0	Right-hand circular
0	45^0	0	Left-hand circular

Table 5.1 The rotation angle of the quarter wave plate and the half wave plate to detect different polarization state if the initial angle for the quarter wave-plate and the half wave-plate is indicated by 0

5.2.2 Results and discussion

There is large spin polarization when a circular polarized laser pumps non-resonantly onto the ridge. In **Figure 5.2,** the left row is the energy and polarization resolved imaging taken at 90mW and 20mW. We can see that at 90mW, the spin polarization is very large at the pump position, while it is very small outside the pump spot. In the right row, we find that there is very small spin polarization at the pump position and outside the pump spot when the laser is linearly polarized.

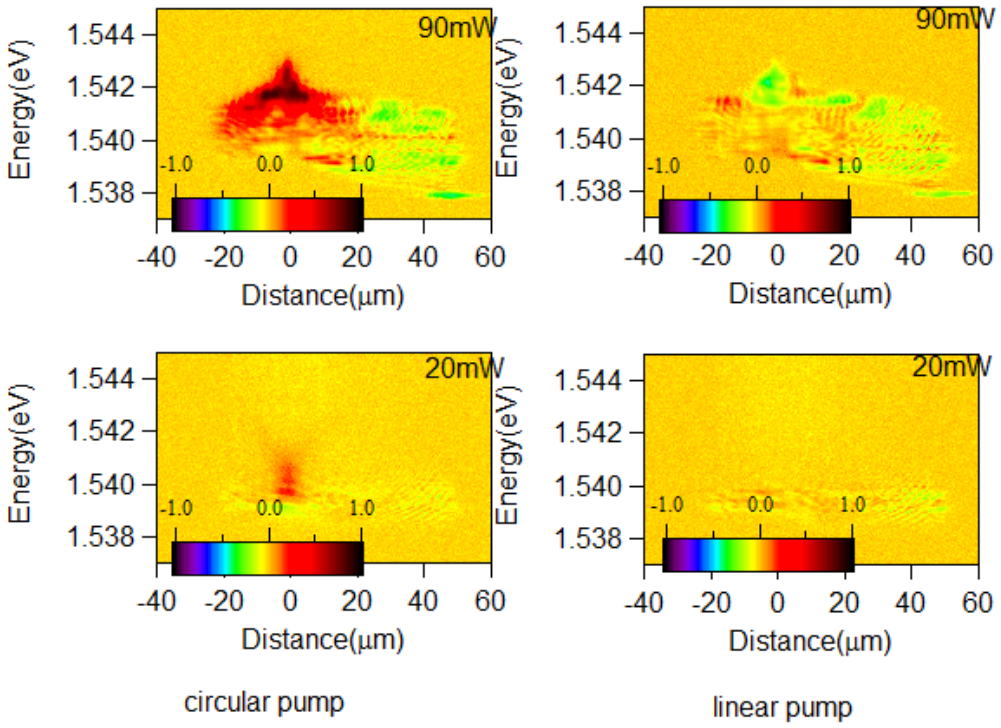

Figure 5.2 Spin polarization along the ridge (The laser pumps at 0, the ridge end is at around 50micrometers). Left row: the power is changed from 20mW and 90mW under a circular polarized pump laser (right hand); Right row: the power is changed from 20mW and 90mW under a linear polarized pump laser.

The increase of the spin polarization of the polaritons with the pump power can be easily understood. When the pump power is low, the spin polarization of the injected polaritons is lost because their energy relaxation time into the ground state (through acoustic phonons, 2 or 3 hundreds of ps) is longer than the spin relaxation time (several tens of ps). The polaritons become un spin polarized before relaxation into the ground state. When the power is higher than the stimulated scattering threshold, the relaxation of the polaritons into the ground state can be very fast (with several ps). Now the spin polarization of the polaritons is kept when they condense macroscopically into the ground states. So the spin polarization of the polaritons is increased a lot.

The spin polarization degree of the exciton polaritons can be expressed as follows if only the effective magnetic field generated by the TE-TM mode splitting is considered **[18]**:

$$\sigma_z = \frac{1}{1+\Omega_{LT}^2 \tau_{rel}^2} \tag{5.1}$$

Where τ_{rel} is the relaxation time of the exciton polaritons; Ω_{LT} is the effective magnetic field.

According to (5.1), the spin polarization of the exciton polaritons increases greatly when stimulated scattering occurs, which needs a much short relaxation time. In the linear polarization case, shown in the right row, stimulated scattering occurs for polaritons with spin σ+ and σ-, so the spin polarization is still very low.

5.3 Spin texture

The previous section does not involve ballistic propagation of polariton condensate, which allows investigating polariton polarization oscillation without scattering in a time period under the effective magnetic field. In the ballistic propagation regime, we find the polariton condensate flow along a microcavity ridge shows specific patterns or structures. At the same time, we observe the spin polarization oscillation due to the effective magnetic field, like the reference **[65]**. This kind of structure is important to understand the polariton propagation dynamics, and can be used in polariton based spin optical circuits.

5.3.1 Observation of spin texture

Real space imaging

In our experiment, we observe polariton textures on the ridge at 40mW, as shown in **Figure 5.3.** The pump laser creates exciton polariton condensate, which is expelled both towards the ridge edge and along the ridge because of interaction between the polariton and exciton reservoir. The polaritons thus gain non zero wave vector kx along the ridge and ky vertical to the ridge.
Now the wave vector of the polaritons is:

$$\vec{k} = k_x \vec{i} + k_y \vec{j} \tag{5.2}$$

When the polaritons reach the ridge edge, they are reflected. The polaritons' wave-vector vertical to the ridge direction changes sign.
So the wave vector of the polaritons becomes:

$$\vec{k} = k_x \vec{i} - k_y \vec{j} \tag{5.3}$$

Now the polaritons propagate with an angle with the ridge edge. The polaritons that have positive +ky and negative –ky interfere with each other when they encounter at the center of the ridge. After interference, these two polaritons continue to move and are reflected again by the ridge edge. The polaritons propagate in thus a way that this texture appears. The interesting thing is that the spin polarization is changed when the polaritons propagate, which is generated by the effective magnetic field. The texture and the spin polarization oscillation are combined and called as "spin texture" here.

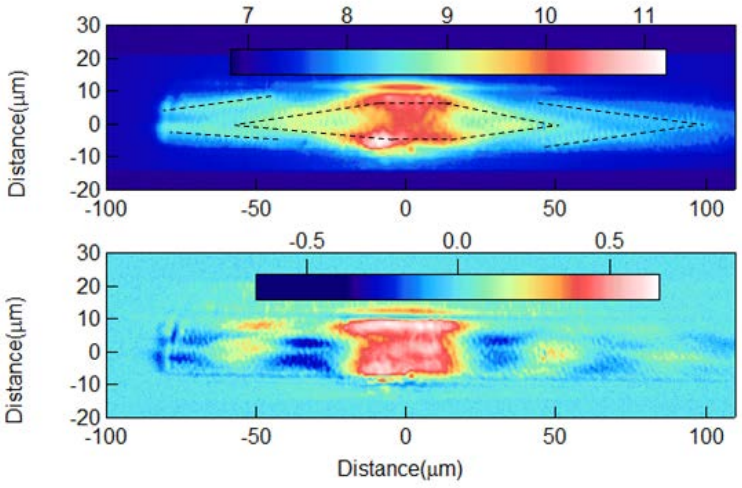

Figure 5.3 Top: total intensity in real space of the ridge; Bottom: spin polarization distribution in real space, the dotted line is for the clarity to see the propagation of polaritons.

Energy resolved imaging

If we measure the energy resolved imaging, we can see more clearly that the spin polarization of the polaritons from the pump spot changes periodically when they ballistically propagate, as shown in **Figure 5.4**. It is obvious that the polaritons have opposite spin polarization at the pump spot. In addition they experience different and independent spin procession, respectively. In **Figure 5.4 (bottom),** we plot the line profile along the ridge at two energies with a difference of 0.9meV. The above result can be seen more clearly from this graph. The oscillation periods vary a little because the TE-TM mode splitting differs for polaritons with different energy.

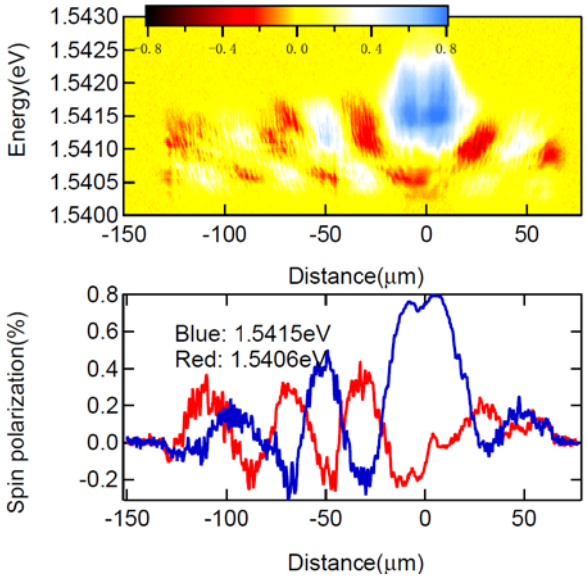

Figure 5.4 Top: spin polarization distribution along the ridge when the pump laser is circularly polarized and with a power of 40mW. Bottom: line profile along the ridge at energy of 1.5415eV and 1.5406eV.

5.3.2 Stokes parameters

As discussed in previous section, the effective magnetic field has a pointing direction which is determined by the polaritons' wave vector. The spin oscillation should be accompanied by the procession of the linear polarization. Here we measure the Stokes-parameters, in **Figure 5.5** under a little different experimental condition than before**.**

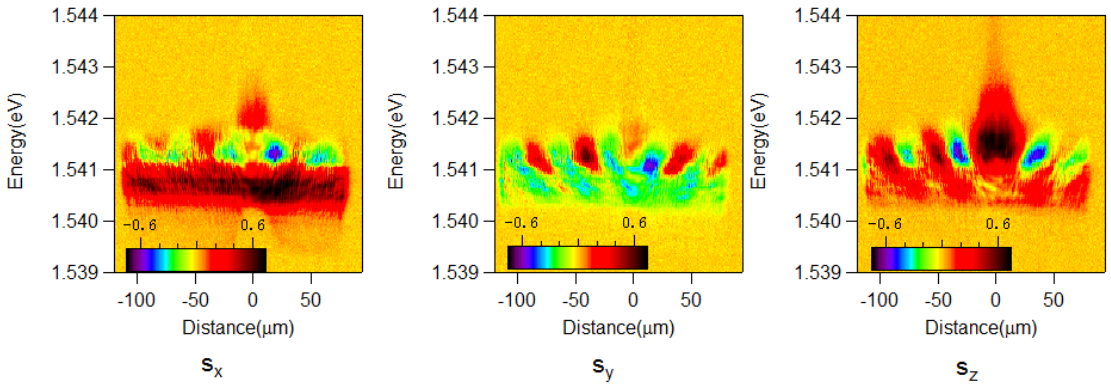

Figure 5.5 Stokes parameters of the exciton polariton condensate when a circular polarized laser pump onto the ridge

In general, the effective magnetic field generated by the TE-TM mode splitting in the microcavity is:

$$\Omega_x = \frac{\Delta_{LT}}{\hbar k^2}(k_x^2 - k_y^2), \text{ and } \Omega_y = \frac{\Delta_{LT}}{\hbar k^2}(k_x k_y) \tag{5.4}$$

where k is the exciton polaritons' in-plane wave vector, k_x, k_y are the wave vector along x and y direction in momentum space, Δ_{LT} is the TE-TM mode splitting. When the exciton polariton condensate propagates along the ridge, the spin polarization oscillates according to **[65]**:

$$v_x \frac{\partial \sigma(x)}{\partial x} = \sigma(x) \times \Omega(k), \tag{5.5}$$

in which x is the distance long the ridge, v_x is the transport velocity of the exciton polariton condensate, $\sigma(x)$ is the pseudospin vector of the exciton polaritons. The pseudospin vector of the exciton polaritons proceeds when they transport along the ridge. In the texture above, we find the polaritons propagate along the ridge with an angle with the edge. In this case, we observe the polaritons change from circular polarization, to vertical (horizontal) or diagonal (antidiagonal) polarization and back to circular polarization again.

5.3.3 Energy resolved results and discussion

To make clear how the exciton polariton condensate propagates with spin oscillation, we measure the real space imaging at different energies and plot the line profile along the center of the ridge, as shown in **Figure 5.6.**

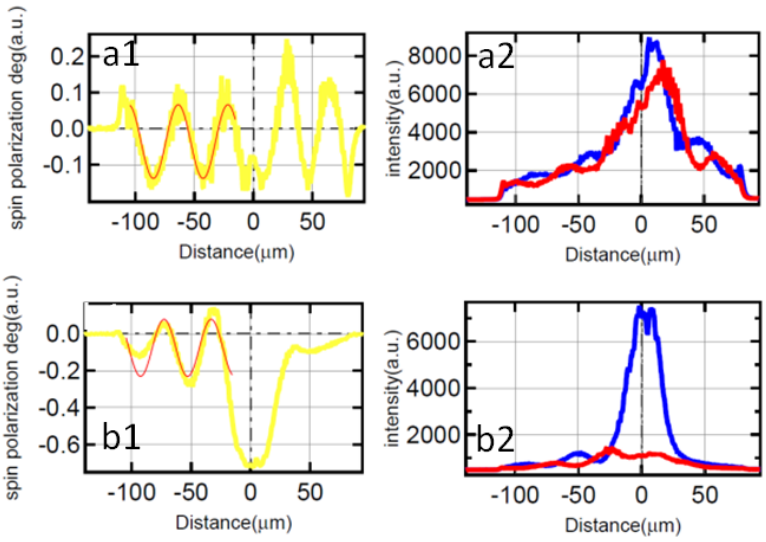

Figure 5.6 a1, b1 the lineprofile of the spin polarization imaging taken at the center of the ridge at energy of 1.5343eV and 1.5348eV; a2, b2, line profile of the σ+ component (blue), σ- component (red) real space imaging of the polariton condensate

Results and discussion

We find that the exciton polariton condensate oscillates at slightly different frequency when their energy changes. In general, the spin oscillation periods should be different when the TE-TM mode splitting changes with the wave vector and energy. For example, the TE-TM mode splitting is larger when the exciton polaritons have higher energy and larger wave vector, as shown in **Figure 5.7**. If we assume the polariton just experiences elastic scattering while keeping the amplitude of the wave vector constant, in the polar system, the circular polarization of the polaritons is **[69]**:

$$\rho(r,\theta) = \sin(2\theta)\sin(\frac{\Omega * r}{v_g}) \tag{5.6}$$

Where θ is the polar angle, v_g is the group velocity. We can find that the oscillation period of the polaritons' spin polarization in real space is

$$T = \frac{v_g}{\Omega} \tag{5.7}$$

The spin polarization of the exciton polariton condensate with a larger TE-TM mode splitting should oscillate faster.

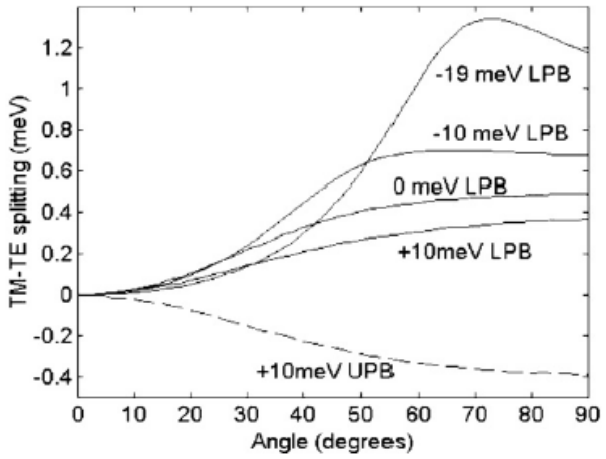

Figure 5.7 Longitudinal-transverse (TM-TE) polariton splitting calculated for a microcavity sample for the lower polariton branch (LPB) and the upper polariton branch (UPB) for different detuning, reprinted from **[18]**.

In **Figure 5.6,** we fit the spin polarization profiles by using a sin function for the two different energies of the polariton condensate: 1.5343eV and 1.5348eV. The spin procession period of the polariton condensate with the energy of 1.5348 eV is 40.95 micrometers, while as the spin procession period of the polariton condensate with the energy of 1.5343 eV is 41.95 micrometers. Here we confirm that the higher-energy polaritons oscillate faster than the lower-energy polaritons. Although the difference is very small (2.5%), this does reveal the effect of the effective magnetic field (and TE-TM mode splitting) on the spin oscillation of the polariton condensate flow.

5.4 spin bullet

The above spin oscillation due to the effective magnetic field disappears when the laser changes from CW to pulse mode (power not changed). The polariton condensate flow is formed without changing spin polarization. We call a polariton condensate flow with non-changing spin polarization a spin bullet. This kind of spin resolved polariton condensate flux forms the basis of spin optical circuits. Spin bullet is observed by reference **[58],** where people use quasi resonant pumping. Here we find the appearance of spin bullet **spontaneously** formed by non-resonant pumping method.

5.4.1 Observation of spin bullet

When a pulse right-hand circular polarized laser is focused onto the ridge, the exciton polariton condensate with spin σ+ propagates from the pump spot earlier than the condensate with spin σ-, as shown in **Figure 5.8.**

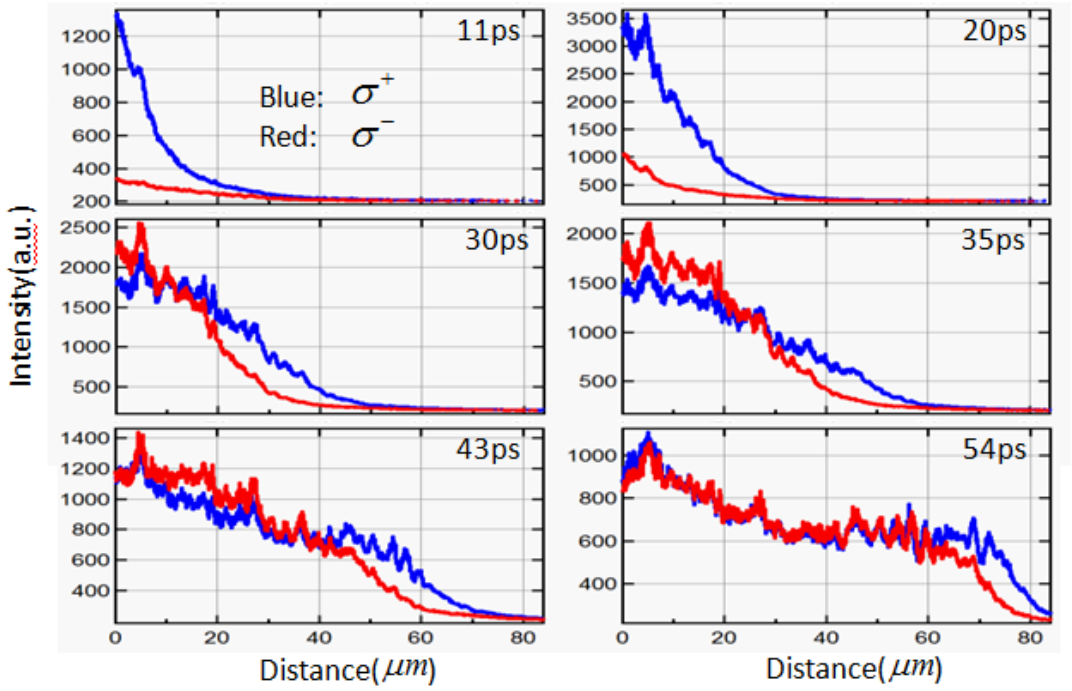

Figure 5.8 Line profile of the real space imaging with spin σ+(blue) and spin σ-(red) at different time

When a left hand circular polarized laser is focused onto the ridge, the exciton polariton condensate with spin σ- is expelled from the pump spot earlier than the condensate with spin σ+ (not shown here), as opposite to the case when a right hand circular polarized laser is used. Finally, if a linear polarized laser is focused onto the ridge, the exciton polariton condensate with spin σ- propagates from the pump position with around the same time as the condensate with spin σ+, now the spin bullet disappears.

To summarize, a circular polarized pulse laser can excite mostly the exciton polariton condensate with firstly the same spin polarization, and secondly with the opposite spin polarization.

Explanation

The above result is confirmed by reference **[70]**. They observe the spin polarization degree changes to become opposite to the pump laser at later time when the power is above the stimulated scattering threshold. For example, they find the spin polarization degree of the lower-branch polaritons starts around 50% and drop quickly to negative values when the power is high enough. In **Figure 5.9,** the above explanation is confirmed if we plot the integrated spin polarization degree at the pump position as a function of time. In the beginning, the spin polarization degree increases quickly from -20% to -80% at 10-20ps, later it jumps to positive values and finally becomes zero.

We can compare this graph with time-resolved spin polarization distribution**.** The polariton condensate with spin σ- transports from the pump spot at around the same time when the integrated spin polarization degree reaches maximal negative value. While as the polariton condensate with spin σ+ is expelled from the pump position at around the same time when the integrated spin polarization degree changes sign and reaches the maximal positive value. This is consistent with the explanation above. When the pump laser becomes linear polarized, the spin polarization of the exciton polariton condensate at the pump position is very small and changes randomly with time, which results in the absence of the spin bullet.

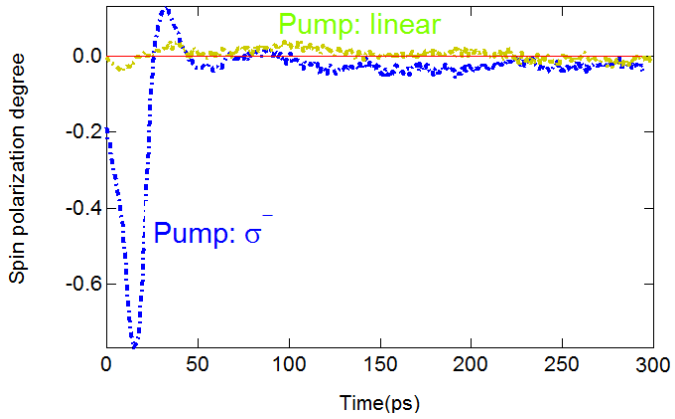

Figure 5.9 Integrated spin polarization degree at the pump position with time when the pump laser is left hand circular polarized (blue dotted line) and linear polarized (yellow dotted line).

To explain simply the time dependent spin polarization degree of polaritons at the pump spot, we can see that the spin polarization increases at first time because the spin polarization of the polaritons is kept above stimulated scattering threshold. The stimulated scattering is spin selective. The polaritons with the same spin polarization with the pump laser macroscopically occupy the ground state firstly. When they occupy the ground states, they are depleted; then the polaritons with opposite spin polarization begin to occupy the ground state slowly. Now the spin polarization degree decreases and finally becomes opposite with the pump laser. Finally polaritons with two different spin polarizations are both depleted and the total spin polarization degree becomes zero.

Why no spin procession

There is a question why the spin polarization of the exciton polariton condensate flow from the pump position does not oscillate along the ridge. Indeed, we find there is weak spin oscillation when the source beam is σ- polarized and in pulse mode, when a spectrometer rather than a streak camera is used, as shown in **Figure 5.10.**

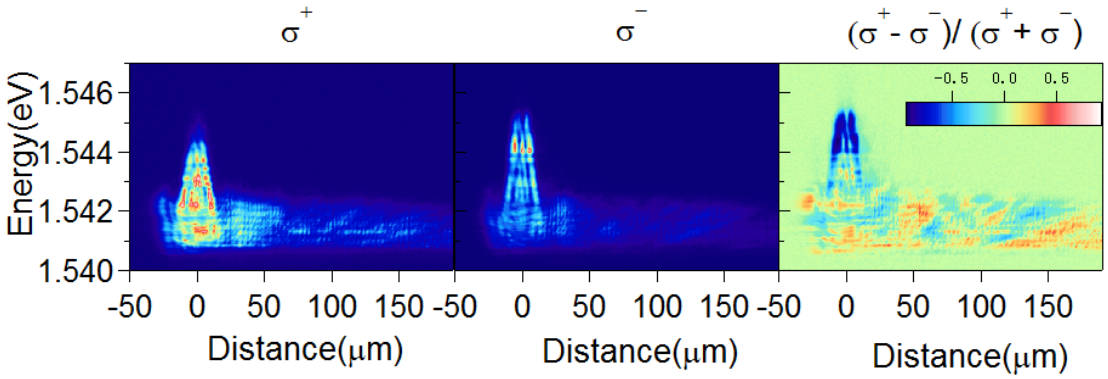

Figure 5.10 Energy resolved imaging for different spin polarization and the calculated spin polarization.

The absence of spin polarization oscillation can be related to the scattering of polaritons with phonons or defects. The TE-TM mode splitting generated effective magnetic field depends on the wave vector. When polariton momentum scattering is quicker, their wave vector will change more frequently. The effective magnetic field is more fluctuating and affects the polarization more weakly **[71]**. In the present experiment, we can see that the polaritons experience more scattering with phonons from the pump spot. This leads to much weaker influence of the effective magnetic field on the polarization of the polaritons. In the ballistic regime where scattering is absent, the effective magnetic field does not experience much fluctuation and results in clear spin polarization oscillation. In addition, there is exchange effective field $\Omega_{exch} \approx E_{ecch}(N_+ - N_-)$ due to the population imbalance in different spin polarization and anisotropic polariton-polariton interaction **[72]**. This exchange field, together with the effective magnetic field generated by the TE-TM mode splitting determines the spin polarization dynamics of polaritons. When the pulse laser is used with around 40 mW, the peak power is much larger than 40mW. This peak power leads to much larger exchange effective field than the TE-TM mode splitting generated field. In this case, the exchange field is collinear with the spin of polaritons. That is why the spin polarization of the polaritons does not show oscillation during propagation. Of course, there is also weak power in the pulse, which renders the TE-TM mode splitting generated effective magnetic field much stronger than the exchange effective field. These weak power leads to the spin inversion of the polaritons at the pump spot to the pump laser and the weak spin polarization oscillation during propagation process in **Figure 5.10**.

5.4.2 Oscillation of spin bullet between source spot and gate spot

If a second laser beam is introduced between the source spot and the ridge end, the polariton condensates with spin σ- and the condensate with spin σ+ have to tunnel through the blueshift created by the gate beam. Because the polariton condensates with spin σ- and σ+ are repelled

from the pump spot at different time, they will propagate independently between the source and gate spots. Thus spin pattern at different time is created. (The polariton condensate components with spin σ- and σ+ have around the same group velocity when they transport between the source and gate position.)

Results and discussion

In **Figure 5.11,** the source laser beam is left-hand circular polarized, the gate beam laser is right-hand circular polarized. At early time such as 47ps, the polariton condensate component with spin σ- propagates earlier than the component with spin σ+, and reaches the gate beam firstly. Because of the blueshift created by the gate beam, the polariton condensate component with spin σ- is reflected and reaches the pump spot earlier than the polaritons with spin σ+, as shown in the imaging at 73ps. At time 119ps, the polariton condensate with spin σ- transports earlier than the component with spin σ+, so the spin patterns appear again.

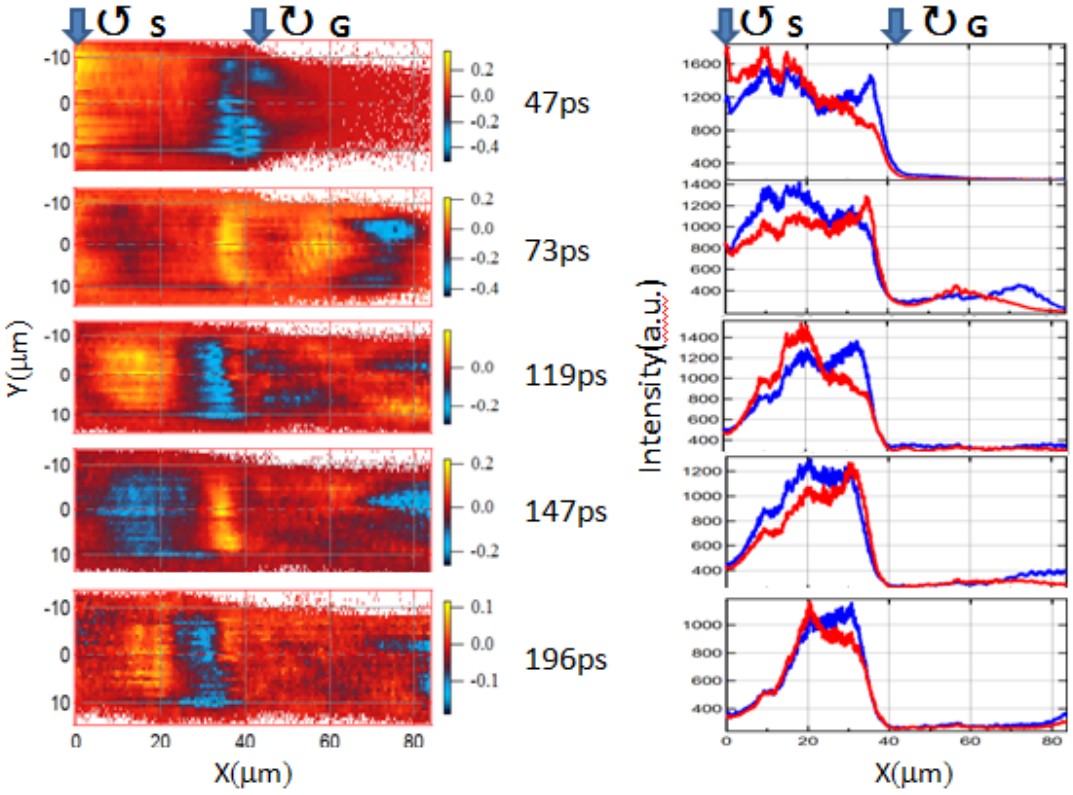

Figure 5.11 Left row: spin polarization imaging at different time; Right row: Integrated spin minus component and integrated spin up component at different time. The source laser is left-hand circular polarized and at 0 micrometers, the gate laser is right hand circular polarized and at 40 micrometers.

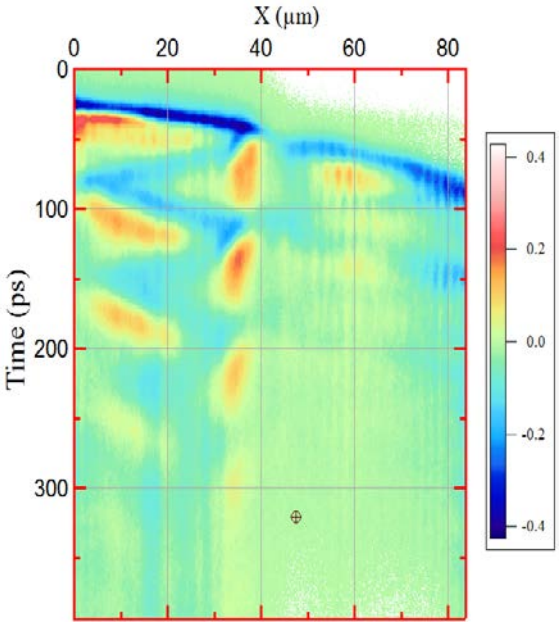

Figure 5.12 Integrated spin polarization distribution along the ridge as a function of time.

In **Figure 5.12,** the integrated spin polarization along the width (20microns) of the ridge is plotted as a function of time. The oscillation of the spin bullet between the source and gate spots can be seen clearly. From this graph, we find that the polariton condensate component with spin σ- is always ahead of the component with spin σ+. Here we observe the independent intensity oscillation of polaritons in different spin polarization between the source and gate spots. As to the transmitted exciton polaritons, the circular polarization of the gate beam does not affect in the experiment. This is due to that the circular polarization of the created exciton reservoir and polaritons is lost when the polariton condensate flow reaches the gate spot.
Next step should be to optimize the circular polarization of the exciton reservoir and polaritons at gate spot, such that the exciton polariton condensate flow with spin σ- and σ+ created by the source beam tunnels through the gate spot differently. Specially, the exciton polariton condensate with spin σ- ejected from the source spot should transmit through the gate spot, if the gate beam is right hand circularly polarized. While as the exciton polariton condensate with spin σ+ should be reflected backwards and oscillate between the source and gate spots.

5.5 spin filter

The oscillation of the polariton spin bullet between source and gate spot should be improved when the polarization of the source and gate beam is considered, as discussed in the above section. We find the polarization of the gate beam affects the polariton condensate flow differently from the above result if proper distance of the source and gate spots is chosen. To start this, we need to discuss basic interaction of excitons in singlet configuration and spin triplet configuration. That is the exciton interaction when their spin polarization orientation is anti-parallel or parallel. This interaction differs greatly; one order of magnitude difference has been found.

The interaction of excitons with the same spin polarization and opposite one

The interaction between the excitons depends on their specific polarization state. In the following **[73],** we discuss firstly the elastic Coulomb scattering of two 1s excitons in the specific polarization state: (this can be applied to exciton polaritons directly.)

$$(1s,Q,S)+(1s,Q^{'},S^{'})\rightarrow(1s,Q+q,S_f)+(1s,Q-q,S_f^{'}) \tag{5.8}$$

The scattering amplitude can be given by the matrix element **[73]**

$$H_{SS^{'}}^{S_fS_f^{'}}(Q,Q^{'},q)=<S\mid S_f><S^{'}\mid S_f^{'}>H_{dir}(Q,Q^{'},q)+<S\mid S_f^{'}><S^{'}\mid S_f>H_{exch}^{X}(Q,Q^{'},q)$$
$$+S_{exch}^{e}(S,S^{'},S_f,S_f^{'})H_{exch}^{e}(Q,Q^{'},q)+S_{exch}^{h}(S,S^{'},S_f,S_f^{'})H_{exch}^{h}(Q,Q^{'},q) \tag{5.9}$$

Where the first part is the direct coulomb interaction between the excitons, the second component is the exciton-exciton exchange interaction, the third and forth parts are the electron-electron and hole-hole exchange interaction. When the exchange wave vector during the scattering process is small enough, the first part and second part can be ignored and the exciton-exciton interaction strongly depends on the spin alignment of the two excitons. The factors S_{exch}^{e} and S_{exch}^{h} are calculated in specific spin channels.

Reference **[73]** calculates the spin exchange caused by electron-electron exchange and hole-hole exchange factors. The permitted spin channels and corresponding spin exchange factors are listed in **Table 5.2**.

S	S'	S_f	S_f'	$\mathcal{S}_{\text{exch}}^{e}(S,S',S_f,S_f')$	$\mathcal{S}_{\text{exch}}^{h}(S,S',S_f,S_f')$
E_α	E_α	E_α	E_α	$\sin^4\alpha+\cos^4\alpha$	$\sin^4\alpha+\cos^4\alpha$
E_α	E_α	$E_{\alpha+\pi/2}$	$E_{\alpha+\pi/2}$	$\frac{1}{2}\sin^2 2\alpha$	$\frac{1}{2}\sin^2 2\alpha$
E_α	E_α	E_α	$E_{\alpha+\pi/2}$	$-\frac{1}{4}\sin 4\alpha$	$-\frac{1}{4}\sin 4\alpha$
E_α	E_α	$+2$	-2	$\frac{1}{2}\sin 2\alpha$	$\frac{1}{2}\sin 2\alpha$
E_α	$E_{\alpha+\pi/2}$	E_α	$E_{\alpha+\pi/2}$	$\frac{1}{2}\sin^2 2\alpha$	$\frac{1}{2}\sin^2 2\alpha$
E_α	$E_{\alpha+\pi/2}$	$E_{\alpha+\pi/2}$	$E_{\alpha+\pi/2}$	$\frac{1}{4}\sin 4\alpha$	$\frac{1}{4}\sin 4\alpha$
E_α	$E_{\alpha+\pi/2}$	$+2$	-2	$-\sin^2\alpha$	$\cos^2\alpha$
E_α	$+2$	E_α	$+2$	$\cos^2\alpha$	$\sin^2\alpha$
E_α	$+2$	$E_{\alpha+\pi/2}$	$+2$	$-\frac{1}{2}\sin 2\alpha$	$\frac{1}{2}\sin 2\alpha$
E_α	-2	E_α	-2	$\sin^2\alpha$	$\cos^2\alpha$
E_α	-2	$E_{\alpha+\pi/2}$	-2	$\frac{1}{2}\sin 2\alpha$	$-\frac{1}{2}\sin 2\alpha$
± 2	± 2	± 2	± 2	1	1

Table 5.2 Allowed scattering spin channels and their corresponding spin exchange factors (reprinted from [73]. $|S>$ and $|S^{'}>$ are initial spin states, $|S_f>$ and $|S_f^{'}>$ are final states; $\{|E_\alpha>,|E_{\alpha+\pi/2}>,|+2>,|-2>\}$ are the basis, where the former two is the elliptically polarized state, the latter two are dark state.

From **Table 5.3**, the excitons in the same circular polarized state cannot change their polarization after scattering; while as the excitons in the opposite circular polarization state can only scatter into the dark states. So if we consider the circular polarization component, we

should only observe the excitons in the same circular polarized state scatter with each other. The excitons in the opposite circular polarized state seem “inactive” with each other.

S	$S^{'}$	S_f	$S_f^{'}$	S_{exch}^{e}	S_{exch}^{h}
|-1>	|-1>	|-1>	|-1>	1	1
|-1>	|-1>	|+1>	|+1>	0	0
|-1>	|-1>	|-1>	|+1>	0	0
|-1>	|-1>	|+2>	|-2>	0	0
|-1>	|+1>	|-1>	|+1>	0	0
|-1>	|+1>	|+1>	|+1>	0	0
|-1>	|+1>	|+2>	|-2>	0	1

Table 5.3 Allowed scattering spin channels and their corresponding spin exchange factors when the excitons are circularly polarized (calculated from reference [73]). Other spin channels like the circular polarized excitons scatter with dark excitons are not plotted here

S	$S^{'}$	S_f	$S_f^{'}$	S_{exch}^{e}	S_{exch}^{h}
|x>	|x>	|x>	|x>	1/2	1/2
|x>	|x>	|y>	|y>	1/2	1/2
|x>	|x>	|x>	|y>	0	0
|x>	|x>	|+2>	|-2>	1/2	1/2
|x>	|y>	|x>	|y>	1/2	1/2
|x>	|y>	|y>	|y>	0	0
|x>	|y>	|+2>	|-2>	-1/2	1/2

Table 5.4 Allowed scattering spin channels and their corresponding spin exchange factors when the excitons are linearly polarized (calculated from reference [73]). Other spin channels like the circular polarized excitons scatter with dark excitons are not plotted here.

Table 5.4 lists the excitons with the same linear polarized state and the opposite ones. They can change their polarization state; and the spin exchange factors do not have much difference compared with the excitons in the opposite linear polarized state.

Proposal of spin filter

From the above results, if we create an exciton polariton condensate flow with linear polarization, the circular polarization components of this condensate flux behave differently when they encounter the circular polarized gate. To be more specifically, the interaction between the polariton condensate with spin σ+ and the excitons or polaritons at gate spot when the gate beam is left hand circular polarized should be much weaker than the polariton condensate with spin σ-.

In addition, the circular polarized gate beam introduces a spin dependent blueshift. The energy of the polariton emission in different spin polarization shows splitting when the gate beam is circular polarized. If we ignore the interaction between the opposite spin polarization excitons (polaritons), the spin dependent blueshift is determined by the number difference of polaritons in different spin polarization.

$$\Delta E = \alpha 1(n_+ - n_-)$$
$$10^{-10} \le \alpha 1 \le 1.6 \times 10^{-10}\, meVcm^2 \qquad (5.10)$$

Large spin dependent blueshift such as 6meV has been found when the pump laser is little blueshifted than the Heavy Hole Excitons and high power. Of course the spin dependent blueshift is smaller when a non resonant and weaker laser is used. But it is already large enough to affect the polariton flow.

From this spin dependent blueshift, if the gate beam is left hand circularly polarized, the polariton condensate with spin σ+ experience smaller blueshift caused by the gate beam and transmits through the gate spot more easily. The polariton condensate with spin σ- encounters a larger blue-shift and tunnels through the gate spot more hardly. So, more polariton condensate with spin σ- will be reflected between the gate spot and source spot. And polaritons with spin σ+ will distribute between the gate spot and the ridge end. Through this spin dependent blueshift, we realize to separate the polariton component with spin σ- and σ+ into two regions, as shown in **Figure 5.13**. The gate beam acts as a spin valve to filter the polariton condensate with the same spin polarization.

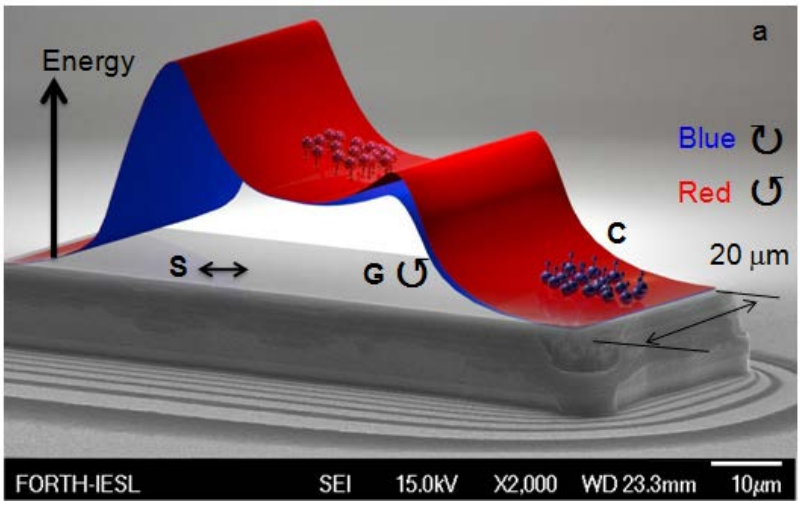

Figure 5.13 Schematics showing the potential energy landscape from the carrier induced blueshift along the ridge. The different blueshift at the gate position arise from the circular polarization of the gate beam.

Results and discussion

The following is done at Crete.

From the discussion of the spin texture, we know the spin oscillation period is around 40microns. If the distance between the source spot and the ridge end is larger than 40microns, the polariton condensate with spin σ- and σ+ will experience spin procession caused by the effective magnetic field. In addition, the circular polarization degree of the excitons or polaritons at gate spot decays quickly with time. The polariton condensate flow with different spin polarization will experience a spin-unrelated blueshift if the distance between the source spot and gate spot is large, as shown in the result of spin bullet in **Figure 5.11**. So we should

reduce the distance between the source and gate spots and use CW laser. In the present experiment, we choose the distance of the source spot to the ridge end to be around 30 micrometers, the distance of the gate spot to the ridge end to be around 15 micrometers.

5.5.1 Energy resolved imaging

When the source laser is linearly polarized, the created polariton condensate should not be spin polarized. From **Figure 5.14 (a)**, we can see that the polariton condensate with different spin polarization have around the same intensity when there is only source beam. The total spin polarization thus is very small. However, the polariton condensate will "feel" differently when they encounter the gate spot induced blueshift. In **Figure 5.14 (b)** where the gate beam is left hand circular polarized, the blueshift in spin polarization σ- is larger than in spin polarization σ+, as shown in **Figure 5.14 (b-4)**, which is the cross section taken just at the gate spot. Here we estimate the spin dependent blueshift is around 0.2meV. The spin dependent blueshift has been observed in resonantly pumped excitons in GaAs/AlGaAs multi quantum wells **[30]**. The difference in the blueshift ranges from 2meV-6meV according to pump power. In our experiment, the laser is non-resonantly pumped and has a low power, the blueshift difference is smaller. However, this spin dependent blueshift leads to observable effect on the propagation of the polariton condensate. In this case, the polariton condensate component in spin polarization σ- "feels" more hardly to transmit through the gate spot. Thus, they will be reflected mostly and located between the source spot and gate spot. On the contrary, the polariton condensate component with spin polarization σ+ experiences a smaller blueshift and transmits through the gate spot more easily, so they are mostly distributed between the gate spot and the ridge end. This can be seen very clearly from **Figure 5.14 (b-1)** and **Figure 5.14 (b-2)**. In **Figure 5.14 (b-3),** we can see that the spin polarization for the transmitted condensate and the reflected condensate can reach around 45%. In this way, the circular polarized gate beam filter the polariton condensate with the same spin polarization and separate the two polariton condensate components with the efficiency of around 45%. If the gate beam changes the circular polarization from σ- to σ+, we should see swapped behavior. **Figure 5.14 (c)** ambiguously shows what we expect.

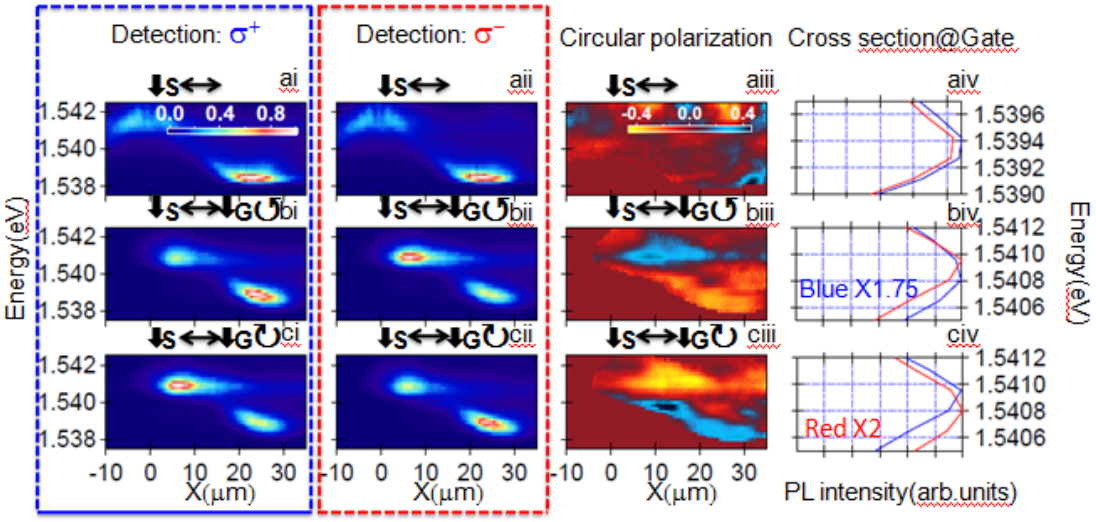

Figure 5.14 Energy vs real-space (X) maps of the emission of a cross section (center) along the ridge, under non resonant CW excitation for different S and G configurations: (a) only S linearly polarized, (b) with a σ- polarized G, (c) with a σ+ polarized G. Column (1)/(2) shows the polariton emission intensity under σ+/σ- detection. Column (3) depicts the degree of circular polarization. Column (4) compiles the cross section at x=8 microns and x=25 microns under σ+ (blue) and σ- (red) detection with energy, the curves are shifted horizontally for clarity to see. The S/G power is 5.7Pth/0.7Pth. The intensity and the degree of circular polarization are coded in a false, log and linear color scale, respectively. To summarize, the above results clearly show the spin filter effect of the circular polarized gate beam.

5.5.2 Real space imaging

To make sure the above phenomenon takes place on the whole ridge, we take the real space imaging at the same experimental condition. **Figure 5.15** shows the near field imaging of the polariton emission under different experimental schemes. The imaging when there is only source beam in linear polarization agrees well with the **Figure 5.14-aiii**. From **Figure 5.15 (b)** and **Figure 5.15 (c),** we can see that the spin filter effect does work in most area of the ridge. This shows that the spin separation by the weak gate beam does function in the present microcavity ridge. Although there is some area where spin separation is not clear, it is caused either from definite spot size of the gate beam or some defect at the ridge edge.

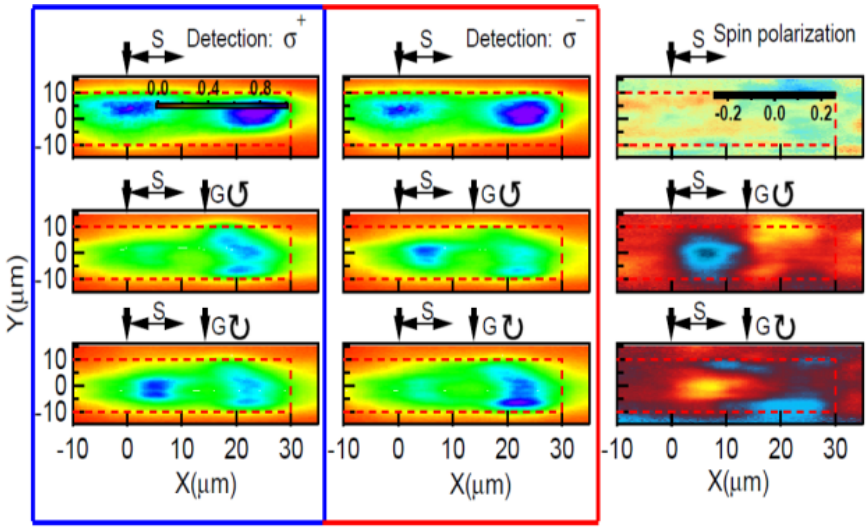

Figure 5.15 Real space polariton emission distribution at the right border of the ridge under non resonant CW excitation for different S and G configurations: (a) only S linearly polarized, (b) with a σ- polarized G, (c) with a σ+ polarized G. Column (1)/(2) shows the polariton intensity distribution under σ+/σ- detection. Column (3) shows the degree of circular polarization. The S/G power is 5.7Pth/0.7Pth. The intensity and the degree of circular polarization are coded in a false, linear color scale.

5.5.3 Change the polarization degree of the gate beam

In view of the sensitivity of the spin dependent blueshift on the polarization of the gate control beam, it is necessary to scan the polarization continuously. Especially a linear polarized gate control beam should not work as a spin filter. Here we change the polarization of the gate beam by rotating the quarter waveplate with the step of 10 degree and detect the polariton emission at both σ- and σ+ conditions. From these energy resolved imaging we integrate the intensity in the region of 1.538eV and 1.542eV. We care specially this region to focus on the polariton condensate and ignore other emission like excitons or Bragg mode. **Figure 5.16 (a 1)** and **Figure 5.16 (a 2)** show the energy integrated intensity as a function of the gate beam polarization under σ- and σ+ detection schemes. It is convincing that the change in the polarization of the gate beam tunes the intensity of the reflected and transmitted polariton condensate emission. When the gate beam is circular polarized such as σ+ and σ-, the spin filter works. However, the TE or TM polarized gate control beam cannot separate the polariton condensate in different spin polarization. In **Figure 5.16 (b 1)** and **Figure 5.16 (b 2)**, a cross section is taken at the position of x=8 microns and x=25 microns. And the topmost is the sum of two cross sections. We can see that the total intensity is around conserved while the intensity of the reflected and transmitted condensate is modulated by the gate beam. An ideal spin filter should allow the crossing at the TE and TM polarization position, which, could be improved in the near future.

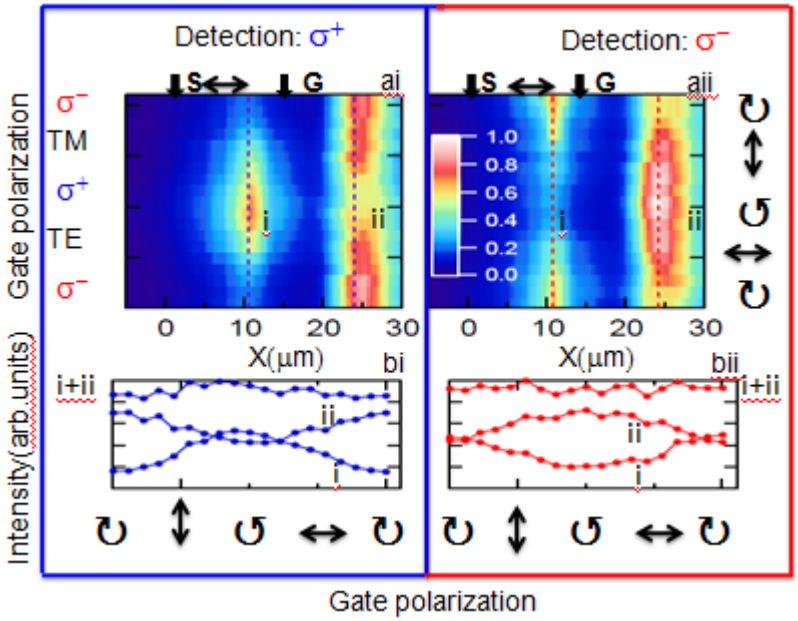

Figure 5.16 (a) Energy integrated intensity along the X-axis of the ridge as a function of the G polarization degree under σ+/σ- detection; (b)The intensity of the cross section taken from (a) at x=8 microns and x=25 microns, and the sum (topmost) of these two cross sections under σ+/σ- detections, respectively, b 1 and b 2 are in the same intensity scale.

5.6 Conclusion

The spin polarization of the polaritons in the microcavity ridge is measured when the laser is circularly polarized. If a continuous wave circular polarized laser is used, the spin procession is observed along the ridge accompanying the condensate ballistic propagation. The polariton condensate flow with non-changing spin polarization (called spin bullet) appears when the pump laser changes to pulse mode. Finally, a non-resonant circular polarized gate beam acts to separate the polariton condensate with different circular polarization by using a spin dependent blueshift.

Chapter 6

Conclusion

Facing more and more limits in the microelectronics by using Silicon and Germanium, the GaAs based microcavity can be used in optical circuits to reduce the consuming power, loss and to increase the operation speed.

Polariton lasing in a high Q planar microcavity and micropillars is observed with a very small threshold. Due to the local blueshift generated by the exciton reservoir, the polariton condensate spontaneously formed is expelled away from the pump spot center and aquire a finite in-plane wave vector. In this case we observe polariton lasing occurs at a higher energy states. At 70K we only see weak coupling lasing. The difference of polariton lasing and photon lasing is compared at low temperature and high temperature. In the strong coupling regime, polariton lasing energy is blueshifted by a nearly constant value. However, in the latter case, the lasing energy is very close to the cavity mode. At positive detuning, the lasing energy is larger than the excitons, which cannot occur in the strong coupling regime. More efficient relaxation scheme is found in micropillars because of stronger lateral confinement. In this case, we observe polariton lasing threshold decreases with pillarsize and detuning. The decreased polariton lasing threshold confirms that the lateral confinement enhances polariton relaxation rate and decreases exciton diffusion. The decrease in the polariton lasing threshold is due to the avoidance of thermal excitation from the ground state. In addition, the polariton lasing at negative detuning needs a smaller critical density, which needs a samller density of states.

A cavity polariton condensate transistor switch is realized by using a high Q microcavity which is etched into ridges. The polariton condensate created at pump spot experiences repulsive interaction from the exciton reservoir. They propagate along the microcavity ridge with a distance of 60 micrometers. It is very interesting because the group velocity of polaritons and their lifetime can propagate along so long this distance. From energy resolved imaging, the propagating polaritons experience energy relaxation. We show in this thesis that the energy relaxation is due to transition between different subbranch polaritons, which is because of the lateral confinement vertical to the ridge. Multiple cavity modes appear and they strongly couple with the excitons and form subbranch polaritons. We show the condensate flow from the source spot can be controlled by a second gate beam which is 20 times weaker. This spatial control with attenuation larger than 90% allows the implementation of all-optical polariton transistors suitable in both optoelectronic and all-optical schemes. In the long future this kind of transistor can be used to replace electron transistors.

The spin of exciton polariton condensate on a microcavity ridge is investigated. Polariton can be seen as a two level system when dark excitons can be ignored. A Pseudospin vector is introduced to describe polariton dynamics. The exciton polaritons have a non-zero TE-TM mode splitting due to the long range electron-hole exchange interaction (for excitons) and cavity mode TE-TM mode splitting. The effective magnetic field generated has a specific pointing direction which lies in the quantum well plane and has a specific angle with the wave

vector. This effective magnetic field rotates the pseudospin of polaritons in a very interesting way, like a Rashba effect on an electron.
Based on this effective magnetic field, novel spin texture in polariton ballistic propagation regime is observed. The spin oscillation is due to the effective magnetic field discussed above. When we measure energy resolved imaging, the high energy condensate or exciton reservoir is located at the pump position and does not show the spin procession, the low energy condensate propagates with clear spin oscillation. When a pulse laser is used, spin bullets are observed without spin oscillation. Two possible reasons are proposed. One is more frequently changing effective magnetic field, which renders it more weak; another is due to the exchange effective magnetic due to polariton population imbalance and anisotropic polariton-polariton interaction.
Finally, a spin filter is realized by using spin dependent blueshift. The weak circular polarized gate control beam can separate the polariton condensate with different circular polarization at different region in the ridge with the efficiency of around 45%. It could be improved in the future.

Outlook and Future

The difference between exciton polariton condensate and cold atom condensate, such as much strong particle interaction, can be used to design new all optical devices.
In the future, studies based on exciton polariton condensate in optical circuits, spin memory and polariton neurons could be investigated by designing novel structures, waveguides, or hybrid materials. For example, polariton confinement can be realized by embedding patterned channels in two dielectric DBRs. With this, we can create polariton condensate flow with well defined in-plane wave vector along these channels and realize manipulation of them. The advantage of polaritons is much larger coherence length which is inversely proportional to the effective mass. In fact, polaritons have been claimed to have a large coherence length of 1 mm. This is several orders of magnitude longer than the electrons. Combining these different polariton devices, the next step should be polariton integrated circuits. The large group velocity and short lifetime can find promising application in these circuits and can replace the current electron based systems.
To be further, polariton-polariton interaction shows promising application potential in photon blockade phenomenon in a polariton dot, which could be explored in quantum optics. The strong polariton-polariton interaction will allow only one polariton in the system. The adding of second one is avoided due to the blueshift larger then polariton linewidth. Especially it is very interesting that polariton with opposite spin attract each other forming bipolaritons like a biexcitons. What will happen if we create resonantly a polariton with definite spin? These are open questions that can be explored. Recently, recently a squeezed light has been realized in a micropillar. It is very interesting to explore whether possible few polariton states can be realized or not.

Bibliography

[1]Gunnar Björk Susumu Machida, Yoshihisa Yamamoto, and Kazuhiro Igeta, Phys. Rev. A 44, 669 (1991).
[2]E. M. Purcell, Phys. Rev. 69, 681 (1946)
[3]Weisbuch, C., M. Nishioka, A. Ishikawa, and Y. Arakawa, Phys. Rev. Lett. 69, 3314(1992).
[4]P. G. Savvidis, J. J. Baumberg, R. M. Stevenson, M. S. Skolnick, D. M. Whittaker, and J. S. Robert, Phys.Rev.Lett 84, 1547(2000); P.G. Savvidis *et. al.* PRB (2002)
[5]Imamoglu, A., R. J. Ram, S. Pau, and Y. Yamamoto, Phys. Rev. A 53, 4250(1996)
[6]R. Butté, G. Delalleau, A. I. Tartakovskii, M. S. Skolnick, V. N. Astratov, J. J. Baumberg, G. Malpuech, A. Di Carlo, A. V. Kavokin, and J. S. Roberts Phys. Rev. B 65, 205310 (2002)
[7]Cho A Y, Advances in molecular beam epitaxy (MBE) Journal of Crystal Growth Vol. 111 1(1991).
[8]E. Wertz, L. Ferrier, D. Solnyshkov, D. Bajoni, A. Miard, A. Lemaitre, G. Malpuech, J. Bloch, Appl. Phys. Lett. 95**,** 51108 (2009)
[9]D. Bajoni, et.al.Phys. Rev. Lett.100, 047401 (2008)
[10]E. Wertz, L. Ferrier, D. Solnyshkov, R. Johne, D. Sanvitto, A. Lemaitre, I. Sagnes, R. Grousson, A. V. Kavokin, P. Senellart, G. Malpuech, J. Bloch, **Nat. Phys. 6**, 860 (2010)
[11]T. Gao, P. S. Eldridge, T. C. H. Liew, S. I. Tsintzos, G. Stavrinidis, G. Deligeorgis, Z. Hatzopoulos, and P. G. Savvidis, Phys.RevB.85.235102(2012).
[12]G. Tosi, G. Christmann, N. G. Berloff, P. Tsotsis, T. Gao, Z. Hatzopoulos, P. G. Savvidis, and J. J. Baumberg, Nat. Phys. 8, 190 (2012).
[13]G. Tosi, G. Christmann, N.G. Berloff, P. Tsotsis, T. Gao, Z. Hatzopoulos, P.G. Savvidis, J.J. Baumberg Nature Comm. 3, 1243 (2012)
[14]Kasprzak, J., *et al.*, 2006, Nature (London) 443, 409.
[15]K. G. Lagoudakis, T. Ostatnický, A. V. Kavokin, Y. G. Rubo and R. André et al. Observation of Half Quantum Vortices in an Exciton-Polariton Condensate, Science, 326, 974(2009).
[16]Alexey Kavokin, Guillaume Malpuech, and Mikhail Glazov, Optical Spin Hall Effect, Phys.Rew.Lett 95, 136601 (2005); C. Leyder et.al.Nature Photonics3, 628(2007)
[17]Giovanna Panzarini, Lucio Claudio Andreani, A Armitage, D. Baxter, M. S. Skolnick, V. N. Astratov, J. S. Roberts, A V. Kavokin, Maria R. Vladimirova, M. A. Kaliteevski Phys. Rev. B59, 5082–5089(1999);
[18]I A Shelykh, A V Kavokin, Yuri G Rubo, T C H Liew and G Malpuech, Semiconductor Sci Technol 25 013001(2010); Maialle M Z, de Andrada e Silva E A and Sham L J 1993Phys. Rev.B47, 15776; K.V. Kavokin, I. A. Shelykh, A.V. Kavokin,G. Malpuech, and P. Bigenwald, PRL92, 017401(2004)
[19]A. Amo, T. C. H. Liew, C. Adrados, R. Houdré, E. Giacobino, A. V. Kavokin, and A. Bramati, Nature Phot. 4, 361 (2010).
[20] A spin filter based on polariton condensate, under preparing and submission.
[21]http://www.ioffe.ru/SVA/NSM/Semicond/GaAs/bandstr.html
[22]Quantum Theory of the Solid State, Joseph Callaway, Academic Press,1976
[23]http://ee.stanford.edu/~dabm/181.pdf

[24]Hui Deng,Hartmut Haug and Yoshihisa Yamamoto, Reviews of Modern Physics 82, 1489(2010)
[25]A.Thilagam and M. A. Lohe, J. Phys. Condens. Matter 18, 3157 (2006).
[26]I.A. Shelykh, L. Viña, A.V. Kavokin, N.G. Galkin, G. Malpuech, R. André, Non-linear coupling of polariton and dark exciton states in semiconductor microcavities, Solid State Communications, 135, 1 (2005)
[27]Ivchenko E L and Pikus G E Superlattices and Other Heterostructures: Symmetry and optical Phenomena (Berlin:Springer),1995
[28]M S Skolnicky, T A Fisherz and D M Whittakerx, Strong coupling phenomena in quantum microcavity structures, semiconductor science and Technology 13, 645(1998); Savona V, Andreani L C, Schwendimann P and Quattropani A 1995 Solid State Commun. 93 733; Andreani L C, Savona V, Schwendimann P and Quattropani A 1994 Superlattices Microstruct. 15 453
[29]Panzarini G, Andreani L C, Armitage A, Baxter D, Skolnick M S, Roberts J S, Kavokin A V, Kaliteevski M A, Astratov V N and Vladimirova M R,PRB 59, 5082(1999)
[30]The physics of semiconductor microcavities, edited by Benoit Deveaud, 2007 WILEY-VCH Verlag GmbH & Co. KGaA, Weinheim
[31]Hopfield, J. J., 1958, Phys. Rev. 112, 1555.
[32]Bryan Nelsen, Gangqiang Liu, Mark Steger, David W. Snoke, Ryan Balili, Ken West, Loren Pfeiffer http://arxiv.org/pdf/1209.4573.pdf
[33]Mermin, N. D., and H. Wagner, Phys. Rev. Lett. 17, 1133(1996); .
[34]CJ Pethick and H Smith, Bose-Einstein condensation in Dilute Gases, Cambridge university press, Second Edition 2008
[35]Christopoulos, S., Baldassarri Höger von Högersthal, G., Grundy, A. J. D., Lagoudakis, P. G., Kavokin, A. V., Baumberg, J. J., Christmann, G., Butté, R., Feltin, E., Carlin, J.-F. and Grandjean, N., Phys. Rev. Lett. 98, 126405 (2007)
[36]M. Z. Maialle, E. A. de Andrada e Silva, and L. J. Sham Phys. Rev. B 47, 15776–15788 (1993); Spin Physics in Semiconductors Editor: M.I. Dyakonov, Springer Series in Solid-State Sciences ISSN 0171-1873, p56
[37]Deng, H., G. Weihs, C. Santori, J. Bloch, and Y. Yamamoto,, Science 298, 199(2002).
[38]Balili, R., V. Hartwell, D. Snoke, L. Pfeiffer, and K. West, 2007, Science 316, 1007
[39]P. Senellart, J. Bloch, **Phys. Rev. Lett. 82**, 1233 (1999)
[40]D. Bajoni, P. Senellart, A. Lemaitre, J. Bloch, **Phys. Rev. B 76**, 201305(R) (2007)
[41]J. Opt.Soc.Am B, 29, A138(2012)
[42]B. Nelsen, R. Balili, D.W. Snoke, L. Pfeiffer, and K. West, "Lasing and Polariton Condensation: Two Distinct Transitions in GaAs Microcavities with Stress Traps," Journal of Applied Physics 105, 122414 (2009)
[43]M. Maragkou, A. J. D Grundy, E. Wertz, A. Lemaitre, I. Sagnes, P. Senellart, J. Bloch, P. G. Lagoudakis, Phys. Rev. B 81, 81307 (2010)
[44]Raphael Butte and Nicolas Grandjean, Semicon.Sci.Technology.26, 014030(2011); Michael Slootsky, Yigan Zhang and S. Forrest, PRB86, 045312(2012), DengHui, PhD thesis, p56
[45]D. J. Frank, R. H. Dennard, E. Nowak, P. M. Solomon, Y. Taur, and H. S. P. Wong, Proc. IEEE 89, 259 (2001); ACTA PHYSICA POLONICA A 3, 113(2008)

[46]R. Doering and Y. Nishi, Proc. IEEE 89, 375 (2001).
[47]M. Anis, M. Allam, and M. Elmasry, IEEE Trans. Circuits Syst. II, Analog Digit. Signal. Process 49, 577 (2002).
[48]R. W. Keyes, Science 195, 1230 (1977)
[49]D. Hisamoto, W. C. Lee, J. Kedzierski, H. Takeuchi, K. Asano, C. Kuo, E. Anderson, T. J. King, J. Bokor, and C. M. Hu, IEEE Trans. Electron Devices 47, 2320 (2000).
[50]E. P. Gusev *et al.*, Electron Devices Meeting, 2001. IEDM Technical Digest. International, (IEEE, Washington DC, 2001), pp. 20.1.1-20.2.4
[51]H. Yan, H. S. Choe, S. W. Nam, Y. J. Hu, S. Das, J. F. Klemic, J. C. Ellenbogen, and C. M. Lieber, Nature (London) 470, 240 (2011).
[52]D. A. B. Miller, Nature Photon. 4, 3 (2010)
[53]K. G. Lagoudakis, M. Wouters, M. Richard, A. Baas, I. Carusotto, R. André, L. S. Dang, and B. Deveaud-Plédran, Nat. Phys. 4, 706 (2008).
[54]A. Amo, D. Sanvitto, F. P. Laussy, D. Ballarini, E. del Valle, M. D. Martin, A. Lemaître, J. Bloch, D. N. Krizhanovskii, M. S. Skolnick, C. Tejedor, and L. Viña, Nature (London) 457, 291 (2009).
[55]J. J. Baumberg, P. G. Savvidis, R. M. Stevenson, A. I. Tartakovskii, M. S. Skolnick, D. M. Whittaker, and J. S. Roberts, Phys. Rev. B 62, 16247 (2000).
[56]T. C. H. Liew, A. V. Kavokin, and I. A. Shelykh, Phys. Rev. Lett. 101, 016402 (2008).
[57]T. K. Paraïso, M. Wouters, Y. Léger, F. Morier-Genoud, and B. Deveaud-Plédran, Nat. Mater. 9, 655 (2010)
[58]C. Adrados, T. C. H. Liew, A. Amo, M. D. Martín, D. Sanvitto, C. Antón, E. Giacobino, A. Kavokin, A. Bramati, and L. Viña, Phys. Rev. Lett. 107, 146402 (2011).
[59]D. Sanvitto, S. Pigeon, A. Amo, D. Ballarini, M. De Giorgi, I. Carusotto, R. Hivet, F. Pisanello, V. G. Sala, P. S. S. Guimaraes, R. Houdré, E. Giacobino, C. Ciuti, A. Bramati, and G. Gigli, Nature Photon. 5, 610 (2011)
[60]T. C. H. Liew, I. A. Shelykh, and G. Malpuech, Physica E 43, 1543 (2011)
[61]Gabriel Christmann, Guilherme Tosi, Natalia G. Berloff, Panos Tsotsis, Peter S. Eldridge, Zacharias Hatzopoulos, Pavlos G. Savvidis, and Jeremy J. Baumberg, Phys. Rev. B 85, 235303 (2012)
[62]G. Dasbach, M. Schwab, M. Bayer, D.N. Krizhanovskii, and A. Forchel Phys. Rev. B 66, 201201(R) (2002)
[63]A. A. High, A. T. Hammack, L. V. Butov, M. Hanson, and A. C. Gossard, Opt. Lett. 32, 2466 (2007)
[64]T. C. H. Liew, A. V. Kavokin, T. Ostatnický, M. Kaliteevski, I. A. Shelykh, and R. A. Abram, Phys. Rev. B 82, 033302 (2010).
[65]E. Kammann, TCH Liew, H. Ohadi, P. Cilibrizzi, P. Tsotsis, Z. Hatzopoulos, P.G. Savvidis, A.V. Kavokin and P.G. Lagoudakis, Physical Review Letters, 109, 036404, 2012
[66]Renucci, P. et al. Microcavity polariton spin quantum beats without a magnetic field: a manifestation of Coulomb exchange in dense and polarized polariton systems. Phys. Rev. B 72, 075317 (2005)
[67]E. Wertz, A. Amo, D. Solnyshkov, L. Ferrier, T.C.H. Liew, D. Sanvitto, P. Senellart, I. Sagnes, A. Lemaitre, A. V. Kavokin, G. Malpuech, J. Bloch, Phys. Rev. Lett. 109, 216404 (2012)

[68]F. Tassone and Y. Yamamoto, Phys. Rev. B, 59, 10830 (1999).
[69] Maria Maragkou's PhD thesis, 2010
[70]M. D. Martín, G. Aichmayr, and L. Viña, R. André PRL 89,077402(2002)
[71] R. I. Dzhioev,Phys. Rev. Lett. 93, 216402 (2004)
[72]Renucci.et.al., PRB72, 075317(2005)
[73]Role of the exchange of carriers in elastic exciton-exciton scattering in quantum wells, C.Ciuti, V, Savona, et al, PRB58, 7926(1998)